INFORMATION TO USERS

This manuscript has been reproduced from the microfilm master. UMI films the text directly from the original or copy submitted. Thus, some thesis and dissertation copies are in typewriter face, while others may be from any type of computer printer.

The quality of this reproduction is dependent upon the quality of the copy submitted. Broken or indistinct print, colored or poor quality illustrations and photographs, print bleedthrough, substandard margins, and improper alignment can adversely affect reproduction.

In the unlikely event that the author did not send UMI a complete manuscript and there are missing pages, these will be noted. Also, if unauthorized copyright material had to be removed, a note will indicate the deletion.

Oversize materials (e.g., maps, drawings, charts) are reproduced by sectioning the original, beginning at the upper left-hand corner and continuing from left to right in equal sections with small overlaps.

Photographs included in the original manuscript have been reproduced xerographically in this copy. Higher quality 6" x 9" black and white photographic prints are available for any photographs or illustrations appearing in this copy for an additional charge. Contact UMI directly to order.

ProQuest Information and Learning
300 North Zeeb Road, Ann Arbor, MI 48106-1346 USA
800-521-0600

DISSERTATION

RADIATIVE DECAY OF $\psi(2S)$ INTO TWO PSEUDO-SCALAR MESONS

Submitted by

Wei Yang

Department of Physics

In partial fulfillment of the requirements

for the Degree of Doctor of Philosophy

Colorado State University

Fort Collins, Colorado

Summer 2000

COLORADO STATE UNIVERSITY

November, 4th 1999

WE HEREBY RECOMMEND THAT THE DISSERTATION PREPARED UNDER OUR SUPERVISION BY WEI YANG ENTITLED RADIATIVE DECAY OF $\psi(2S)$ INTO TWO PSEUDO-SCALAR MESONS BE ACCEPTED AS FULFILLING IN PART REQUIREMENTS FOR THE DEGREE OF DOCTOR OF PHILOSOPHY.

Committee on Graduate Work

Adviser

Department Head

ABSTRACT OF DISSERTATION

Radiative Decay of $\psi(2S)$ into Two Pseudo-Scalar Mesons

The existence of pure gluon bound states, the glueballs, is predicted by the Standard Model and several candidate of glueball states have been pursued for years in pp and $p\bar{p}$ central production on fix-target experiments, and in J/ψ radiative decay on e^+e^- collision experiments. This dissertation presents a study of the radiative decay of the radially excited counterpart of the J/ψ, the $\psi(2S)$, into two pseudo-scalar mesons pairs, i.e. $\pi\pi$, $K\overline{K}$ and $\eta\eta$. The $\sim 3.79 \times 10^6$ $\psi(2S)$ data sample we used for this analysis was collected by a e^+e^- collision experiment at the Beijing Electron-Position Collider with the Beijing Spectrometer.

We give the first measurement of the decay branching fractions of $\psi(2S) \to \gamma f_2(1270)$, $\psi(2S) \to \gamma f_J(1710) \to \gamma K\overline{K}$, $\psi(2S) \to \gamma f_J(1710) \to \gamma\pi^+\pi^-$ and $\psi(2S) \to \gamma f_2'(1525)$. These results agree with the predicted "15% rule", when compared with the corresponding J/ψ decay branching fractions. The spin-parity of the glueball candidate $f_J(1710)$ is yet to be determined. The χ_{c0} and χ_{c2} decay into $\pi^0\pi^0$ and $\eta\eta$ branching fractions have also been measured with a pattern that follows the SU(3) flavor symmetry.

Wei Yang
Physics Department
Colorado State University
Fort Collins, CO 80523
Summer 2000

Acknowledgments

I would like to thank the BES Collaboration and the high energy physics group of Colorado State University for the help they gave me, in particular my advisor Dr. Walter Toki who made it all possible.

Dr. Robert Wilson and Dr. John Harton and other HEP group members of CSU have given me many constructive suggestion during my four years of study at CSU, especially during the thesis writting. I have had a wonderful time during these four years with this team.

Many thanks go to Dr. William Dunwoodie, Dr. Joseph Izen, Dr. Fred Harris, Dr. Xinchou Lou, Dr. Xinhua Li and Dr. Li Haibo and Mr. Jinlong Zhang of the BES Collaboration for their wonderful suggestions, discussions and comments on the physics analysis and results, and Dr. Jim Panetta and Derrick Kong for computing issues.

Thanks also go to Prof. Zheng Zhipeng, Prof. Yan Wuguang, Prof. Li Jin, Prof. Zhang Changchun, Dr. Zhao Zhengguo, Prof. He Ju and Dr. Zhang Xueyao of IHEP for their help during the time I was there.

I thank Bonnie Gilmore, Marilyn Anderson and Sandy Demlow of our department for the help they offered during my staying at CSU.

Finally, I would like to thank my parents and my brother for their years of care, encouragement and help.

Contents

List of Figures

List of Tables

Chapter 1

Introduction to J/ψ and $\psi(2S)$ Decay

A century ago in 1897, J.J. Thompson's discovery of electron and Rutherford's famous scattering experiment first touched elementary particles. In 1900 Max Planck opened the door to the quantum world. Since then the experimental research expanded from the atomic level to the nuclear level and then to the quark level. And the quantum theory has grown from Niels Bohr's theory to Schrödinger and Heisenberg's non-relativistic quantum mechanics to Quantum Electrodynamics and to the finally Standard Model and beyond.

The Quark Model proposed by Gell-Mann and Zweig was very successful at the beginning but suffers from two profound embarrassment before November 1974: absence of free quarks experimentally and the inconsistency with the Pauli principle. Ideas of quark confinement and the color hypotheses had been proposed to save the model but were not well accepted. It was the discovery of the $c\bar{c}$ quark bound state.

the J/ψ that proved the quark model and allowed the *partons*, lumps inside the proton, to be identified as quarks. This chapter will give a brief introduction of the basic particle physics including generations of quarks and leptons and the simplest vertices of various interactions. It will also cover the physics of J/ψ, $\psi(2S)$ and χ_c states decays.

1.1. Basic Elementary Particle Physics

Elementary particle physics addresses at the most fundamental level of the question, "What is matter made of?". Fifty years ago, they were the proton, neutron, electron and photon. As the research progressed and more powerful and sophisticated accelerators and particle detectors were built around the world, today we see hundreds of new particles. They are no longer been considered as fundamental. Instead, quarks and leptons which are point-like, spin-$\frac{1}{2}$ fermions, along with their spin-1 mediator bosons are considered to be the fundamental constituents of matters.

There are six flavors of quarks. They are spin-$\frac{1}{2}$ fermions. They carry fractional electrical charges ($\frac{1}{3}$ or $\frac{2}{3}$), weak "charges" and strong force "charges" referred as "red", "green" and "blue" colors. They are classified as three generations.

$$\begin{pmatrix} u \\ d \end{pmatrix} \cdot \begin{pmatrix} c \\ s \end{pmatrix} \cdot \begin{pmatrix} t \\ b \end{pmatrix} \tag{1.1}$$

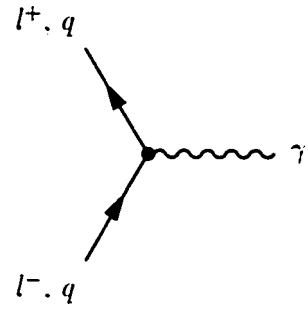

Figure 1.1: The vertex of electro-magnetic interaction

Also corresponding to this three generation of quarks are three generations of leptons.

$$\begin{pmatrix} \epsilon^- \\ \nu_e \end{pmatrix} \cdot \begin{pmatrix} \mu^- \\ \nu_\mu \end{pmatrix} \cdot \begin{pmatrix} \tau^- \\ \nu_\tau \end{pmatrix} \tag{1.2}$$

Among the four kinds of interactions, gravity is considered to be too weak to take into account in particle physics so it is not considered in the Standard Model. The String Theory explains and unifies the gravity and other interactions.

The strong interaction (color interaction), the electro-magnetic interaction and weak interaction are what is considered in particle physics. Fig. 1.1 shows the vertex of the electro-magnetic interaction. The mediator, the photon, is a massless charge-free, spin-1 particle. The strength of the electro-magnetic interaction is characterized by a coupling constant $\alpha = 1/137$.

The fundamental vertex of color interaction is shown in Fig. 1.2. The interaction is done by exchanging gluons which are massless spin-1 particle. There are eight

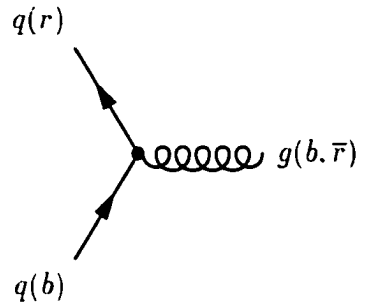

Figure 1.2: The vertex of color interaction

of them and they are bi-colored. Particles that can be observed in experiments are color-free. The fact that gluons carry color charge allow gluons to interact among themselves, which add additional primitive gluon-gluon vertices (Fig. 1.3) and make it possible for the existence of glueballs. The strength of the color interaction is characterized by strong coupling constant α_S which is really not a fixed constant. It is much larger than α and it varies with momentum exchanges. It is difficult to apply the perturbative theory.

The weak interaction vertices involving leptons and quarks can be found in Fig. 1.4 and Fig. 1.5. Weak interaction vertexes involving W, Z and photon only are not listed here.

Color interaction and electro-magnetic interaction do not change the quark flavor, as one can see from these fundamental Feynman diagrams. However quark flavor does change in charged weak interactions. Actually weak interactions not only change quark flavor, but also allow cross-generation vertex or mixing. This is described by

Figure 1.3: Three-gluon vertex and four-gluon vertex of color interaction

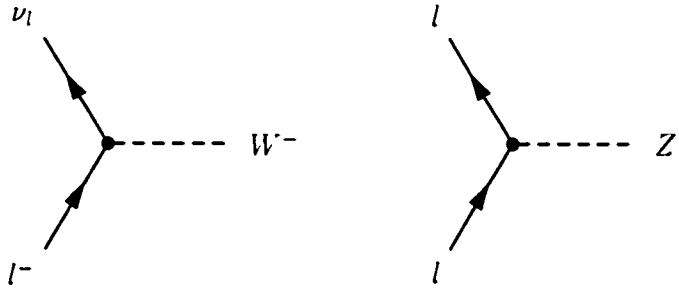

Figure 1.4: Weak interaction vertexes involving leptons

Cabibbo-Kobayashi-Maskawa mixing matrix.

$$\begin{pmatrix} d' \\ s' \\ b' \end{pmatrix} = \begin{pmatrix} V_{ud} & V_{us} & V_{ub} \\ V_{cd} & V_{cs} & V_{cb} \\ V_{td} & V_{ts} & V_{tb} \end{pmatrix} \begin{pmatrix} d \\ s \\ b \end{pmatrix} \tag{1.3}$$

For example, V_{ud} measures the coupling of u to d. The diagonal elements in the CKM matrix are almost 1 and off-diagonal elements are close to zero — the fact that mixing

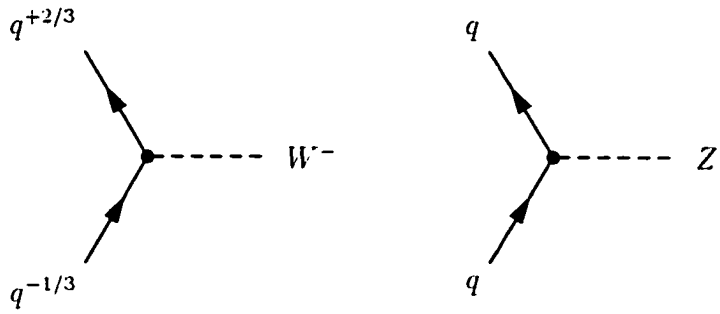

Figure 1.5: Weak interaction vertexes involving quarks

only happens in weak interaction.

1.2. J/ψ and $\psi(2S)$ Decay

The existence of the charm quark was predicted by Glashow, Iliopoulos and Maiani [1]. One of charm quark-antiquark bound states, the J/ψ, was first discovered in 1974 [2] [3]. The bound states of charmed quark and charmed antiquark, often referred as charmonium states, has a spectrum similar to positronium, as shown in Fig. 1.6. Since its discovery, the decay of J/ψ has received considerable attention while other states such as triplet χ_c states and singlet η_c and η_c' have not been studied extensively. This is partly because they don't have the same quantum number as photon ($J^{PC} = 1^{--}$) and thus could not be produced directly in e^+e^- collisions. The only other state below charm open threshold that can be produced directly in e^+e^- collision experiment is the $\psi(2S)$, which has several decay modes that are not available to the J/ψ because of its higher mass. But the mechanism of J/ψ and $\psi(2S)$ decays is expected to be

the same.

J/ψ has $J^{PC} = 1^{--}$ and thus is forbidden from decaying into two gluons by C-parity conservation [4]. The lowest order of the J/ψ decay in QCD is into three gluons, as in Fig. 1.7(b). The decay width is

$$\Gamma(J/\psi \to ggg) = \frac{40}{81}(\pi^2 - 9)\alpha_S^3 \frac{|\Psi(0)|^2}{m_c^2}(1 + 4.9\alpha_S/\pi) \tag{1.4}$$

where α_S is the strong coupling constant. $m_c \simeq M_{J/\psi}/2$ is the mass of charm quark. The annihilation probability represented by $|\Psi_{n0}(0)|^2$, the wave function at origin squared, must be determined by experiment. It can be calculated from the decay width of J/ψ into leptons through the following formula (Fig. 1.7(a)).

$$\Gamma(J/\psi \to l^+l^-) = 16\pi\alpha^2\epsilon_c^2 \frac{|\Psi(0)|^2}{M_{J/\psi}}(1 - \frac{16}{3}\alpha_S/\pi) \tag{1.5}$$

where $\alpha = 1/137$ is the QED coupling constant and $\epsilon_c = 2/3$ is the charge of charm quark in unit of electron charge. The lepton mass effect is neglected in Eq. (1.5). This relation can also be used to measure α_S, which turns out to be

$$\alpha_S = 0.160 \pm 0.007 \tag{1.6}$$

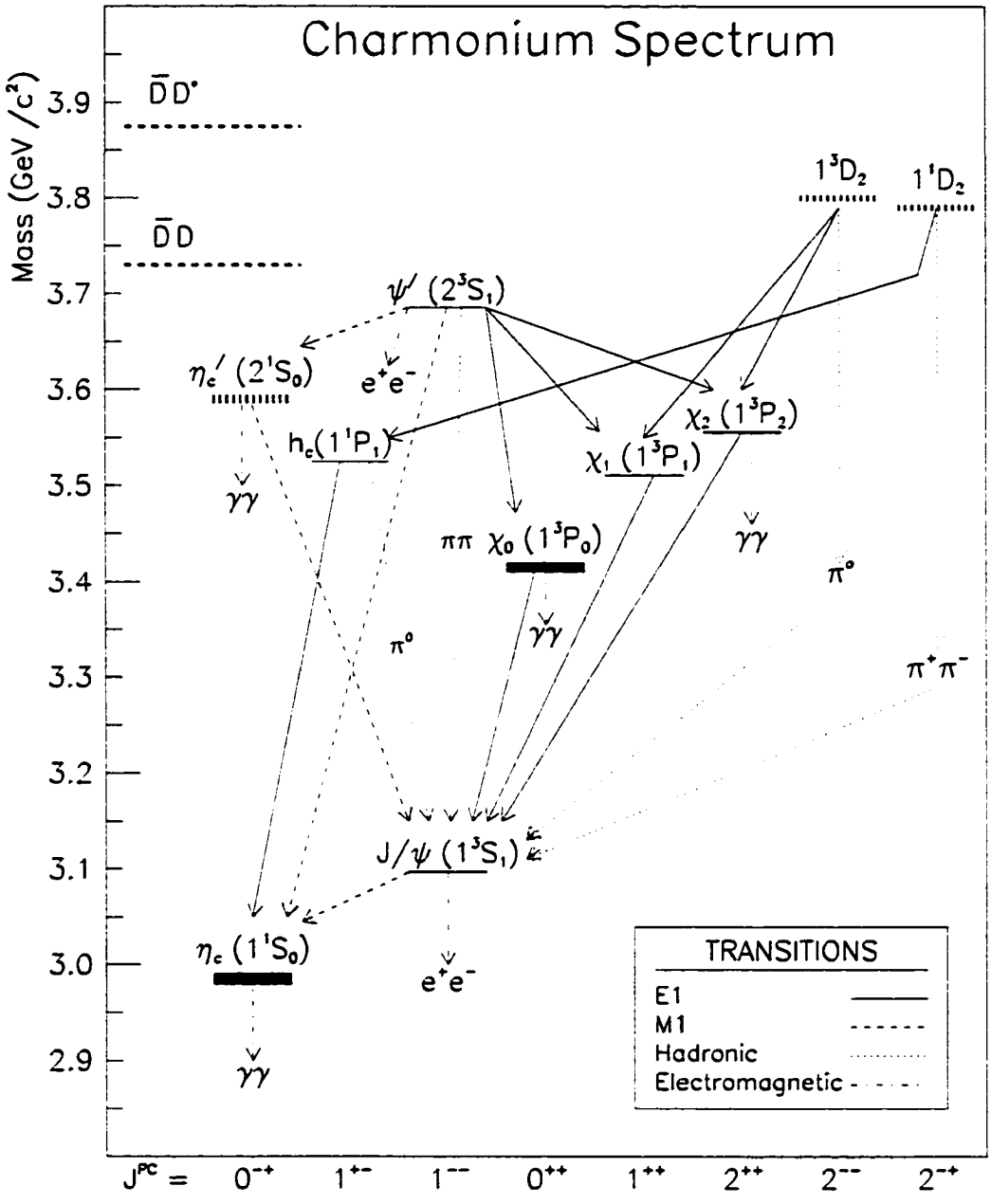

Figure 1.6: The Charmonium bound states. The open charm threshold is the line marked as $D\overline{D}$. The predicted state 1^1P_1 has not been discovered yet. Different notations have been used in this picture and the rest of the text: $\psi'(2^3S_1)$ stands for $\psi(2S)$, or ψ', the $\chi_{c0,1,2}$ states are represented by $\chi_J(1^3P_J)$, $J = 0, 1, 2$.

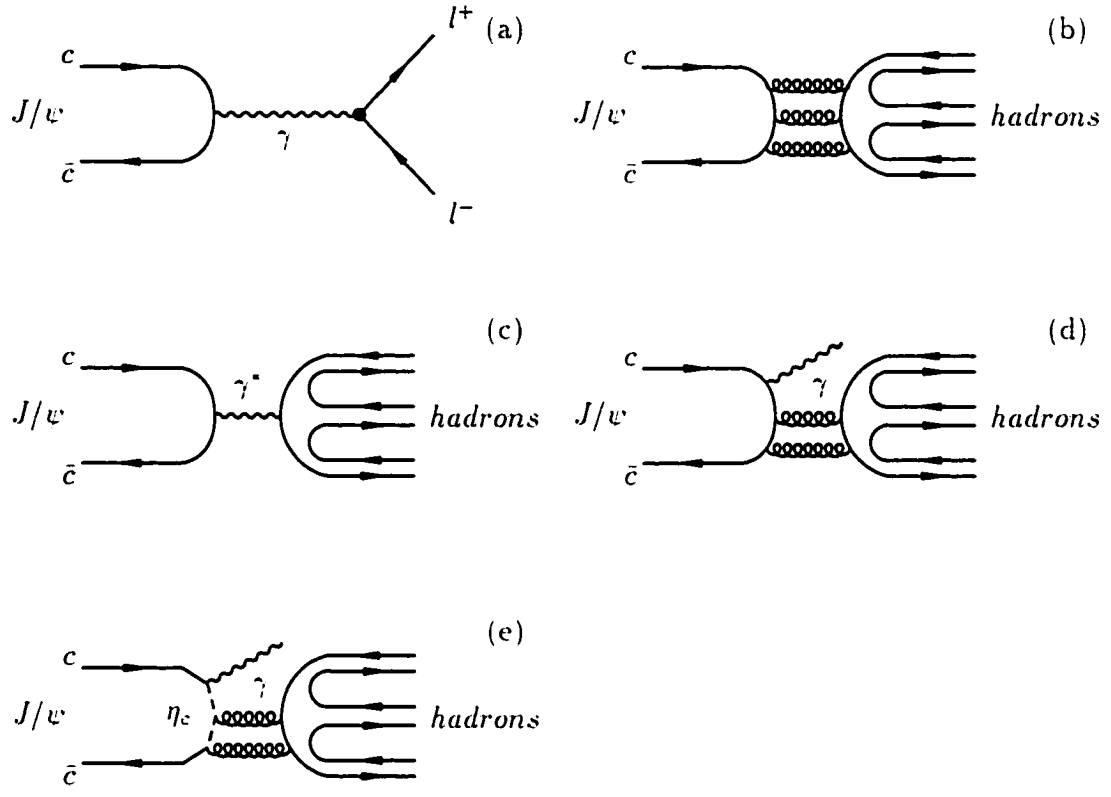

Figure 1.7: Lowest order Feynman diagrams of J/ψ decay (a) decay into di-lepton (b) decay into three gluon (c) decay into virtual photon (d) radiative decay (e) decay via η_c.

It follows that

$$\Gamma(J/\psi \to ggg) = \frac{5}{18\pi}(\pi^2 - 9)\frac{\alpha_S^3}{\alpha^2}\Gamma(J/\psi \to l^+l^-)(1 + 10.3\alpha_S/\pi) \simeq 48KeV \quad (1.7)$$

Other J/ψ partial decay width includes the J/ψ electro-magnetic decay width (Fig. 1.7(c)).

$$\Gamma(J/\psi \to q\bar{q}) = 3\Sigma\epsilon_q^2\Gamma(J/\psi \to l^+l^-) = (10.2 \pm 0.6)KeV \quad (1.8)$$

the radiative decay width (Fig. 1.7(d)).

$$\Gamma(J/\psi \to \gamma gg) = \frac{32}{9}(\pi^2 - 9)\alpha_S^2\alpha\epsilon_c^2\frac{|\Psi(0)|^2}{m_c^2}(1 - 0.9\alpha_S/\pi) \simeq 5\ KeV \quad (1.9)$$

and the decay via η_c (Fig. 1.7(e)) which is measured by Crystal Ball experiment [5] as,

$$\Gamma(J/\psi \to \gamma\eta_c) = (940 \pm 285)eV \quad (1.10)$$

The partial widths in Eq. (1.8) and Eq. (1.7) are comparable, hence the width J/ψ decay into three gluons are not large at all. It is just in the same order with its electro-magnetic transition. This is due to the consequence of the OZI rule which states that decays with the initial quark line discontinuous in the final quark line are suppressed. In the J/ψ case, the initial quark lines, the c and $\bar{c}$ don't appear in

L	J^{PC}
0	$0^{++}, 2^{++}$
1	$0^{-+}, 1^{-+}, 2^{-+}$
2	$0^{++}, 2^{++}, 4^{++}$
3	$2^{-+}, 3^{-+}, 4^{-+}$

Table 1.1: Possible spin-parity combination for glueball states

the final states (they annihilated) because the mass of J/ψ is lower than the open threshold in the charmonium spectrum. the D and $\overline{D}$ mesons in Fig. 1.6.

1.2.1. The Search of Glueballs

In the previous section. we mentioned that gluons carry color charges and thus interact with other gluons and can form bound states out of themselves. They are called glueballs. Since the glueballs contain no quarks. they are flavor singlets. Gluons are spin-1 vectors . Two gluons in a bound state with orbital angular momentum $L = 0$ (S wave) must be symmetric and will have $J^{PC} = 0^{++}$ or 2^{++}. With $L = 1$. they must be also asymmetric spin state ($S = 1$) and thus $J^{PC} = 0^{-+}, 1^{-+}, 2^{-+}$. Table 1.1 listed the combinations.

Some modes in the table are also possible to form from $q\bar{q}$ meson states. The same J^{PC} glueball state and $q\bar{q}$ meson state can be mixed. makes the identification of glueballs rather complicated. Possible hybrid states with $g + q\bar{q}$ could also add more complexity to the search of glueballs.

Lattice QCD predicted that the lowest mass glueballs are scalar glueballs ($J^{PC} =$

0^{++}). The mass is expected to be in the $1 \sim 2$ GeV region. The width was not predicted by Lattice QCD but a rough estimation was made to be

$$\Gamma_G = \sqrt{\Gamma_{OZIsuppressed} \times \Gamma_{OZIallowed}} \sim 10 \sim 100\ MeV$$

The width of ρ and ϕ may give a good estimation of OZI allowed $q\bar{q}$ decay and suppressed $q\bar{q}$ decay.

The radiative decay of J/ψ are good hunting grounds for glueball. The ratio of decay width of J/ψ radiative decay and three-gluon decay is

$$\frac{\Gamma(J/\psi \to \gamma gg)}{\Gamma(J/\psi \to ggg)} = \frac{16}{5}(\alpha/\alpha_S)(1 - 5.8\alpha_S/\pi) \simeq 10.3\% \qquad (1.11)$$

We can further classify J/ψ radiative decay into four modes, as are shown in Fig. 1.8. The order of magnitude in terms of α and α_S for these four modes are

$$\begin{aligned}
\Gamma(J/\psi \to \gamma G) &\sim O(\alpha\alpha_S^2) \\
\Gamma(J/\psi \to \gamma H) &\sim O(\alpha\alpha_S^3) \\
\Gamma(J/\psi \to \gamma M) &\sim O(\alpha\alpha_S^4) \\
\Gamma(J/\psi \to \gamma F) &\sim O(\alpha\alpha_S^4)
\end{aligned}$$

The decay into glueballs dominates the J/ψ radiative decay. Other channels that

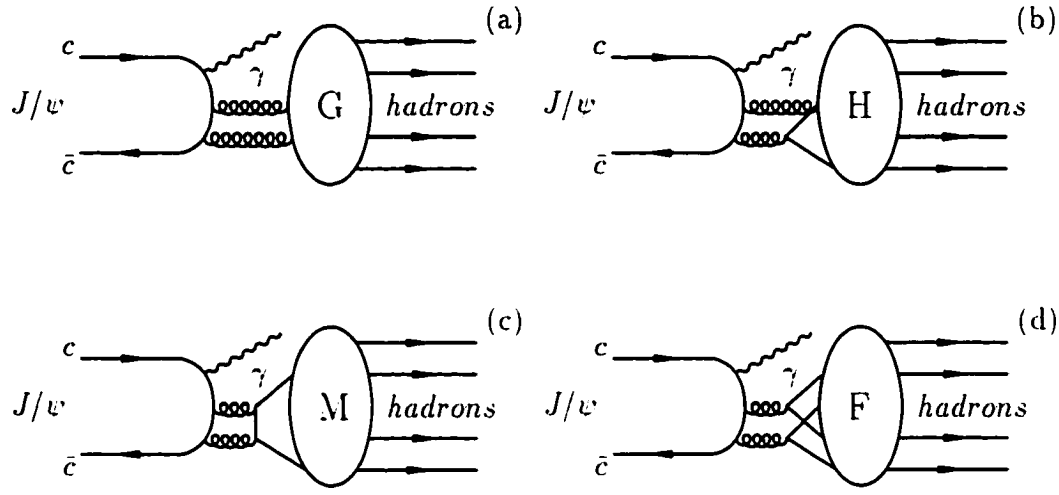

Figure 1.8: Feynman diagrams of J/ψ radiative decay into (a) glueball (b) hybrid states (c) quark molecule (d) Four-quark states

may produce glueballs include OZI violating decay channels and Pomeron exchange channels in central production.

Evidence of these light glueballs have existed for many years. The lightest possible one, the $f_0(1500)$ has been seen by several pp or $p\bar{p}$ central production experiments in $\pi\pi$ and $K\overline{K}$ final states. It was also seen in radiative J/ψ decay channels in e^+e^- experiment by DM2 and Mark III, but not Crystal Ball. Evident of another glueball candidate, the $f_J(1700)$, formerly called $\theta(1720)$, has been seen in both central production and J/ψ radiative decay. However it is difficult to analyze the signal due to the overlapping tensor and scalar signals and also due to the backgrounds such as $J/\psi \to K^*\overline{K}$. (This actually gives an advantage of studying $\psi(2S)$ radiative decay

because $\psi(2S) \to K^*\overline{K}$ is severely suppressed). The Mark III and BES collaboration also reported the evidence of another glueball candidate $\xi(2.2)$ in $\pi\pi$, K^+K^- and $K_S^0K_S^0$ final states.

1.2.2. The Relation of J/ψ and $\psi(2S)$ Decay

The $\psi(2S)$ differs from the J/ψ only by the radial wave function. So the underlying mechanism of J/ψ and $\psi(2S)$ decays via $c\bar{c}$ annihilation are expected to be the same. We expect that the above formula for J/ψ decays remain unchanged for the $\psi(2S)$ decay. One of the interesting aspects is to look at the J/ψ and $\psi(2S)$ three-gluon decay branching fractions.

$$\begin{aligned} B(J/\psi \to ggg) &\sim \frac{\alpha_S^3}{M_{J/\psi}^2}\frac{|\Psi(0)|^2}{\Gamma_{full}(J/\psi)} \\ &\sim \frac{\alpha_S^3}{M_{J/\psi}^2}\frac{\Gamma(J/\psi \to l^+l^-)M_{J/\psi}^2}{\Gamma_{full}(J/\psi)} \\ &\sim \alpha_S^3 B(J/\psi \to e^+e^-) \end{aligned} \tag{1.12}$$

The derivation is identical for the $\psi(2S)$. If we assume that α_S doesn't change significantly from J/ψ mass to $\psi(2S)$ mass, and also the process of hadronization of the gluons are the same for both, we expect that,

$$\frac{B(\psi(2S) \to X)}{B(J/\psi \to X)} = \frac{B(\psi(2S) \to ggg)}{B(J/\psi \to ggg)} \simeq \frac{B(\psi(2S) \to l^+l^-)}{B(J/\psi \to l^+l^-)} = (14.6 \pm 2.2)\% \tag{1.13}$$

where X is a non-charmonium state. The relation is sometimes called the "15% rule". Note that this prediction is made for the total decay width of three-gluon decay, not for the partial decay widths of individual modes. Since each exclusive decay proceeds through a three-gluon annihilation, the partial decay widths are expected to be functions of the wave function of the charmonium states at the origin. So we expect that the rule is generally valid for any processes involving the annihilation of the initial quarks. However, we do not expect the agreement between the prediction and experiment results to be perfect due to many factors that are not considered here.

The radiative decay of J/ψ and $\psi(2S)$ are similar to their three-gluons decays expect that one of the gluon lines is replaced by a radiative photon (Fig. 1.7(b) and Fig. 1.7(d)). The partial decay width of a quarkonium state to a photon plus two gluons is then similar to Eq. (1.4) with one power of the coefficient α_S be replaced by a α and a modification of the SU(3) color factor. Moreover, the "15% rule" relation should hold in the J/ψ and $\psi(2S)$ radiative decay.

The Mark II experiment did a systematic study by using their $\sim 1 \times 10^6$ $\psi(2S)$ data. They found that most of $\psi(2S)$ decay channels are consistent with the "15% rule". However, puzzling things exist in the $\psi(2S) \to \rho\pi$ and $K^*\overline{K}$ modes which are severely suppressed from the "15% rule" [6]. Recently, the BES experiment has collected about 3.7×10^6 $\psi(2S)$ data and performed a more detailed study. The

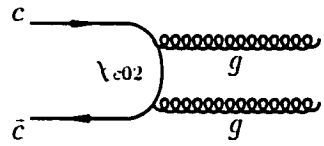

Figure 1.9: χ_{c0} and χ_{c2} decay into two gluons

result from BES experiment not only confirmed the suppression in the $\psi(2S)$ decay into vector-pseudo-scalar modes such as $\psi(2S) \to \rho\pi$ and $K^*\overline{K}$, but also in vector-tensor modes such as ρa_2, $\omega f_2(1270)$ and $\phi f_2'(1525)$ [7] as well as $K_1^{\pm}(1270)K^{\mp}$ mode (axial-vector plus pseudo-scalar) [8].

1.2.3. The χ_c Decay

Unlike J/ψ, χ_{c0} and χ_{c2} have even C-parity and thus can decay into two gluons. The lowest diagrams is shown in Fig. 1.9 and the two-gluon decay width are

$$\Gamma(\chi_{c0} \to gg) = 96\alpha_S^2 \frac{|\Psi'(0)|^2}{M^4} \tag{1.14}$$

$$\Gamma(\chi_{c0} \to gg) = \frac{128}{5}\alpha_S^2 \frac{|\Psi'(0)|^2}{M^4} \tag{1.15}$$

The decay width formula involve the derivative of the wave functions at the origin because the P state wave functions themselves vanish at the origin. Since wave functions must be supplied from phenomenology, a more interesting thing would be

to consider the ratio of these two width.

$$\begin{aligned} \frac{\Gamma(\chi_{c0} \to gg)}{\Gamma(\chi_{c2} \to gg)} &= \frac{15}{4} \quad or \\ &= \frac{15}{4}(1 + 12\alpha_S/\pi) \end{aligned} \tag{1.16}$$

The second formula involving the high order diagram contributions.

According to Fermi's "Golden Rule", the partial decay width of the χ_c two-body decay into two pseudo-scalar mesons can be expressed as

$$d\Gamma \sim |\mathcal{M}|^2 \delta^4(p_1 - p_2)\left(\frac{cd^3\mathbf{p_1}}{(2\pi)^3 2E_1}\right)\left(\frac{cd^3\mathbf{p_2}}{(2\pi)^3 2E_2}\right) \tag{1.17}$$

$$\sim |\mathcal{M}|^2 \frac{p}{M^2} d\Omega \tag{1.18}$$

where p_1 and p_2 are the four momentums of the two final particles. $\mathbf{p_1}$ and $\mathbf{p_2}$ are their spatial components. $|\mathbf{p_1}| = |\mathbf{p_2}| = p$. M is the mass of χ_c. The last two terms in the parentheses in Eq. (1.17) describe the relativistic phase of the two final particles.

$$\mathcal{M} \sim p^s \tag{1.19}$$

is the matrix element. s is the spin of χ_c.

According to the SU(3) flavor symmetry, the expression of the matrix element $\mathcal{M}$ of the decay of χ_{c0} to $\pi^0\pi^0$ and the decay of χ_{c0} to $\eta\eta$ should be the same. So the

two decay branching fractions are the same, except a factor $p^{(2s+1)}$ due to the Eq. (1.18) and Eq. (1.19). Here, p is the momentum of the π^0 or η in χ_c's rest frame and s is the spin of χ_c's. The momentum of π^0 in χ_{c0}'s rest frame is 1702 MeV and the momentum of η in χ_{c0}'s rest frame is 1617 Mev. Thus the ratio of $B(\chi_{c0} \to \pi^0\pi^0)$ and $B(\chi_{c0} \to \eta\eta)$ is 0.95. The decay of χ_{c2} has similar property. And the corresponding ratio is 0.79.

In the following chapters, we will study the $\psi(2S)$ radiative decay into $\pi\pi$, $K\overline{K}$ and $\eta\eta$. The "15% rule" related to $\psi(2S) \to \gamma f_2(1270)$ and $\psi(2S) \to \gamma f_J(1710)$ branching fractions will be looked at. The χ_{c0} and χ_{c2} decay into $\eta\eta$ and $\pi^0\pi^0$ will also be studied.

Chapter 2

The BES Detector

2.1. The BEPC

The Beijing Electron Positron Collider (BEPC) was designed to study $\tau-c$ physics. It was built in Beijing, China in 1988. It consists of a 202 meter linear accelerator and a 76 × 66 meter storage ring with a circumference of 240 meters (Fig. 2.1). The electrons and positrons are accelerated to 1.1 $\sim$ 1.4 GeV in a linear accelerator and then injected into the storage ring. In the storage ring, the electrons and positrons circulate in opposite directions around the ring and are accelerated by the electromagnetic fields in four Radio-Frequency (RF)cavities called klystrons. When the electron and positron beam reach a certain energy, they interact with each other at the Interaction Point (IP). There are two interaction points on the storage ring. The Beijing Spectrometer (BES) is located at southern IP. The other IP has not been used. Fig. 2.1 is the schematic diagram of the LINAC and the storage ring.

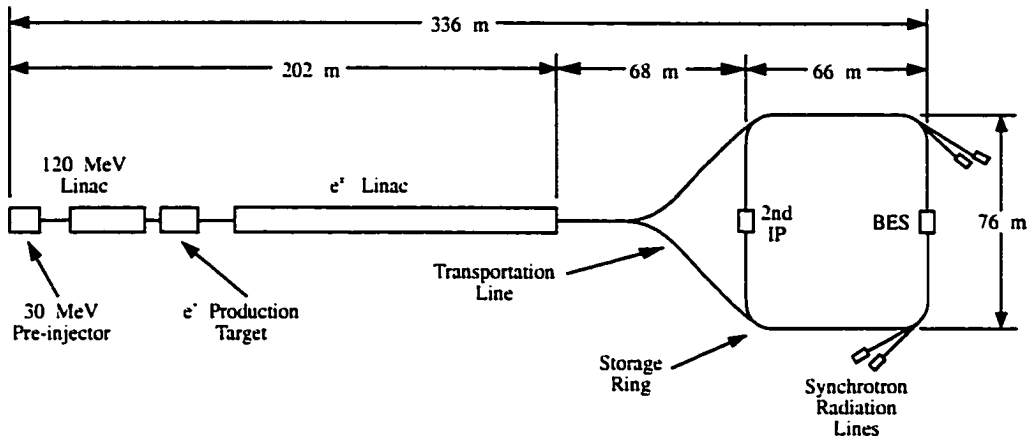

Figure 2.1: Schematic diagram of BEPC accelerator and storage ring

The designed peak luminosity of BEPC is $1.7 \times 10^{31} cm^{-2} s^{-1}$ when the center of mass energy $\sqrt{s} = 5.6 GeV$. The highest luminosity it ever achieved was $6.0 \times 10^{30} cm^{-2} s^{-1}$ when $\sqrt{s} = 3.56 GeV$. BEPC also provides synchrotron radiation for other research.

2.2. The BES Detector

The BES detector consists of several major subsystems for the tracking and particle identification. They are the Central Drift Chamber (CDC), Main Drift Chamber (MDC), Time-of-Flight system (TOF), Shower Counter (SC), and Muon Chamber. Other detector apparatus includes luminosity monitors and magnet systems. Fig. 2.2 and Fig. 2.3 show the schematic diagram of the BES detector.

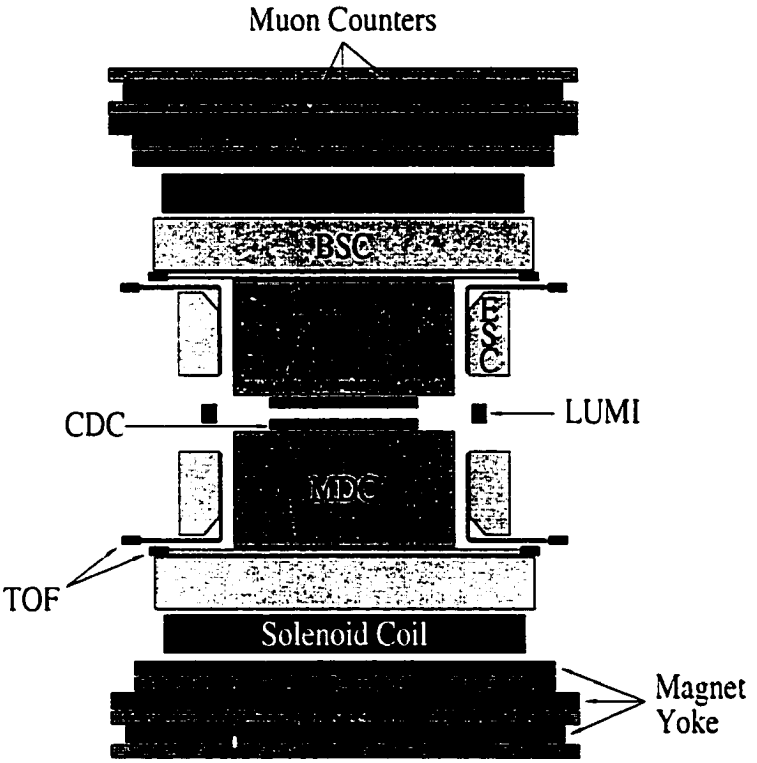

Figure 2.2: Side view of the BES detector

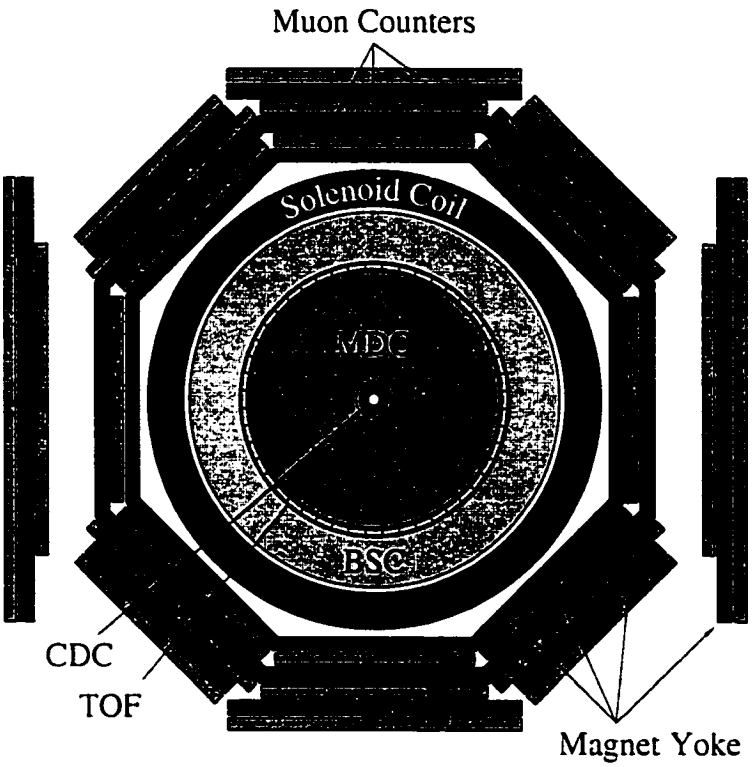

Figure 2.3: Axial view of the BES detector

2.2.1. Beam Pipe

The beam pipe is part of the storage ring. It is made of Aluminum which is light material (low Z) in order to reduce multiple scattering. It is 2 mm thick and has a diameter of 150 mm. The total radiative thickness before Main Drift Chamber. include the beam pipe. the inner and outer wall of Central Drift Chamber and the inner wall of Main Drift Chamber is 6.46×10^{-2} r.l.

2.2.2. Center Drift Chamber(CDC)

The central drift chamber is a cylindrical drift chamber located just outside the beam pipe with an inner diameter of 18.4 cm and an outer diameter of 30.2 cm. Its effect length is 1.1 m covering $4\pi \times 98\%$ solid angle. It has four layers of axial sense wires (48 wires per layer). The resolution is 220 μm in the xy plane and 1 cm along the z direction. It covers a 98% solid angle. The working gas is a mixture of 89% Argon. 10% CO_2. and 1% CH_4 at one atmosphere pressure.

The CDC can be used with the main drift chamber to measure the charged particle's track and its momentum. It can also be used with the Time-of-Flight system for triggering. The BES has used it for triggering only.

After the 95 $\psi(2S)$ data run. the CDC was replaced by A straw vertex chamber constructed at Colorado State University. It has a total of 640 straw cells distributed in 8 axial layers and 4 stereo layers. It provides a superior single wire resolution of

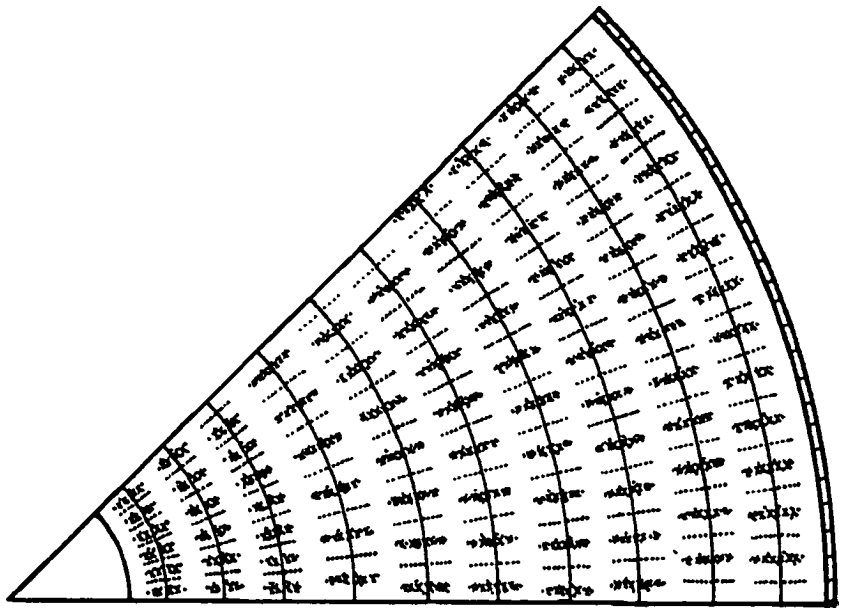

Figure 2.4: Schematic diagram of Main Drift Chamber cell structure

$\sim$ 60 μm.

2.2.3. Main Drift Chamber(MDC)

The Main Drift Chamber is located outside of CDC. It has an inner diameter of 31.0 cm. an outer diameter of 230.0 cm and an effective length of 220.0 cm. Five axial-cell layers and 5 stereo-cell layers are alternated in the MDC and each cell has 4 radial arranged sense wires. The cell number of each layer is different. ranging from 48 to 108. with total of 702 cells. Fig. 2.4 shows the schematic cell structure.

The MDC measures the momentum of charged tracks. The second layer of MDC

covers 95% of 4π. The 4th layer covers 90% of 4π and the 10th layer covers 70% of 4π. The momentum resolution is $\sigma_p/p = 1.7\% \times \sqrt{1 + p^2(GeV/c)}$. The spatial resolution for single wire is $200 \sim 250$ μm for XY plane and $2.3 \sim 5$ cm for Z direction. The θ and ϕ resolution are 3.7 mrad and 8.3 mrad respectively.

The MDC also provides measurements of the energy loss of the particle when it travels through MDC (dE/dx) by measuring the charge output by sense wires. From the Bethe-Bloch formula

$$\frac{dE}{dx} = \frac{4\pi N_0 z^2 e^4 c^2}{m\beta^2} \frac{Z}{A}[ln(\frac{2mc^2\beta^2}{I(1-\beta^2)}) - \beta^2]$$

we know the energy loss for different particle mass, and thus provide particle identification information. Fig. 2.5 show the distribution of dE/dx verses the momentum of charged particles measured by BES. The quantity XS which is defined as

$$XS = \frac{(\frac{dE}{dx})_{meas} - (\frac{dE}{dx})_{exp}}{\sigma_{dE/dx}}$$

is used to describe how good a particle mass hypotheses is. $\sigma_{dE/dx}$ is the dE/dx resolution which is $\sim 9\%$.

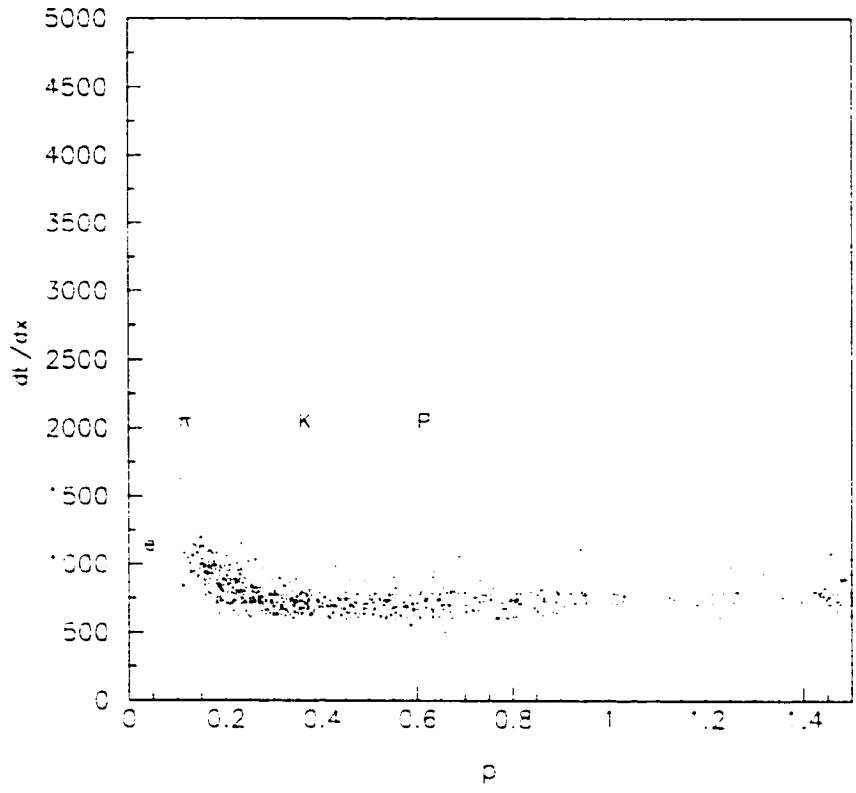

Figure 2.5: The MDC dE/dx distribution

2.2.4. Time of Flight(TOF)

The barrel Time-of-Flight counter is a relatively thin layer surrounding the Main Drift Chamber. It is composed of 48 scintillator along the Z-axis with photo-multiplier tubes on both sides of the scintillators. The mechanism is to excite molecular level of the organic plastic scintillator which then emits UV light. The UV light is converted into visible light by wavelength shifter in the scintillator, which is then collected by photo-multiplier. Each scintillator is 284 cm long, 15 cm wide and 5 cm thick. The time resolution for barrel TOF is $\sim$ 330 ps for Bhabha events and $\sim$ 450 ps for hadron events. There are also endcap Time-of-Flight on both ends. Each is composed of 24 scintillators. The barrel TOF covers 76% of 4π and east and west endcap TOF covers 20% of 4π. The endcap TOF information has not been used for analysis.

The flight time information of charged particles provided by TOF is used along with the particle's momentum and trajectory from Main Drift Chamber to compute the mass of the particle, which in turn identifies the particle. The mass formula

$$m = p\frac{\sqrt{1-\beta^2}}{\beta}; \qquad \beta = \frac{l}{t}$$

where p is the particle's momentum, l is the length of flight trajectory in MDC, t is the measured flight time and β is the velocity in unit of speed of light c. In order to test how good a particle hypotheses is, we define the TOF weight w for each particle

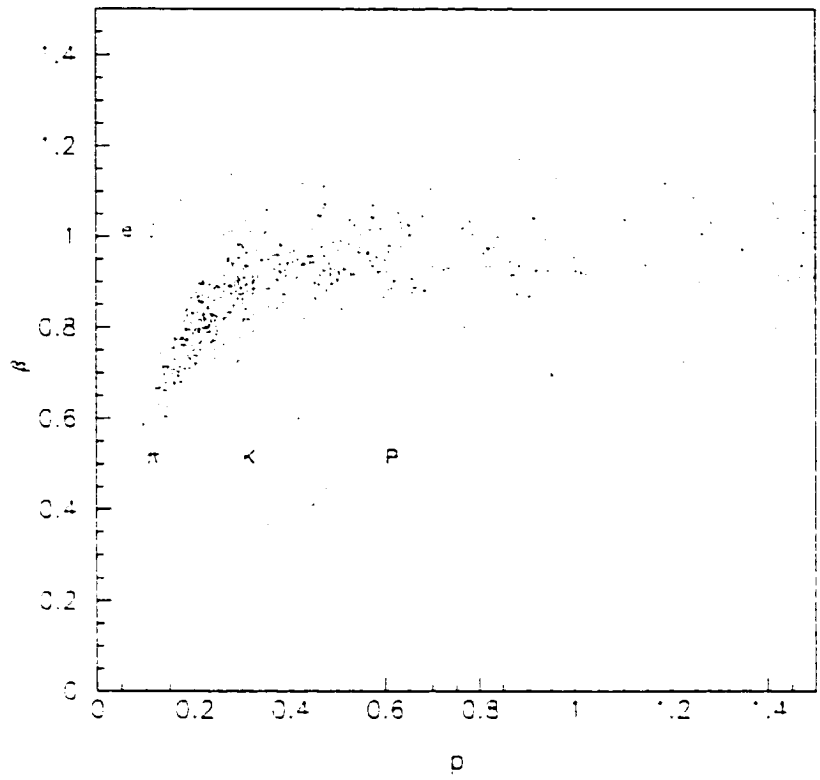

Figure 2.6: The TOF particle velocity distribution

hypotheses:

$$w = \epsilon^{-\frac{1}{2}(t_{meas}-t_{exp})^2/\sigma_t^2}$$

where σ_t is TOF time resolution. Fig. 2.6 shows the scatter plot of β verse particle momentum. The Time-of-Flight information is also used by trigger system to remove the background.

2.2.5. Electro-Magnetic Calorimeter(SC)

The electro-magnetic calorimeter consists of electro-magnetic shower counters of both barrel and endcaps, outside of Time-of-Flight. The barrel shower counter (BSC) is 12 radiation lengths thick separated into 24 layers. Each layers has 540 cells along circumference. Each cell has a 0.5 r.l. Al-Pb-Al plate absorbing energy deposited by electro-magnetic interaction, followed by a SQS gas-counter to measure the energy loss. Barrel shower counter has inner diameter of 247.0 cm, outer diameter of 338.2 cm and length of 385.0 cm, see Fig. 2.7. BSC covers 80% of 4π. Endcap shower counter is outside of endcap Time-of-Flight and has inner diameter of 74.6 cm, outer diameter of 192.0 cm and thickness of 41.0 cm. It consists of an alternative of 23 layers of Al-Pb-Al plates and 24 layers of SQS counters. Information from endcap shower counter has not been calibrated and reconstructed.

The BSC has 6 electronic readout layers corresponding to a 2-2-2-3-3-12 physicals layer scheme. The Z position is read out at both ends via charge division. The gas in use is a 33% Argon and 67% CO_2 mixture bubbled through 0^oC n-pentane. Energy and position resolution are $\sigma_E/E = 22\%/\sqrt{E(GeV)}$ and $\sigma_\phi = 4.5mrad$ and $\sigma_Z = 2cm$.

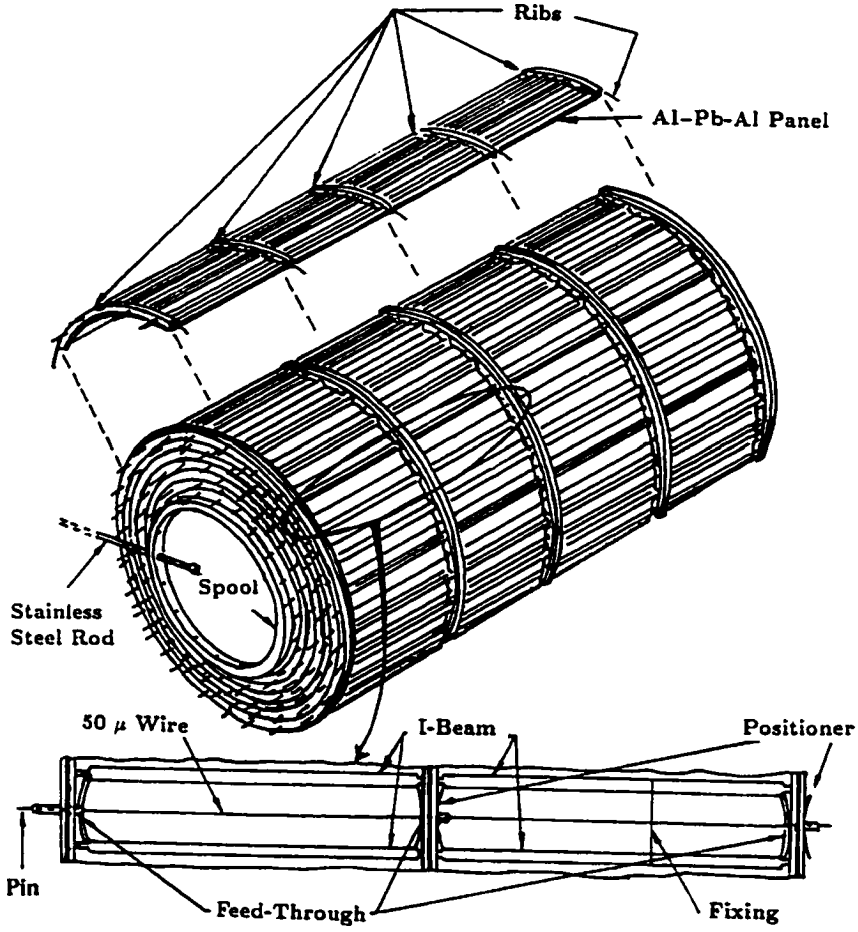

Figure 2.7: Schematic diagram of the barrel shower counter

2.2.6. Magnetic Field

An Aluminum coil of inner diameter 3.48 m. outer diameter 4.14 m and length 3.6 m provides a 0.4 Tesla of magnetic field. The homogeneity of the field within the tracking volume is better than 3%.

2.2.7. Muon Counter

The muon system is the outer most part of the detector. It consists of three double layers of proportional counter sandwiched with iron absorber which also serve as magnetic field flux return. The muon detector covers 68% of 4π solid angle. The position resolution is $\sigma_Z = 5cm$ and $\sigma_{r\phi} = 3cm$. The Z position is read out by charge division method.

2.2.8. Luminosity Monitor

The structure of luminosity monitor is shown in Fig. 2.8. It consists of four combined scintillator (P and C) and shower counter telescope (S) in two pairs. being placed symmetrically about the interaction point. Its purpose is to measure the number of small angle Bhabha events which then tells us the luminosity.

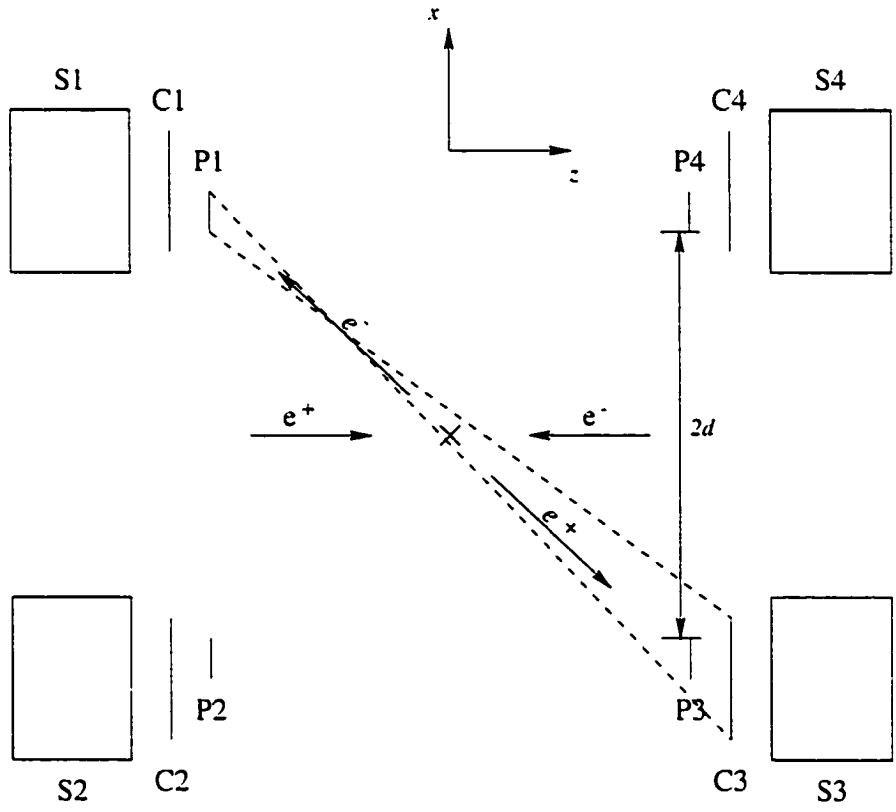

Figure 2.8: Schematic diagram of luminosity monitor

2.2.9. The Trigger and Online Data Acquisition

In the storage ring, the beam crossing rate is 1.25Mhz. Only $0.2 \sim 5$ of them per second are good events. For example, at J/ψ mass region, $\sigma_{J/\psi} \times \mathcal{L} = 2500\ nb \times 2 \times 10^{-3}\ nb^{-1}s^{-1} = 5$ Hz. The cosmic rays also contribute several kilo hertz. In the mean time, it takes 10 msec for the electronic to read out the detector and 20 msec for the online VAX/785 computer to store the result. So a 10% dead-time is introduced even at 3 events/sec rate. The goal of a triggering system is to make a fast and good decision and reject those 99.99% of the background and read out only those few events with high probability of physical interests.

The interval between beam crossing is only 800 nsec. So a multi-level trigger is designed to respond at that time frame. Fig. 2.9 shows the flowchart of this multi-level trigger. Table. 2.1 shows the triggering condition for the $\psi(2S)$ data runs.

2.3. The Off-line Data Analysis System

The main purpose of the offline system is to reconstruct physical quantities such as momentum, energy, position, etc. out of the digitized data taken from the detector, and also provide a simulation frame. The conversion from voltage and wire numbers to these physical quantities is handled by means of various calibration constants such as drift velocity an time zero point, which reflect the detector conditions during the data taken. These constants are adjusted for each runs by using well-known QED processes

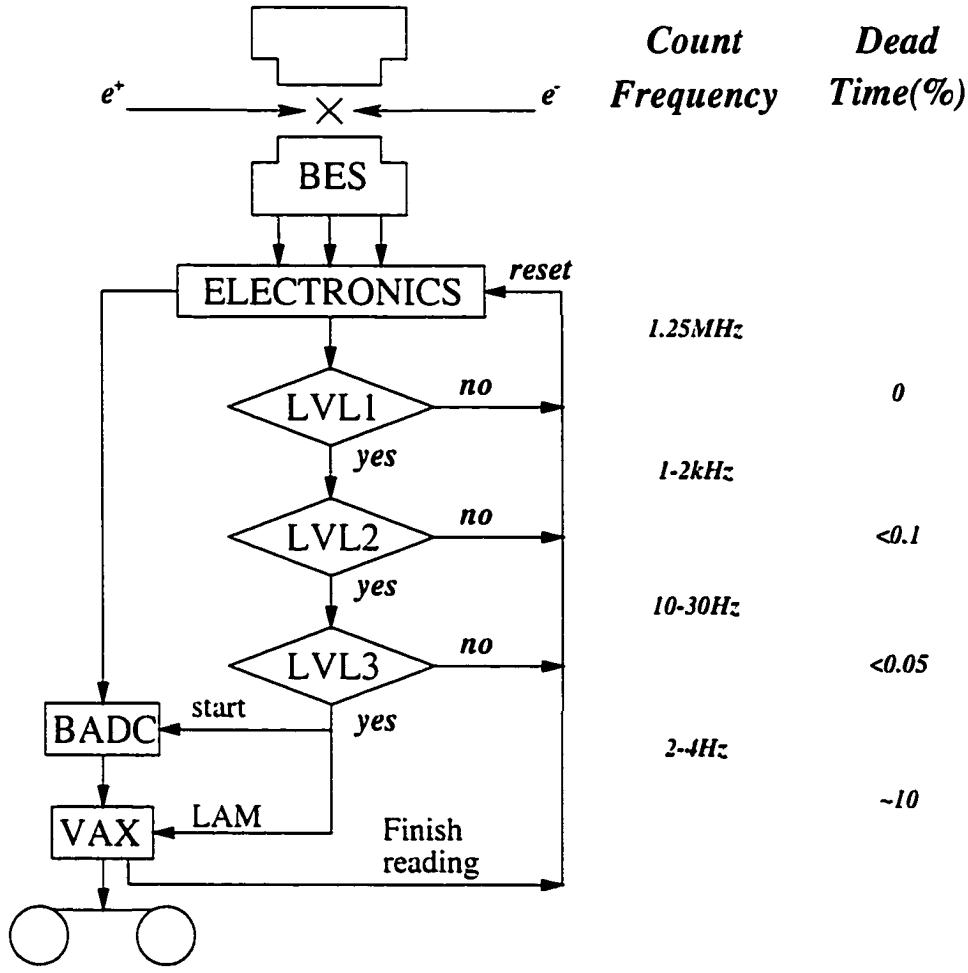

Figure 2.9: The BES multi-level triggering system

Table 2.1: The $\psi(2S)$ data triggering condition

Data set	1993/94				1995			
Channel	CHRG	MUON	Neutral	ESC	CHRG	MUON	Neutral	ESC
Active?	Y	Y	Y	Y	Y	Y	Y	Y
$N_{tof} \geq 1$	Y	Y	-	-	Y	Y	-	-
RADIAL	-	-	Y	-	-	-	Y	-
END B-B	-	-	-	Y	-	-	-	Y
$N_{trk} \geq 1$	Y	Y	-	-	Y	Y	-	-
$N_{trk} \geq 2$	-	-	N	-	-	-	N	-
$N_{trk} \geq 5$	-	-	N	-	-	-	N	-
ESC-Etot>6	-	-	-	Y	-	-	-	Y
MUON-OR	-	Y	-	-	-	Y	-	-
CDC	Y	Y	-	Y	Y	Y	-	Y
BSC-Etot>6	Y	-	-	-	Y	-	-	-
BSC-Etot>40	-	-	Y	-	-	-	Y	-

such as Bhabha-scattering and $e^+e^- \rightarrow \mu^+\mu^-$ because the physical quantities such as momentum, energy and angler distributions of these processes can be precisely calculated from QED. The constants will be used by the reconstruction program to rebuild physical interesting quantities, or detector simulation program to do a reverse process — generating the digital data out of momentum, energy etc. Also, the offline system provides a frame for physical analysis. Fig. 2.10 show the flow chart of the offline system.

The BES offline analysis software was originally ported to VAX/VMS platform in the middle of 1980s from the Mark III software running on IBM VM/CMS. Later,

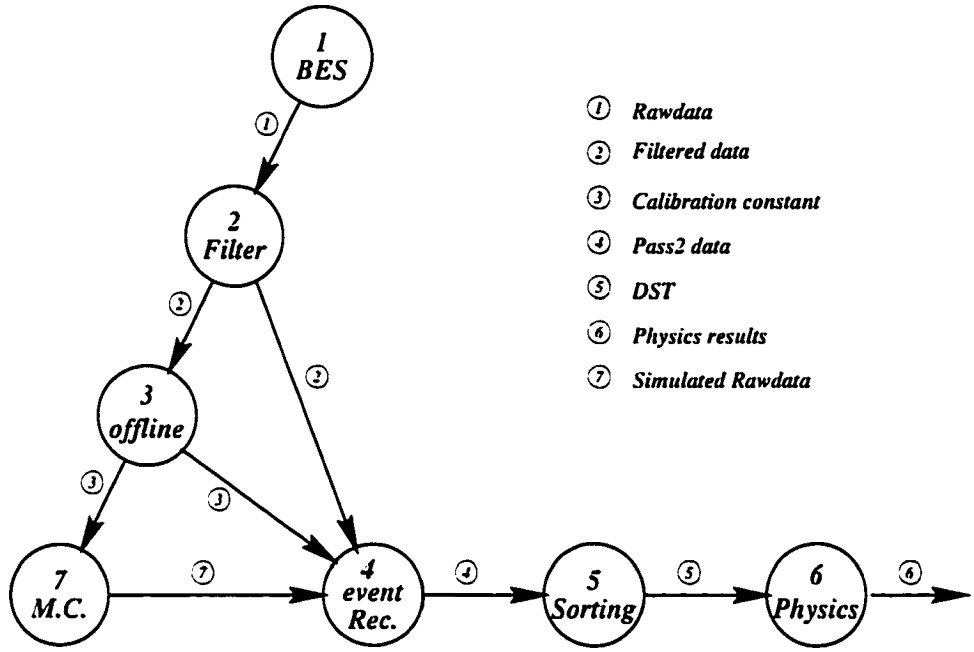

Figure 2.10: The BES offline data analysis system

several flavors of UNIX, such as HP-UX, IBM/AIX, DEC/OSF were also supported. The analyses were done at different sites in P.R.C. and the US. Consistency of the code was implemented by the CODEMAN system developed at BES. A central dispatch server (CODEMAN server) receives the modification request from BES users and dispatches them to all BES sites (CODEMAN clients) for compilation and installation. All is done via electronic mail. Exclusive locks are generated on the server to prevent simultaneous modifications. The BES calibration constant files, documents, utility packages are also distributed by the CODEMAN system. All changes are recorded into the RCS/CVS archive system on server.

The Linux platform for the BES analysis was first started in the summer of 1996 at Colorado State University. It was motivated by a fact in the personal computer market that the PC hardware and the free Linux operating system can provide a workstation level performance at a fraction of the price of UNIX workstations. Software commonly used by the high energy physics community such as C/C++ compiler, FORTRAN compiler, CERN libraries are also available for free. Starting from 5MB of some 1300 source code files and scripts, we overcame the difficulties caused by the widely used VAX/VMS FORTRAN extension and other operating system related issues. To compare the performance, we ran BES reconstruction and simulation jobs on both Linux PCs and HP 735/99 workstations. On average, a Pentium 166 Linux PC has similar speed as a HP 735/99 workstation while a Pentium-II 400 Linux PC is about

3 times faster than them. Today, the Linux version of the BES code and CODEMAN client system are officially supported by the BES collaboration.

Chapter 3

General Event Selection

Since it first collision in 1989. the BEPC/BES has collected many data sets for $e^+e^- \rightarrow J/\psi$. $e^+e^- \rightarrow \psi(2S)$. $e^+e^- \rightarrow \tau\tau$. $e^+e^- \rightarrow D_s\overline{D}_s$ and for R value scan. Table. 3.1 listed those data sets up to the summer of 1995. The total number of data collected for $\psi(2S)$ at center of mass energy $\sqrt{s} = 3.686$ GeV is $3.67 \pm 0.01 \pm 0.30 \times 10^6$ events[1] [9] for the two $\psi(2S)$ data samples. These are the data we used in this study.

3.1. Selection of Good Photons

Two $\psi(2S)$ decay channels we will discuss later. $\psi(2S) \rightarrow \gamma\pi^0\pi^0$ and $\psi(2S) \rightarrow \gamma\eta\eta$ have pure five photon final state. The selection of good photons is critical for these channels. A shower in the BES TRKLST can be a fake photon. So the selection of good photons starts with rejecting false photons. Noise in shower counter usually

[1]This number corresponds to good quality runs. Other analysis may use addition fair quality runs as well. which yield to $(3.79 \pm 0.01 \pm 0.31) \times 10^6$ $\psi(2S)$ events.

Table 3.1: Various Data Sets Collected by BES up to the Summer of 1995

Period	Purpose	Number of Events
Sep. 89 - Jan. 90	Testing and Calibration	3×10^5
Jan. 90 - Jun. 90	First J/ψ Run	2.5×10^6
Nov. 90 - Jan. 91	Second J/ψ Run	2.85×10^6
Apr. 91 - May. 91	Third J/ψ Run	2.65×10^6
Nov. 91 - Jan. 92	τ Mass Run	$5pb^{-1}$
Jan. 92 - Jun. 92	First D_s Run	$3.2pb^{-1}$
May. 92	Fourth J/ψ Run	1.0×10^6
Dec. 92 - May. 93	Second Ds Run	$7.1pb^{-1}$
Dec. 93 - Jan. 94	First $\psi(2S)$ Run	1.3×10^6
Jan. 94 - May. 94	Third Ds Run	$15pb^{-1}$
Jan. 95 - Mar. 95	Second $\psi(2S)$ Run	2.4×10^6

shows up with a relatively small amount of energy and leaves only a few isolated layers and cells fired. A few simple cuts were applied to remove them. We require that a good shower should have:

- Deposit more than 10 MeV of energy in barrel shower counter.
- Hit at BSC for more than 2 layers and more than 3 cells.

In addition, the barrel shower counter rib region, which is the aluminum support bar region, should be avoided because that is the region shower counter can not provide accurate measurements. The rib regions are in the region $|z| < 4cm$ and $1.25m < |z| < 1.3m$.

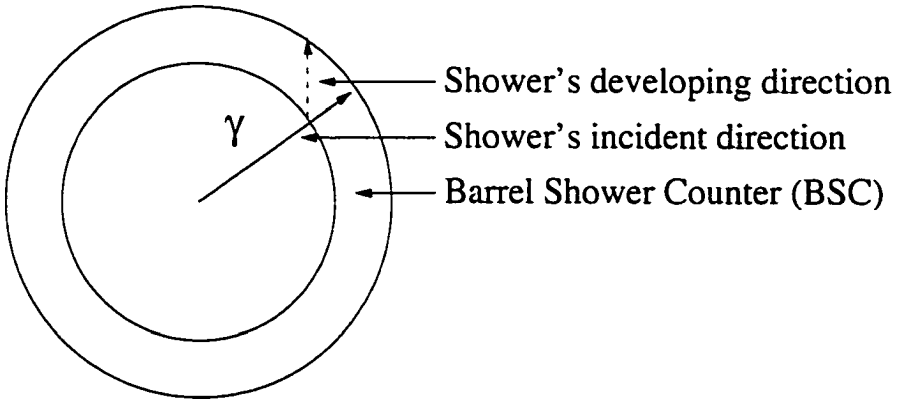

Figure 3.1: Angle between shower's incident direction and the shower's developing direction

A charged track may leave shower in shower counter while itself is not detected by the Main Drift Chamber. In this case, the angle between shower's incident direction, which is the direction from interaction point to the shower's starting point, and shower's developing direction (see Fig. 3.1) may be large. This may also happen to split showers described below. So we imposed a very loose requirement:

- Angle between shower's incident direction and the shower's developing direction should be smaller than 60°.

A real photon may have several showers corresponding to it (split showers), each carries part of the photon's energy. This may either because of dead channels in shower counter that can not be read out, or because the photon interacts with material before it reaches the shower counter and create high energy electron-positron pair which then fly to different directions, or because the reconstruction program is not perfect to make a correction decision. These split showers' energy should be combined

together. This raises a problem of how close two showers can be without being identified as split showers. We will look at this question below.

A high energy π^0 may decay into two photons with very small opening angle. The smallest opening angle happens when the two photons decaying direction are perpendicular to the π^0 moving direction. which is given by

$$2tan^{-1}(\frac{m_{\pi^0}}{p_{\pi^0}})$$

In case the momentum of a π^0 is much larger than the mass of the π^0. for example. closing to the beam energy of the $\psi(2S)$ data. which is the maximum it can have. the opening angle reaches its minimum value of 8.4^o. That has no problem to separate by the BES barrel shower counter. Showers within 8^o of opening angle are unlikely to be independent and should be combined. So we adapted the following method:

- If shower i and shower j are within 8^o of opening angle and $E_j < E_i$. then combine the energy and error matrix of shower j into shower i and then remove shower j from the event TRKLST.

Fig. 3.2 shows the minimum opening angle of any two showers[2]. A clear dip at $\sim 8^o$ appears in the plots. This requirement may reject most split showers within 8^o but may leave split showers with an opening angle larger than 8^o untouched. More

[2]This figure is obtain after a simple pre-selected set of events. which asks that there are at least 5 photons hit at barrel shower counter and a $\psi(2S) \rightarrow \gamma\gamma\gamma\gamma\gamma$ 4-constraint fit with fitting χ^2 smaller than 50.

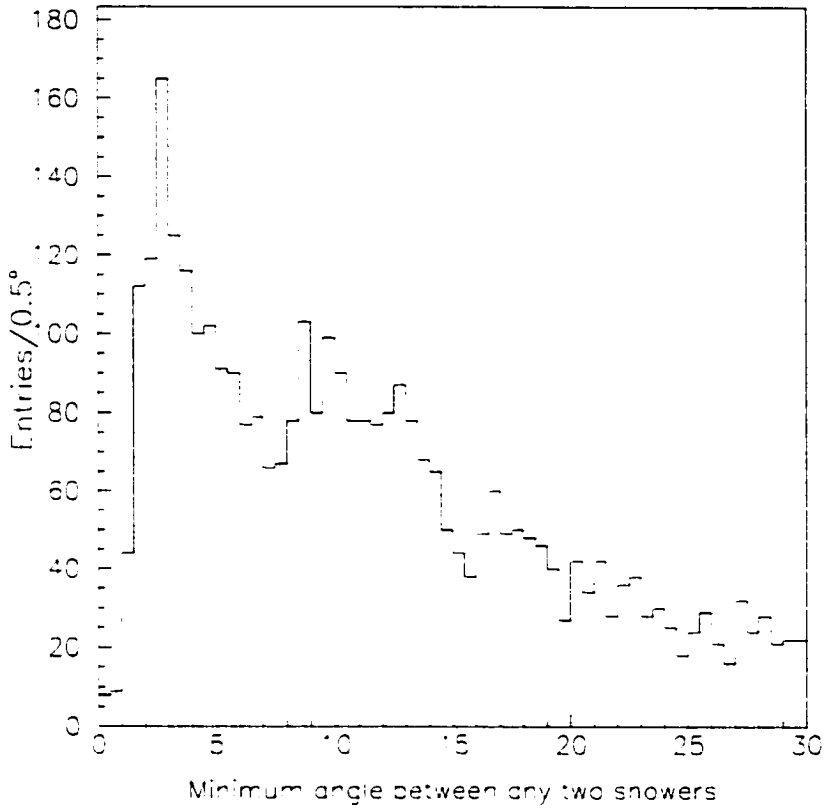

Figure 3.2: Minimum opening angle of any two showers

investigation may be needed because distinguishing two merged photons from split showers is especially important to the identification and reconstruction of π^0.

Another method is to look at the helicity angle of π^0 decay. This angle is defined in π^0's rest frame as the angle between photon and the π^0's moving direction. Fig. 3.3 shows the definition of this angle. Fig. 3.4 shows the distribution from data before applying kinematic fit and after kinematic fit. Since π^0 is spin-0 particle. this distribution should be flat. The accumulation of events at $|cos(\theta_{helicity})| \sim 1$ in Fig.

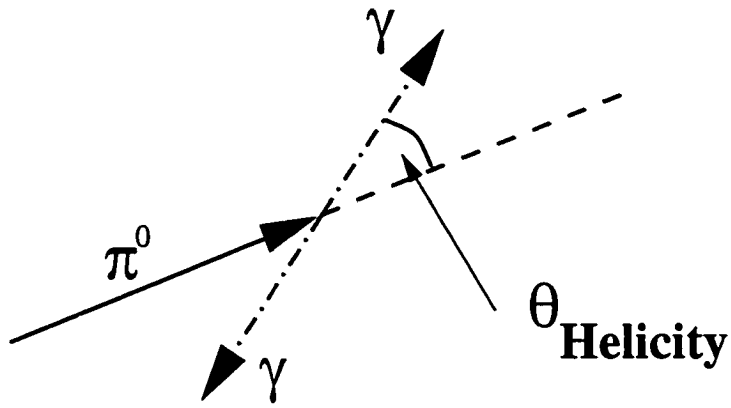

Figure 3.3: Helicity Angle of $\pi^0 \rightarrow \gamma\gamma$

3.4 indicates fake photons being picked up as photons decay from π^0. In order to remove them, we imposed a cut:

- $|cos(\theta_{helicity})| < .99$

3.2. Selection of Charged Tracks

We selection charged tracks with $|cos(\theta)| < 0.85$, $R_{xy} < 2cm$ and $|Z| < 15cm$, where θ is the polar angle of the track (angle between track and the Z axis). R_{xy} is the closest approach to the interaction point (the primary vertex) in X-Y plane. Fig. 3.5 shows the distribution of R_{xy} and z. The exception are those tracks from K^0_S decay which will be discussed in Section 5.2. A charged track should also have at least 60 MeV of transverse momentum so that they do not loop inside the Main Drift chamber.

If the final state has only two charged tracks involved, the difference of the z-

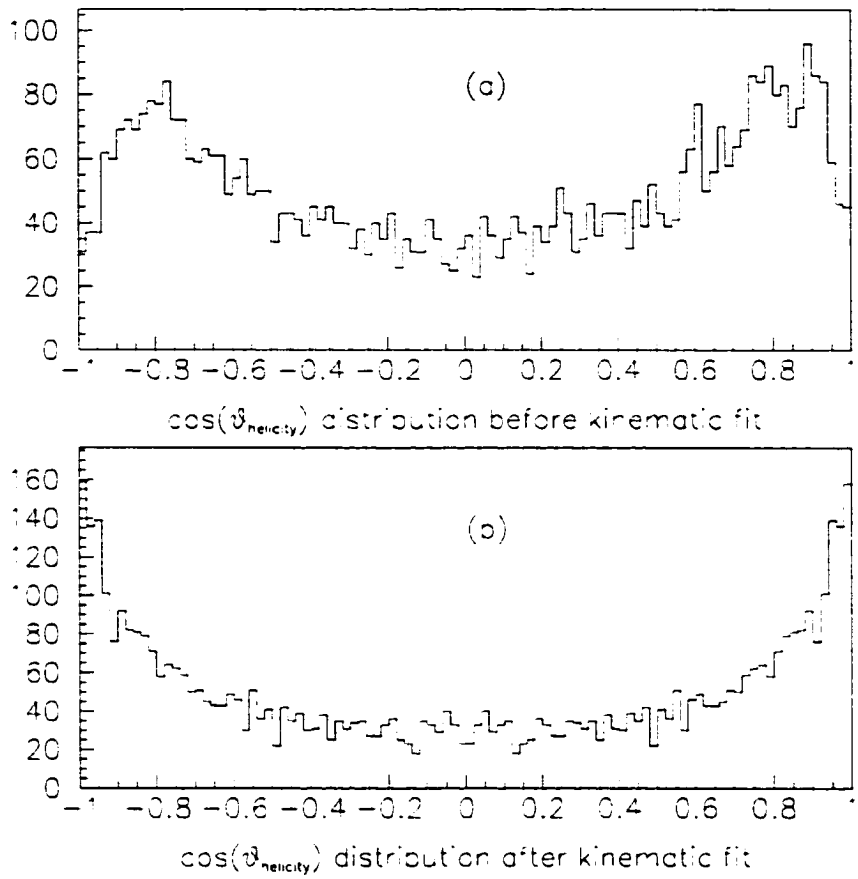

Figure 3.4: $\pi^0 \rightarrow \gamma\gamma$ helicity angle distribution before kinematic fit(a) and after kinematic fit(b).

position of these two tracks, $|z_1 - z_2|$ should be smaller than 5 cm. We will try to reconstruct a vertex out of these two tracks. The z-position of this vertex, Z_V, should be within 15 cm from origin. This will help to remove more beam-gas.

The main background of two charged final states are Bhabha events $e^+e^- \rightarrow e^+e^-$ and radiative dimuon events $e^+e^- \rightarrow (\gamma)\mu^+\mu^-$. Just like the photon, electrons and positrons deposit almost all their energy in Electro-magnetic shower calorimeter. This

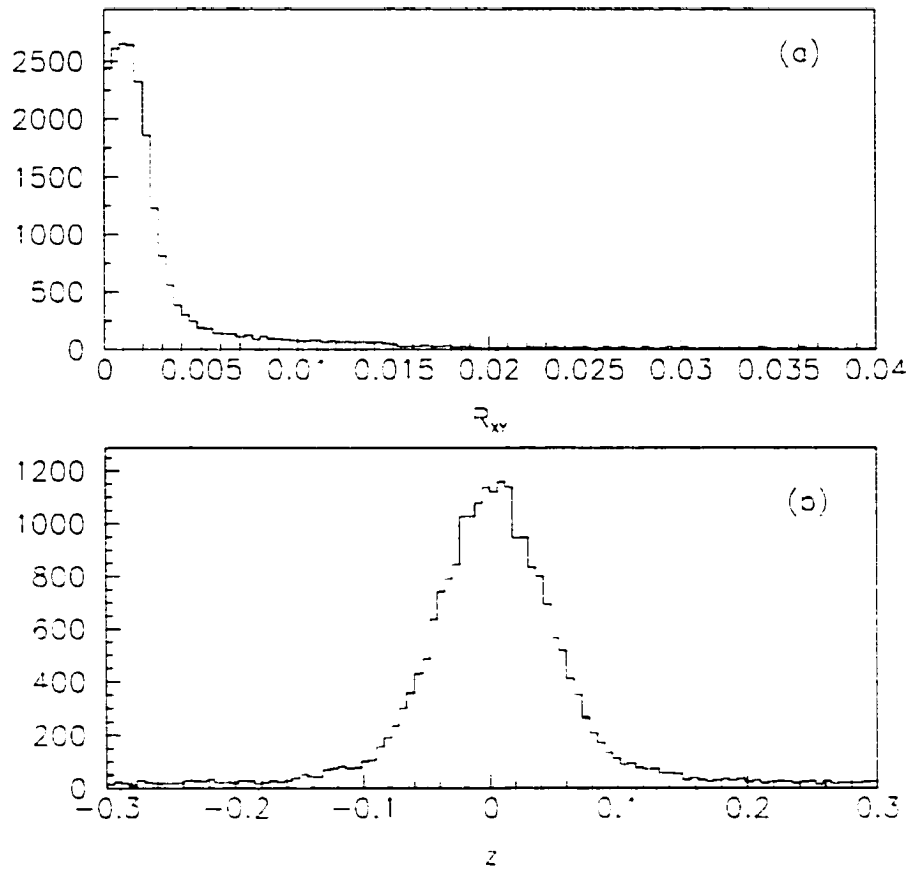

Figure 3.5: (a) R_{xy} distribution (b) z distribution

character can help us to remove Bhabha background. In Fig. 3.6, the electron and positron are clearly shown up at the up side of the plot above line $E = 0.75p$. So we impose a cut $E/p < 0.75$ for all charged tracks with momentum larger than 700 MeV to exclude electron and positron.

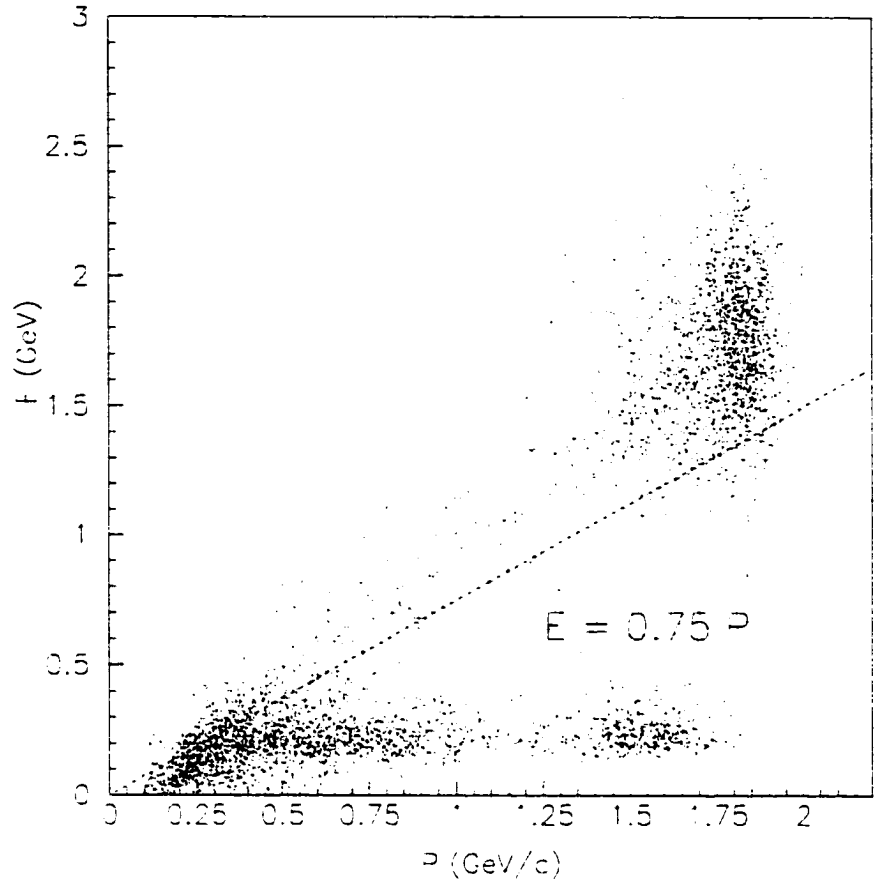

Figure 3.6: Energy vs Momentum

In addition, we define

$$(E_+/p_+ - 1)^2 + (E_-/p_- - 1)^2$$

where E_+ and p_+ are defined as the energy and momentum of positively charged track and E_- and p_- are defined as the negatively charged track's. The distribution of this

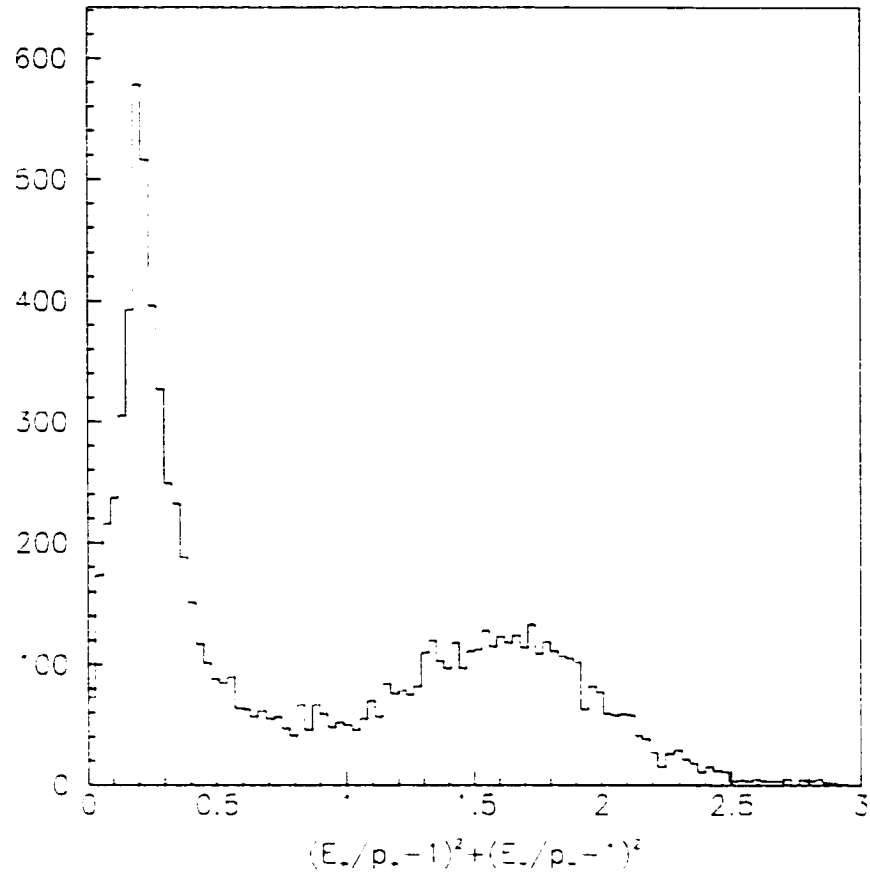

Figure 3.7: Using the ratio of energy and momentum from both tracks to remove Bhabha background

value can be found in Fig. 3.7. A cut of

$$(E_+/p_+ - 1)^2 + (E_-/p_- - 1)^2 < 0.4$$

is imposed for any events with charged track momentum larger than 700 MeV.

For radiative Bhabha events, we also looked at the angle between photon and $\pi^{\pm}$

— the $\theta(\gamma\pi)$. Fig. 3.8 is the distribution of this angle obtained from a Monte Carlo simulated radiative Bhabha process. We cut at $\theta_{(\gamma\pi)} > 15^{\circ}$.

Di-μ events is another source of QED background. Muon counter information has been used to reject them. A good Muon chamber hit is defined as a hit with the distance between the hit point and the projected point from MDC smaller than 4cm. 5cm or 6cm at the first, second and third layers of the counter respectively. A event is removed if a total of more than 3 Muon chamber layers being hit by both tracks. This clearly is not enough to remove much of this background. As we will see later, the mass of π and μ are so close that it is also almost impossible to use the BES particle identification subsystems to separate them. Other method has to be introduced to further removing the background, which will be discussed in section 4.1.

π and K is what we always try very hard to separate at BES. From Fig. 2.5 and Fig. 2.6 we can see very clear that we can't separate high momentum π from K by using the Time-of-Flight and dE/dx individually. Instead, we try to combine information from TOF, dE/dx and Kinematic fit together in the following way.

Assuming the measured time-of-flight is a gauss distribution, for each hypotheses H, where H is π or K, we define:

$$\chi^2_{TOF}(H) = \frac{(TOF_{meas} - TOF_{pred}(H))^2}{\sigma^2_{TOF}}$$

where TOF_{meas} and $TOF_{pred}(H)$ are measured time-of-flight and predicted time-of-

flight for hypotheses H. The degree of freedom is 1 for each track. Since BES TRKLST defines quantity $w(H) = e^{-\chi^2_{TOF}(H)/2}$ as TOF weight for each hypotheses H, $\chi^2_{TOF}(H)$ can be extracted directly from TRKLST.

Similarly, assuming Gaussian distribution for the dE/dx measurement, we define

$$\chi^2_{dE/dx}(H) = \frac{(dE/dx_{meas} - dE/dx_{pred}(H))^2}{\sigma^2_{dE/dx}}$$

where dE/dx_{meas} and $dE/dx_{pred}(H)$ are measured dE/dx and predicted dE/dx for hypotheses H. The degree of freedom is 1 for each track. $\chi^2_{dE/dx}(H)$ can be extracted from TRKLST variable $XS(H) = (dE/dx_{meas} - dE/dx_{pred}(H))/\sigma_{dE/dx}$.

Kinematic fitting returns the fitting χ^2 for $\psi(2S) \to \gamma\pi^+\pi^-$ and $\psi(2S) \to \gamma K^+K^-$ hypotheses. The degree of freedom of each hypotheses equals the number of constraints applied for the fit.

To combine TOF, dE/dx and kinematic fit (see Appendix D) information for particle identification, we define:

$$\chi^2_{PID}(H) = \chi^2_{TOF}(H) + \chi^2_{dE/dx}(H) + \chi^2_{KF}(H)$$

The corresponding degree of freedom is the sum of these three individual degree of

freedoms

$$Ndof(H) = Ndof_{TOF}(H) + Ndof_{dE/dx}(H) + Ndof_{KF}(H)$$

The probability density function of a χ^2 distribution is:

$$f(z,n) = \begin{cases} \frac{z^{n/2-1}e^{-z/2}}{2^{n/2}\Gamma(n/2)}: & z \geq 0 \\ 0: & z < 0 \end{cases}$$

where n is the degree of freedom. The corresponding confidence level is the integration of the tail of $f(z,n)$:

$$\begin{aligned} CL(\chi^2,n) &= \int_{\chi^2}^{\infty} f(z,n)dz \\ &= \frac{1}{\sqrt{2^n}\Gamma(n/2)} \int_{\chi^2}^{\infty} e^{-\frac{t}{2}} t^{\frac{n}{2}-1} dt \end{aligned}$$

The distribution of the confidence level function (CL) should be flat. Fig. 3.9 is a actual distribution from one of our channels with the $\psi(2S) \rightarrow \gamma\pi^+\pi^-$ hypotheses. A cut of $CL > 0.01$ or $CL > 0.05$ is generally applied in order to remove the high peak at the left side of the plot.

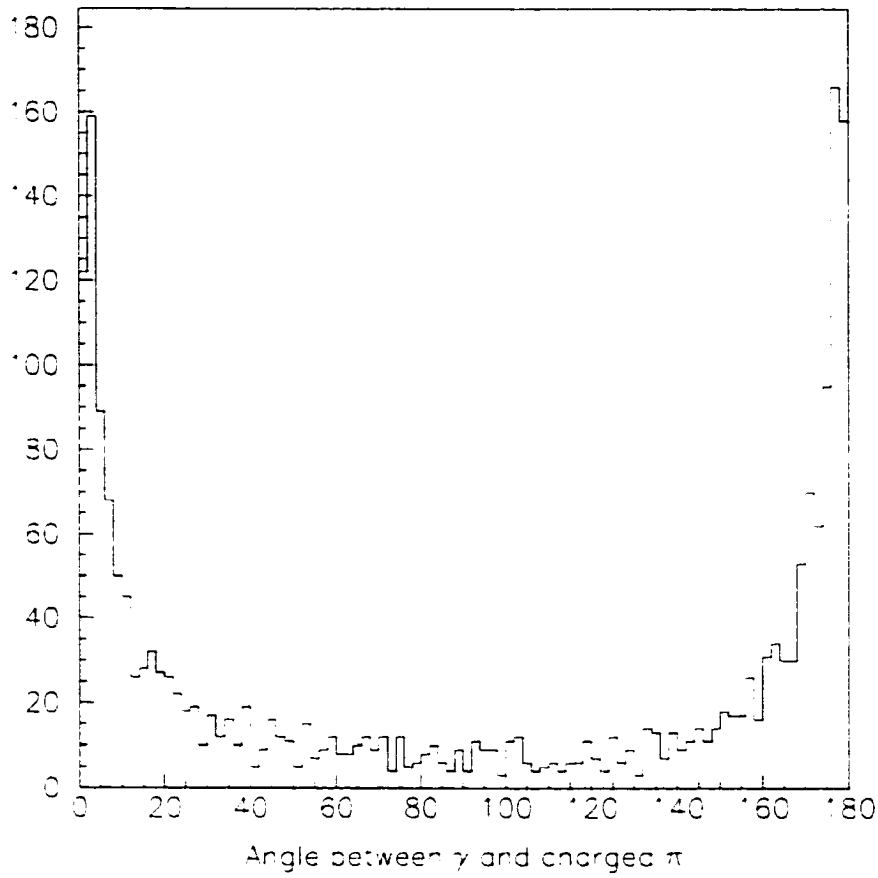

Figure 3.8: $\theta_{(\gamma\pi)}$ distribution from Monte Carlo data of $e^+e^- \rightarrow \gamma e^+e^-$. Note that each event contributes two entries in this plot. That is why the plot sharply rises at both ends instead of only at around zero. Cuts $\theta_{(\gamma\pi^+)} > 15^\circ$ and $\theta_{(\gamma\pi^-)} > 15^\circ$ will cut out the end peaks.

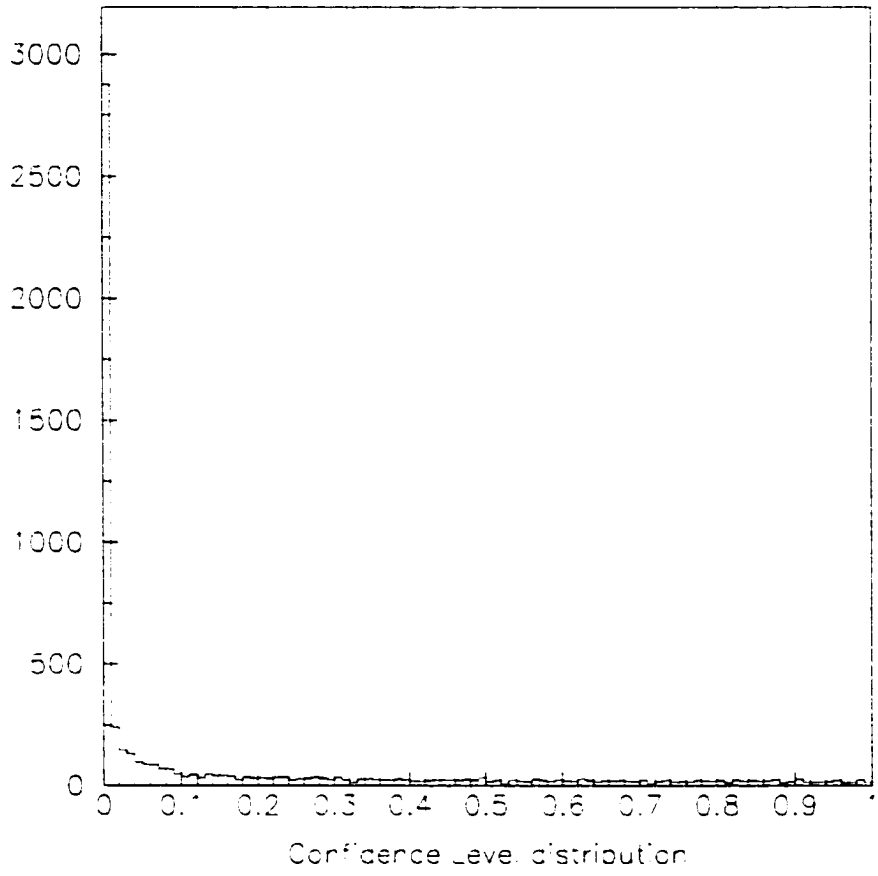

Figure 3.9: Confidence level distribution with $\psi(2S) \rightarrow \gamma\pi^+\pi^-$ hypotheses.

Chapter 4

Study of $\psi(2S) \to \gamma\pi\pi$ Final States

From the $c\bar{c}$ radiative decay diagram, one expects that the $\psi(2S)$ can directly decay into $\gamma\pi\pi$ final states, or through charmonium mesons χ_c's, or non-charmonium mesons. Apart from the possible glueball states, $\psi(2S)$ radiative decays into $\pi\pi$ through non-charmonium mesons is also interesting because of the theoretical "15%" rule. The decay of χ_{c0} and χ_{c2} into $\pi^+\pi^-$ and K^+K^- have been studied by the Mark I [10] and DASP [11] [12] and the BES collaborations [13]. The branching fractions of χ_{c0} and χ_{c2} into $\pi^+\pi^-$ from PDG and the recently paper published by BES are not consistent. The $\psi(2S)$ decay into $\gamma\chi_{c0,2}$ and $\gamma f_2(1270)$ with $\gamma\pi^0\pi^0$ final states have also been studied by Crystal Ball [14] and BES [15] but the results were not published.

By studying χ_{c0} and χ_{c2} decays into $\pi^0\pi^0$, we can add more information to these channels. It can also interesting to compare the branching fractions of χ_{c0} and χ_{c2} into $\eta\eta$ and check for the consistency with the SU(3) flavor symmetry.

4.1. Study of $\psi(2S) \to \gamma\pi^+\pi^-$

4.1.1. Signals and Backgrounds

We start with events containing two oppositely charged tracks and at least one photon. Requirements described in the Chapter 3 should be satisfied. In addition, we also impose the following requirement in order to separate π and K.

$$CL_{(\chi^2_{TOF}+\chi^2_{dE/dx}+\chi^2_{KF})}(\gamma\pi^+\pi^-) > CL_{(\chi^2_{TOF}+\chi^2_{dE/dx}+\chi^2_{KF})}(\gamma K^+K^-) \qquad (4.1)$$

$$CL_{(\chi^2_{TOF}+\chi^2_{dE/dx}+\chi^2_{KF})}(\gamma\pi^+\pi^-) > 0.01 \qquad (4.2)$$

The invariant mass of $\pi^+\pi^-$ is shown in Fig. 4.1(a). A $f_2(1270)$ signal is clearly present in the plot along with a ρ^0 signal and continuum background. The ρ^0 signal in the plot indicates that it may come from the QED initial state radiation process of $e^+e^- \to \gamma\rho^0 \to \gamma\pi^+\pi^-$. The line shape of the continuous background indicates the $e^+e^- \to \gamma\mu^+\mu^-$ background. This process may contribute to the continuous background because of the difficulty to distinguish between π and μ particles by the detector. To remove these backgrounds, we use the BES τ scan data.

The BES collaboration collected $e^+e^- \to \tau^+\tau^-$ data in its 1992 run (Table. 3.1). The CMS energy of the BES $\psi(2S)$ data ($\sqrt{S}$) is 3.686 GeV and the CMS energy of BES τ data is $3.55 \sim 3.60$ GeV [16]. Thus the τ data should give a good description

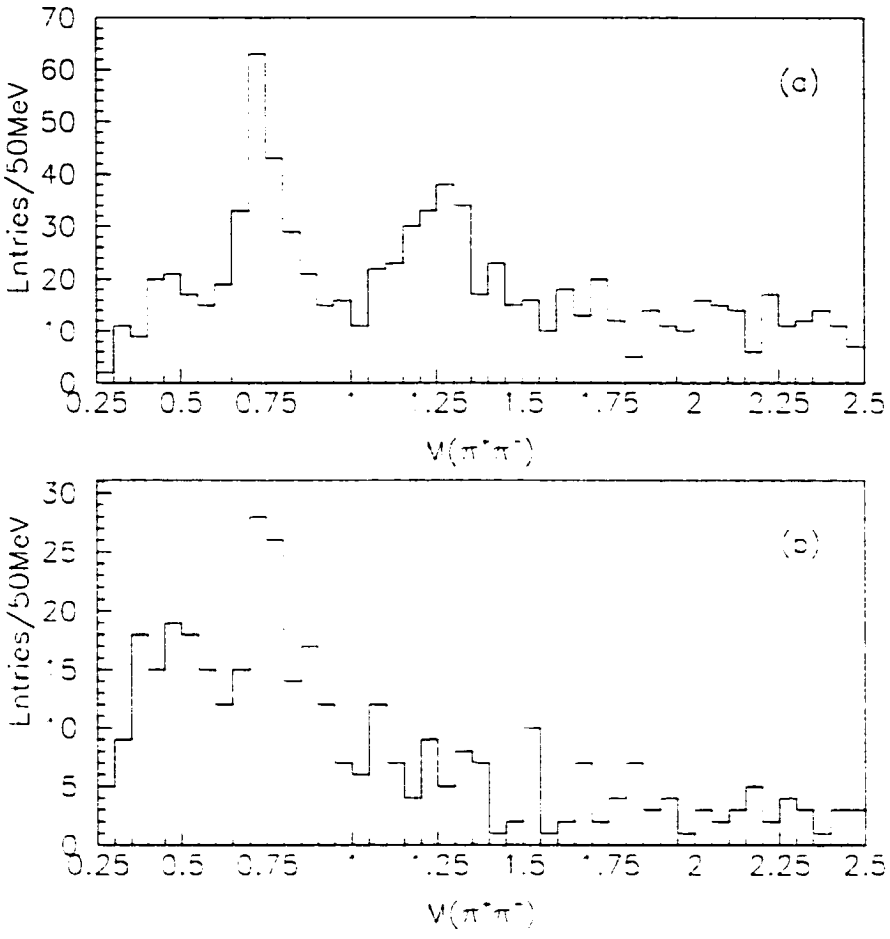

Figure 4.1: Invariant mass of $\pi^+\pi^-$ from $\psi(2S)$ data(a) and τ data(b)

of the QED background we observed in $\psi(2S)$ decay. We analyze the BES τ data with our analysis program, and we see the same ρ^0 signal and the continuous line shape in Fig. 4.1(b). A straight forward approach is to normalize the two histograms obtained from $\psi(2S)$ data and τ data according to the QED cross-section at each data point and the integrated luminosity of each data set. In this way, the QED background in the $M_{\pi^+\pi^-}$ histogram in Fig. 4.1(a) can be subtracted by assigning each τ event with

a negative weight in the likelihood function of mass fit.

One thing that should be considered carefully is the $e^+e^- \to \tau^+\tau^-$ process itself. Since both BES τ scan data and $\psi(2S)$ data are around or just above the $\tau^+\tau^-$ production threshold, the τ scan data can not describe the $\tau^+\tau^-$ production at the $\psi(2S)$ energy region. τ has larger branching fractions decaying into $\nu\pi$ and $\nu\rho$. These decay modes have similar final particles as $\gamma\pi^+\pi^-$, except the number of photons. Fortunately, the neutrino will take away around $800 \sim 900$ MeV of energy without been detected by the BES. It is thus not likely that a event with two of such energetic neutrinos missed can pass the $\gamma\pi^+\pi^-$ kinematic requirement. In fact, we generated 13616 $e^+e^- \to \tau^+\tau^-$, $\tau \to \nu\pi$ or $\nu\rho$ events and none of them can pass the cuts.

The integrated luminosity of the $\psi(2S)$ data is ~ 6.011 nb $^{-1}$ [17]. Unfortunately the integrated luminosity of the τ data is not known exactly due to various problems. Most problems are due to the imperfect running status of the BES detector. Different studies of the total luminosity of the τ set resulted in different numbers [18]. The approach we choose in our analysis is to normalize the two histograms according to the number of events with $\pi^+\pi^-$ invariant mass below 900 MeV because they can considered as pure QED contribution. This approach results in a ratio of

$$\omega = \frac{L_{\psi(2S)} \times \sigma_{\sqrt{S}=M_{\psi(2S)}}}{L_\tau \times \sum_i \sigma_{\sqrt{S_i}\simeq 2M_\tau}} = \frac{N_{\psi(2S)}(M_{\pi^+\pi^-} < 900\ MeV)}{N_\tau(M_{\pi^+\pi^-} < 900\ MeV)} = 1.43 \qquad (4.3)$$

This result is very close to the newest and most reliable result obtained from the total

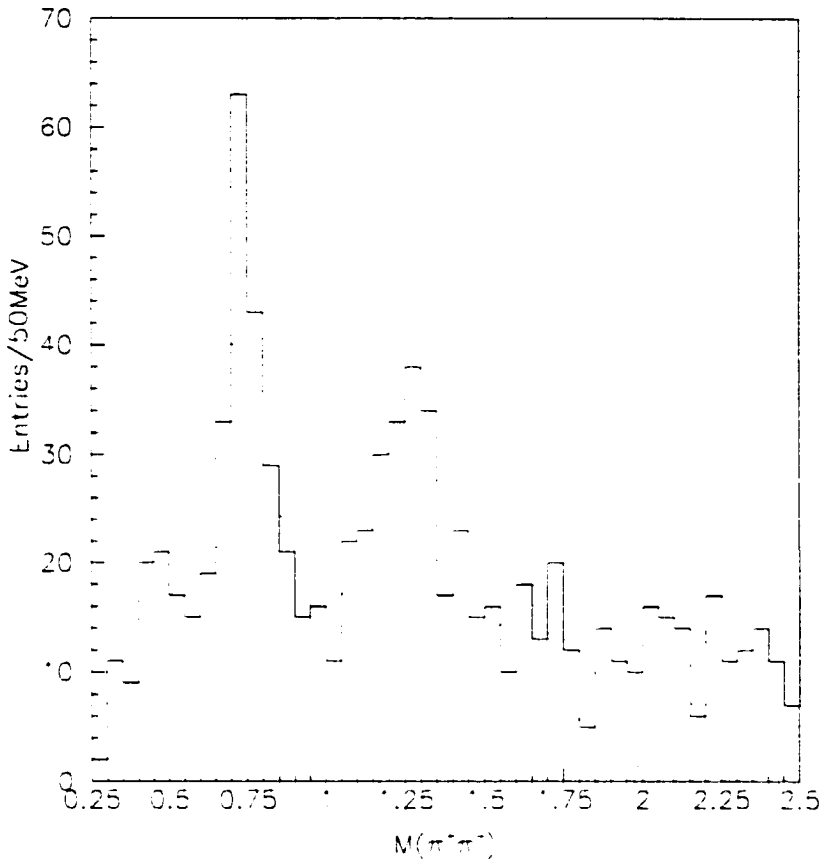

Figure 4.2: Invariant mass of $\pi^+\pi^-$ from $\psi(2S)$ data and τ data (in dot-line histogram) after normalization

luminosity analysis of the τ data by using large angle Bhabha events [18]. Fig. 4.2 shows the same two histograms after normalization of the τ data according to Eq (4.3).

4.1.2. The Breit-Wigner and the Likelihood Function

The decay width of $f_2(1270)$ is rather large according to the PDG (185±20 MeV). We adopted a special form of relativistic Breit-Wigner function with energy dependent width and the spin-2 amplitude, based on the fact that the $f_2(1270)$ mainly decays into $\pi\pi$ and $K\overline{K}$ ($\sim$ 84.7% branching fraction to $\pi\pi$ and $\sim$ 4.6% to $K\overline{K}$) as described in more detail in Appendix A [19]:

$$\frac{d\sigma}{dm^2} = C|T|^2 \frac{P}{m_{\psi(2S)}} \frac{Q}{m} \tag{4.4}$$

where:

- C is a constant that will be computed numerically based on the normalization.
- m is the invariant mass of the two pseudo-scalars.
- P is the momentum of the $\pi^+\pi^-$ resonant in $\psi(2S)$ rest frame.
- Q is the momentum of the $\pi^\pm$ in the $\pi^+\pi^-$ rest frame.
- T is the invariant amplitude describing the production and decay of $f_2(1270)$.

If T has the form

$$T = \frac{Q^s}{m_0^2 - m^2 - i \times m_0 \times \Gamma_{total}(E)}$$

where S is the orbital angular momentum of a π in the $\pi\pi$ system. which equals to the spin of the resonant (which is 2 here for $f_2(1270)$ ($J^{PC} = 2^{++}$)). $\Gamma_{total}(E)$ is the energy dependent width.

Consider that $f_2(1270) \to \pi\pi$ and $K\overline{K}$ has 90% of its total decay width. we can make an approximation on $\Gamma_{total}(E)$

$$\Gamma_{total}(E) = \Gamma_0 \frac{m_0}{m} \frac{B(f_2 \to \pi\pi)[\frac{Q_\pi(m)}{Q_\pi(m_0)}]^{2s+1} + \theta B(f_2 \to K\overline{K})[\frac{Q_K(m)}{Q_K(m_0)}]^{2s+1}}{B(f_2 \to \pi\pi) + B(f_2 \to K\overline{K})} \tag{4.5}$$

$$\theta = \begin{cases} \theta(m - (m_K + m_{\overline{K}})): & m > m_K + m_{\overline{K}} \\ 0: & m < m_K + m_{\overline{K}} \end{cases}$$

Γ_0 is the width of $f_2(1270)$ on PDG. By putting Eq. (4.5) and T back to Eq. (4.4). we obtain a D-wave Breit-Wigner describing the mass distribution of $f_2(1270)$. It is then folded with a Gaussian function describing the mass resolution

$$f(m) = \int \frac{d\sigma}{dm'^2} \frac{1}{\sqrt{2\pi}\sigma_m} \epsilon^{-\frac{(m'-m)^2}{2\sigma_m^2}} dm' \tag{4.6}$$

The rest of the likelihood function is a rather standard technique. We use a Legendre polynomial to describe the background shape.

$$BG(m) = \frac{1}{m_{max} - m_{min}} \sum_{i=1}^{N_{poly}} b_i p_i(x) P(m) Q(m) \tag{4.7}$$

where $p_i(x)$'s are Legendre polynomials and $b_0 = 1$ for normalization reason. m_{max} and m_{min} are the mass fitting range and

$$x = 2\frac{m - m_{min}}{m_{max} - m_{min}} - 1; \quad x \in [-1, 1]$$

P and Q are here in order to ensure compatibility of the Lorentz invariant phase space behavior. Normalization of $f(m)$ and $BG(m)$ are done numerically.

Sum all these together (Eq. (4.6) and Eq. (4.7)), we have

$$prob(m) = \alpha f(m) + (1 - \alpha)BG(m) \tag{4.8}$$

where α is the ratio of events. The logarithm likelihood function we are going to maximize is

$$\ln(\mathcal{L}) = \ln(\prod_{events} prob(m)) = \sum_{events} \ln(prob(m_i)) \tag{4.9}$$

in which parameters to fit are m_0, Γ_0, α, $b_1 \ldots b_n$. σ_m can be obtained from Monte Carlo.

In order to use the τ scan data to remove the background line sharp in Fig. 4.2, we employed negative weight likelihood approach: For each event from $\psi(2S)$ data set, we give a weight of 1 to the cross-section expression Eq. (4.4). For each τ data set, we give a weight of $-\omega$:

$$(\frac{d\sigma}{dm^2})^{-\omega}$$

where ω is defined in Eq. (4.3). Thus Eq. (4.9) can be written as

$$\begin{aligned} \ln(\mathcal{L}) &= \sum_{\psi(2S)events} \ln(prob(m_i)) + \sum_{revents} \ln(prob^{-\omega}(m_i)) \\ &= \sum_{\psi(2S)events} \ln(prob(m_i)) - \omega \sum_{revents} \ln(prob(m_i)) \end{aligned}$$

4.1.3. The Invariant Mass Fitting Results

Monte Carlo data has been generated by using a uniform phase space Monte Carlo simulation program from the BES software library with the Breit-Wigner function being replaced by Eq. (4.4) and Eq. (4.5). Fig. 4.3 shows the $f_2(1270)$ signal from Monte Carlo data. Of the Monte Carlo events generated, 12912 out of 28610 pass various cuts — showing the analysis' efficiency for this channel is $\epsilon = 43.8\%$. The mass resolution obtained from Monte Carlo simulation is around 8 MeV.

The fitting results from the data can be found in Fig. 4.4. Data points with error bars are the difference between the two histograms in Fig. 4.2. The error bar in each bin is determined by

$$\Delta_{bin} = \sqrt{N_{bin}(\psi(2S)) + \omega^2 N_{bin}(\tau)} \tag{4.10}$$

We fix the mass and width of the $f_2(1270)$ at the PDG value of 1275 MeV and 185 MeV when we performs the mass fitting. Underneath of the fitting curve there are 209.8 ± 24.9 events [1]. This error is statistical. The number of events that survive

[1] In the actual mass fit, the background function we turn off by setting α in Eq. (4.8) to 1.

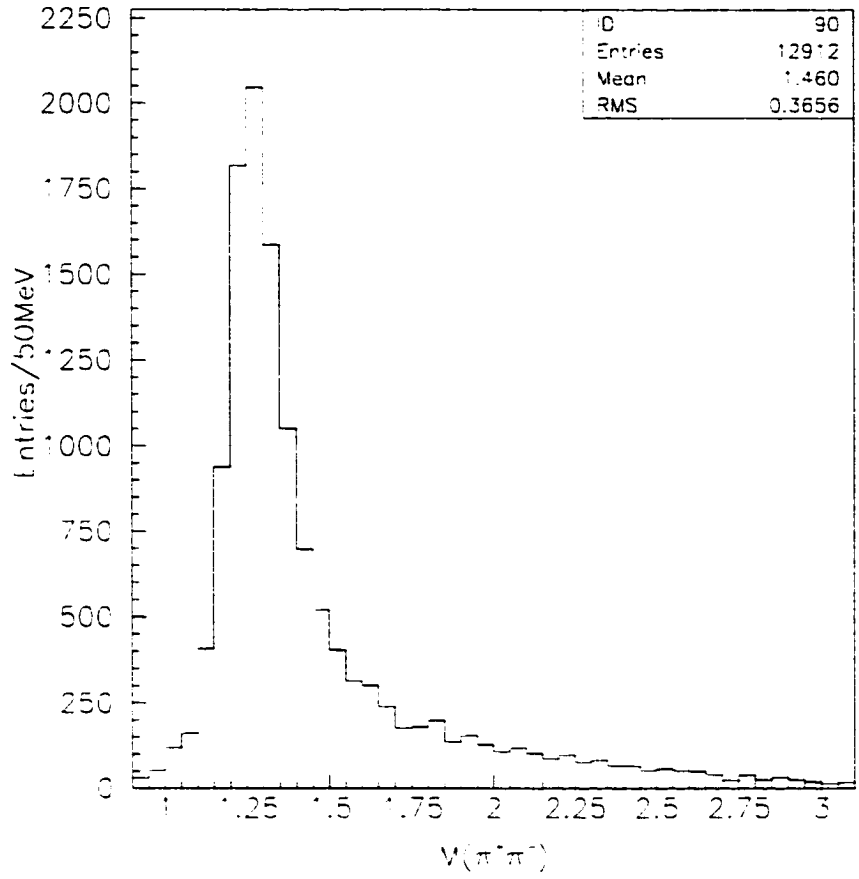

Figure 4.3: Monte Carlo results generated by using Breit-Wigner function described by Eq. (4.4).

various cuts (both real data and Monte Carlo data) are listed in Table. 4.1.

The branching fraction of $\psi(2S) \to \gamma f_2(1270)$ can be calculated based on the following relation:

$$B(\psi(2S) \to \gamma f_2(1270) \to \gamma\pi^+\pi^-) = \frac{N}{N_{\psi(2S)} \times \epsilon \times B(f_2(1270) \to \pi^+\pi^-)}$$

Cuts	Data	Monte Carlo
Initial number of events	4786432	28610
$\sum Q_i = 0$; $N_\gamma > 0$; mfit=2	1062523	21082
γ hit at BSC, $E_\gamma > 10MeV$	971176	18620
$\lvert Z_1 - Z_2\rvert < 5cm$; $\lvert Z_V\rvert < 15cm$; $\theta_{\pi^+\pi^-} < 175^\circ$	402323	18178
Total μ layers< 3; $\lvert\cos(\theta_\pi)\rvert < 0.85$; $R_{xy} < 2cm$; $Z < 15cm$; $E/P < 0.75$; $(E_+/P_+ - 1)^2 + (E_-/P_- - 1)^2 > 0.4$	222326	16447
$P_{(\chi^2_{TOF}+\chi^2_{dE/dx}+\chi^2_{KF})}(\gamma\pi^+\pi^-) > P_{(\chi^2_{TOF}+\chi^2_{dE/dx}+\chi^2_{KF})}(\gamma K^+K^-)$ $P_{(\chi^2_{TOF}+\chi^2_{dE/dx}+\chi^2_{KF})}(\gamma\pi^+\pi^-) > 0.01$	1783	13085
$\theta_{\gamma\pi} > 15^\circ$	1715	13010

Table 4.1: Number of $\gamma\pi^+\pi^-$ events survive various cuts

where N is the number of $f_2(1270)$ after the mass fit. $N_{\psi(2S)}$ is the total $\psi(2S)$ number of the data set. ϵ is the efficiency of the analysis given by Monte Carlo.

The $f_2(1270)$ is a isospin-0 particle. Its isospin wave function can be expanded as:

$$\begin{aligned} |f_2(1270).0.0> &= \sqrt{\frac{1}{3}}|\pi^+.1.1>|\pi^-.1.-1> \\ &- \sqrt{\frac{1}{3}}|\pi^0.1.0>|\pi^0.1.0> \\ &+ \sqrt{\frac{1}{3}}|\pi^-.1.-1>|\pi^+.1.1> \end{aligned}$$

or

$$< f_2(1270)|f_2(1270) >= \frac{2}{3} < \pi^+\pi^-|\pi^+\pi^- > + \frac{1}{3} < \pi^0\pi^0|\pi^0\pi^0 > \qquad (4.11)$$

Thus we have $B(f_2(1270) \to \pi^+\pi^-) : B(f_2(1270) \to \pi^0\pi^0) = 2 : 1$, and

$$\begin{aligned} B(\psi(2S) \to \gamma f_2(1270)) &= \frac{N}{N_{\psi(2S)} \times \epsilon \times \frac{2}{3} \times B(f_2(1270) \to \pi\pi)} \\ &= (2.31 \pm 0.27 \pm 0.39) \times 10^{-4} \end{aligned} \tag{4.12}$$

Again the first error is statistical. The second error is systematic. A detail discussion of systematic error will be done in Section 4.1.4.

Comparing our result of $B(\psi(2S) \to \gamma f_2(1270))$ with $B(J/\psi \to \gamma f_2(1270)) = (13.8 \pm 1.4) \times 10^{-4}$ on PDG, we get the ratio of these two branching fractions:

$$Q = \frac{B(\psi(2S) \to \gamma f_2(1270))}{B(J/\psi \to \gamma f_2(1270))} = (16.7 \pm 2.0 \pm 2.4)\%$$

The PDG value of $B(J/\psi \to \gamma f_2(1270))$ is actually obtained from a slightly improperly handled analysis. If we use the Mark III's result of $B(J/\psi \to \gamma f_2(1270)) = (15.6 \pm 1.4) \times 10^{-4}$ [21], we then have:

$$Q = \frac{B(\psi(2S) \to \gamma f_2(1270))}{B(J/\psi \to \gamma f_2(1270))} = (14.8 \pm 1.7 \pm 2.1)\%$$

The $B(\psi(2S) \to \gamma f_2(1270))$ we measured clearly shows that "*The 15% rule hold for $\psi(2S)$radiative decay into $\gamma f_2(1270)$*".

In addition, we also know from the mass fit that the number of events under the

$f_J(1710)$ signal is 39.2 ± 4.4. The detection efficiency from Monte Carlo simulation is 45.4%. Assuming isospin conservation, $B(f_J(1710) \to \pi^+\pi^-) : B(f_J(1710) \to \pi^0\pi^0) = 2 : 1$, we have:

$$\begin{aligned} B(\psi(2S) \to \gamma f_J(1710) \to \gamma\pi\pi) &= \frac{N}{N_{\psi(2S)} \times \epsilon \times \frac{2}{3}} \\ &= (3.51 \pm 0.90 \pm 1.46) \times 10^{-5} \end{aligned}$$

where $N = 39.2 \pm 10.1$ is the number of events and $\epsilon = 45.4\%$ is the efficiency. The first error is statistical and the second error is systematic. Table. 4.3 listed sources contributed to systematic error.

Mark III measured the corresponding branching fractions in J/ψ decay (See Fig. 4.5) and gave $B(J/\psi \to \gamma\theta(1720) \to \gamma\pi^+\pi^- = (1.6 \pm 0.4 \pm 0.3) \times 10^{-4}$ [22] ($\theta(1720)$ was the old name of $f_J(1710)$). The ratio of our result in $\psi(2S)$ decay and Mark III's result is

$$\frac{B(\psi(2S) \to \gamma f_J(1710) \to \gamma\pi\pi)}{B(J/\psi \to \gamma f_J(1710) \to \gamma\pi\pi)} = (14.7 \pm 3.8 \pm 5.9)\%$$

4.1.4. The Systematic Uncertainty

The systematic uncertainty of branching fraction results can be estimated by varying major cuts by one standard deviation and then recalculate the branching fraction values. However, the definition of one standard deviation of those cuts are

not always clear. Fortunately, the change of cuts also influence the analysis efficiency calculation from Monte Carlo. At the lowest approximation, we expect the relative change of the branching fraction results (the percentage errors) are independent of the changes of the cuts, if the changes are small.

Table. 4.2 lists the major source of systematic error and their contribution to the total systematic error for $\psi(2S) \to \gamma f_2(1270) \to \gamma\pi^+\pi^-$ channel. The $|Z_{VC}|$ cut is changed by one standard deviation, which is the spatial resolution of the z coordinate of the Main Drift Chamber. As for other cuts such as the $P_{\chi^2}(\gamma\pi^+\pi^-)$, $(E_+/P_+ - 1)^2 + (E_-/P_- - 1)^2$, and the fitting range of the $\pi^+\pi^-$ invariant mass, we varied them in a way that a more clear event sample can be obtained so that the total systematic error is not under estimated. The uncertainty of the total number of $\psi(2S)$ events collected by the BES is 8% [9] and should go to the systematic error in our branching fraction results. A 10% uncertainty is included in systematic error due to the problem of kinematic fitting package TELESIS [20].

Table. 4.3 lists the major source of systematic error for $\psi(2S) \to \gamma f_J(1710) \to \gamma\pi^+\pi^-$ channel. We estimated the systematic error of this channel in the same way we do for the $\gamma f_2(1270)$ channel. Since the number of events underneath of the $f_J(1710)$ signal is much smaller than the $f_2(1270)$ signal, the fluctuation of the change of each cuts is also much larger, and thus the total systematic error.

Major cuts	$\delta B(\psi(2S)' \to \gamma f_2(1270))$ (%)
$P_{\chi^2}(\gamma\pi^+\pi^-) > 0.01 \to 0.05$	1.5%
$\|Z_V\| < 15cm \to 10cm$	0.8%
$\theta_{\gamma\pi} > 15^o \to 10^o$	4.1%
$(E_+/P_+ - 1)^2 + (E_-/P_- - 1)^2 > 0.4 \to 0.6$	8.2%
Fitting Region from $0.3 \sim 2.5$ GeV to $0.3 \sim 2.0$	6.3%
Number of $\psi(2S)$ events	8%
Kinematic fitting package TELESIS error	10%
Total	16.9%

Table 4.2: Systematic error estimation of $B(\psi(2S) \to \gamma f_2(1270))$ from channel $\gamma\pi^+\pi^-$

4.2. Study of $\psi(2S) \to \gamma\pi^0\pi^0$

The measurement of $\psi(2S) \to \gamma\pi^0\pi^0$ is interesting because of several previous inconsistent measurements. We start from events with at least 5 photons and no more than 10 photons and with no charged tracks. At least 5 good photons should be identified by photon selection criteria described in section 3.1. After fake or spurious showers are removed and split energy shower are recombined, a six-constraint kinematic fit of $\gamma\pi^0\pi^0 \to \gamma_1\gamma_2\gamma_3\gamma_4\gamma_5$ with two π^0 resonants was applied to all $\gamma\pi^0\pi^0$ combination. The one with smallest χ^2 and with extra photons' total energy smaller than 150 MeV is selection as the final topology of $\gamma\pi^0\pi^0$. The fitting χ^2 should have a confidential level higher than 0.01.

We also apply a four-constraint kinematic fit with no π^0 mass constraint. The invariant mass of both of the two γ pairs decaying from π^0 should be within 70 MeV

Major cuts	$\delta B(\psi(2S)' \to \gamma f_J(1710) \to \gamma\pi\pi)$ (%)
$P_{\chi^2}(\gamma\pi^+\pi^-) > 0.01 \to 0.05$	28.0%
$\|Z_V\| < 15cm \to 10cm$	1.4%
$\theta_{\gamma\pi} > 15^o \to 10^o$	16.4%
$(E_+/P_+ - 1)^2 + (E_-/P_- - 1)^2 > 0.4 \to 0.6$	17.6%
Fitting Region from $0.3 \sim 2.5$ GeV to $0.3 \sim 2.0$	14.0%
Number of $\psi(2S)$ events	8%
Kinematic fitting package TELESIS error	10%
Total	41.5%

Table 4.3: Systematic error estimation of $B(\psi(2S) \to \gamma f_J(1710)) \to \gamma\pi\pi)$ from channel $\gamma\pi^+\pi^-$

of π^0 mass, e.g.

$$|M_{\gamma\gamma} - M_{\pi^0}| < 70MeV$$

the "Data" column of Table 4.4 shows how many real events survive the various cuts. Fig. 4.6 is the invariant mass of two photons pairs. A peak at π^0 region is observed.

4.2.1. $\chi_{c0,2} \to \pi^0\pi^0$

As we mentioned at the beginning of this chapter, the Crystal Ball experiment measured $B(\chi_{c0} \to \pi^0\pi^0) = (3.1\pm0.4\pm0.5)\times10^{-3}$ and $B(\chi_{c2} \to \pi^0\pi^0) = (1.10\pm0.20\pm 0.20) \times 10^{-3}$. The result has not been published [14] [2] The corresponding charged

[2]The original Crystal Ball's results [14] used $B(\psi(2S) \to \gamma\chi_{c0}) = (8.2 \pm 1.4) \times 10^{-3}$ and $B(\psi(2S) \to \gamma\chi_{c2}) = (7.4 \pm 1.3) \times 10^{-3}$, which are different from listed values in current PDG. The $\chi_{c0,2} \to \pi^0\pi^0$ branching fractions we quoted were obtained from the PDG 96 whose number are based on R.A. Lee's work [14] but with new $\psi(2S) \to \gamma\chi_{c0,2}$ branching fractions.

decay modes' branching fraction on PDG are $B(\chi_{c0} \to \pi^+\pi^-) = (7.5 \pm 2.1) \times 10^{-3}$ and $B(\chi_{c2} \to \pi^0\pi^0) = (1.9 \pm 1.0) \times 10^{-3}$. They were measured many years ago by Mark I and DASP. Recently BES has re-measured these two channels and the results are $B(\chi_{c0} \to \pi^+\pi^-) = (4.68 \pm 0.26 \pm 0.65) \times 10^{-3}$ and $B(\chi_{c2} \to \pi^+\pi^-) = (1.49 \pm 0.14 \pm 0.22) \times 10^{-3}$ [13]. Apparently they are not in good agreement. Measuring the decay branching fractions of χ_{c0} and χ_{c2} into $\pi^0\pi^0$ final state is useful to resolve the difference.

The decays of the χ_{c0} and the χ_{c2} into $\pi^0\pi^0$ were studied in a decay chain process of

$$\begin{aligned} \psi(2S) &\to \gamma \quad \chi_{c0,2} \\ &\hookrightarrow \pi^0\pi^0 \end{aligned}$$

From phase space Monte Carlo simulations we know that the overall efficiency of detecting and analyzing the events are $\epsilon(\chi_{c0}) = 10.5\%$ and $\epsilon(\chi_{c2}) = 8.2\%$. Also we know from the simulation are the mass resolution of 39.7 MeV at χ_{c0} mass region and 31.9 MeV at χ_{c2} region. The difference between these two mass resolutions may be because of the difficulty to identify soft photons radiated from $\psi(2S) \to \gamma\chi_{c2}$.

Fig. 4.7 shows invariant mass of $\pi^0\pi^0$. The χ_{c0} signal and χ_{c2} signal are clearly observed along with little background. We fit these two signals with two Breit-

Wigners of form:

$$\frac{1}{\pi}\frac{\Gamma/2}{(m-m_0)^2+\Gamma^2/4}$$

plus polynomial background function with $\Gamma_{\chi_{c0}}$, $\Gamma_{\chi_{c2}}$, $M_{\chi_{c0}}$ and $M_{\chi_{c2}}$ fixed at PDG and we the number of events underneath the fitting curving are

$$N(\chi_{c0}) = 96.9 \pm 11.1$$

$$N(\chi_{c2}) = 20.8 \pm 5.8$$

which then gives us the following branching fraction numbers:

$$B(\chi_{c0} \to \pi^0\pi^0) = (2.80 \pm 0.32 \pm 0.60) \times 10^{-3}$$

$$B(\chi_{c2} \to \pi^0\pi^0) = (9.2 \pm 2.7 \pm 5.3) \times 10^{-4}$$

The first error is statistical and the second error is systematic.

4.2.2. $\psi(2S)$ Decay into $\gamma\pi^0\pi^0$ Through Non-charmonium Resonants

In the region where that $\pi^0\pi^0$ masses are lower than that in Fig. 4.7, we see a $f_2(1270)$ signal. We fit it with a D-wave Breit-Wigner described by Eq. (4.4) and by Eq. (4.5), as shown in Fig. 4.8. The mass resolution from Monte Carlo is 38.2 MeV and the detecting and analyzing efficiency is $\epsilon = 9.6\%$. From the mass fitting

we know there are $N = 29.9 \pm 11.1$ $f_2(1270)$ events, and

$$\begin{aligned} B(\psi(2S) \to \gamma f_2(1270)) &= \frac{N}{N_{\psi(2S)} \times \epsilon \times \frac{1}{3} B(f_2(1270) \to \pi\pi)} \\ &= (3.01 \pm 1.12 \pm 1.12) \times 10^{-4} \end{aligned} \tag{4.13}$$

in which we used the ratio from Eq. (4.11). Compared to the Crystal Ball experiment's measurement of $B(\psi(2S) \to \gamma f_2(1270)) = (1.5 \pm 0.4 \pm 0.5) \times 10^{-4}$, our result is twice as that of Crystal Ball's result and is consistent with our previous measurement in $\gamma\pi^+\pi^-$ final state. Table 4.4 is a list of number of events survived various cuts[3]. Table 4.5 listed the source of systematic error of the branching fraction. The source of systematic uncertainty in this table are estimated in the same way described in section 4.1.4. Since the Monte Carlo can not simulate the creation of extra photons in the shower counter, and there is no well understood $\psi(2S)$ decay into all-photon channel that can be used to determine the distribution of total extra photon energy, we included a maximum possible uncertainty of 32.8% by removing the upper limit of the total extra photon energy requirement so that the systematic error is not under estimated.

The two results of $B(\psi(2S) \to \gamma f_2(1270))$ from Eq. (4.12) and Eq. (4.13) are

[3]The 4-C fit cut off some of the Monte Carlo events because some of the shower hit at the aluminum supporting frame (rib) region in Barrel Shower counter

combined to obtain a single best estimation (See Appendix B),

$$B(\psi(2S) \to \gamma f_2(1270)) = (2.37 \pm 0.25 \pm 0.39) \times 10^{-4} \tag{4.14}$$

$$Q = \frac{B(\psi(2S) \to \gamma f_2(1270))}{B(J/\psi \to \gamma f_2(1270))} = (17.2 \pm 1.8 \pm 2.5)\% \tag{4.15}$$

The $\psi(2S) \to \gamma\pi^0\pi^0$ channel has relatively fewer backgrounds compared to the $\psi(2S) \to \gamma\pi^+\pi^-$ channel. This allows us to look at the helicity angle distribution of the $\pi^0\pi^0$ decay. The angle is defined as the polar angle of a π^0 in the $\pi^0\pi^0$ system rest frame. A distribution is shown in figure 4.9 alone with a curve showing the probability function describing $\psi(2S) \to \gamma 2^{++}$ and $2^{++} \to 0^-0^-$ decay mode:

$$P(cos(\theta_m) = \frac{4\pi}{3}(3cos^2\theta_m - 1)^2 + 8\pi x^2 cos^2 o_x cos^2\theta_m sin^2\theta_m + 2\pi y^2 cos^2 o_y sin^4\theta_m$$

where

$$x = \frac{|A_{11}|}{|A_{10}|} = 0.88; y = \frac{|A_{21}|}{|A_{10}|} = 0.04; o_x = o_y = 0$$

are the ratio of helicities and their phase obtained from $J/\psi \to \gamma f_2(1270)$ [24].

The $f_0(1500)$ scalar was perhaps observed by an earlier BNL experiment. In recent years, it has also been observed in $\pi^0\pi^0$ mass by Crystal-Barrel experiment [25] and E760 experiment in $p\bar{p} \to \pi^0\pi^0\pi^0$ reaction and in $K_S^0K_S^0$ final state in central production experiment $pp \to p_{fast}(K_S^0K_S^0)p_{slow}$ at E690 [26]. In J/ψ radiative decay

experiment, both Mark III and DM2 claimed signal of $f_0(1500) \to 4\pi$ in $J/\psi \to \gamma 4\pi$ [27]. However, in the $J/\psi \to \gamma\pi^0\pi^0$, the Crystal Ball experiment observed no signal of $f_0(1500)$ [14].

We also tried to fit the small narrow peak at around ~ 1.55 GeV in Fig. 4.8 with a S-wave Breit-Wigner function with either the mass and width fixed at PDG value of $f_0(1500)$ or with them values allowed to vary in the fit, as shown in figure 4.10 and 4.11. They both give $B(\psi(2S) \to \gamma f_2) = (2.85 \pm 0.91) \times 10^{-4}$. They also result in ~ 2.4 and ~ 4.7 events underneath the peak (~ 1.55 GeV) respectively. We estimate the upper limit of the branching fraction of $\psi(2S)$ radiative decay to X($1500 \sim 1550$) via two π^0's are 1.9×10^{-5} and 2.6×10^{-5} from the above two fits respectively.

4.2.3. Backgrounds of $\gamma\pi^0\pi^0$ Final State

The branching fraction of $\psi(2S) \to \gamma\eta \to 3\gamma$ is $\sim 20 \times 10^{-5}$ [28]. This is not very small compare to the $B(\psi(2S) \to \gamma f_2(1270) \to \gamma\pi^0\pi^0) = 8.5 \times 10^{-5}$. Extra fake photons may present in shower counter for various reasons. Since these kind of background events do not have two π^0 resonances, we do not expect a large fraction of them can pass the kinematic fit.

$\psi(2S) \to \gamma\eta'$ and $\eta' \to \gamma\gamma$ or $\pi^0\pi^0\eta \to \pi^0\pi^0\gamma\gamma$ may have a total of $\sim 1.5 \times 10^{-5}$ of branching fractions [28]. Their contribution to the background should also be small because they either do not have two π^0 resonances, or the total energy of two photon

Cuts	Data	MC
# of events come in	3318477	42915
$Q_i = 0$; 5 $\leq$# of γ's$\leq$ 10	186455	19463
Good γ selection	38030	5500
4-C fit	5486	5210
6-C kinematic fit $P(\chi^2) > 0.01$	458	5034
$\lvert M_{\gamma\gamma} - M_{\pi^0}\rvert < 70 MeV$	266	4134
$E_{extra-\gamma} < 100 MeV$	117	4127

Table 4.4: Number of $\gamma\pi^0\pi^0$ events survive various cuts

from a η is too large to pass the extra photon total energy cut.

The two-photon annihilation process $e^+e^- \to \gamma\gamma$ (see Fig. 4.12) have the cross-section piled up at small polar angle. So it may not have a big contribution to the $\gamma\pi^0\pi^0$ final state. The two photon process $e^+e^- \to e^+e^-\gamma^*\gamma^* \to e^+e^-X$ (see Fig. 4.13) have very energetic e^+ and e^- in the final state that fly almost alone the beam pipe direction. These events may be misidentified as all-photon events. But they can not pass the kinematic fit due to the large fraction of energy been taken away by the e^+ and e^-.

Cuts	% change to $B(\psi(2S) \to \gamma f_2)$
# good γ's $= 6 \to 5$	2.8%
$P(\chi^2) > 0.01 \to 0.02$	3.1%
$\lvert M_{\gamma\gamma} - M_{\pi^0} \rvert < 70 MeV \to 90 MeV$	4.1%
$\lvert M_{\gamma\gamma} - M_{\pi^0} \rvert < 70 MeV \to 50 MeV$	3.0%
Extra photon energy $< 100 MeV \to 150 MeV$	13.0%
Remove the extra photon energy upper limit	32.8%
# of $\psi(2S)$ events error	8%
Background shape change	1.0%
χ_c contamination	11%
Uncertainty from the TELESIS	10%
Total	37.4%

Table 4.5: $B(\psi(2S) \to \gamma f_2(1270))$ systematic error estimations from channel $\psi(2S) \to \gamma\pi^0\pi^0$

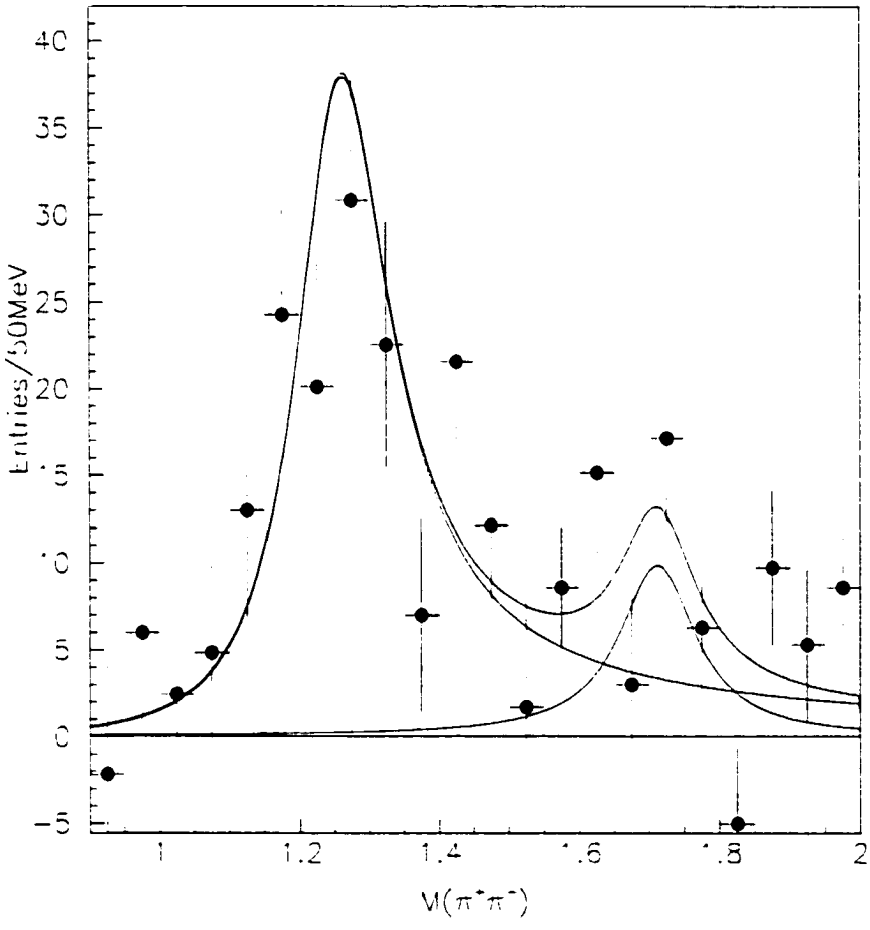

Figure 4.4: Data points with error bars are the difference between the two histograms in Fig. 4.2. The curve is the fit result with Breit-Wigner function described by Eq. (4.4).

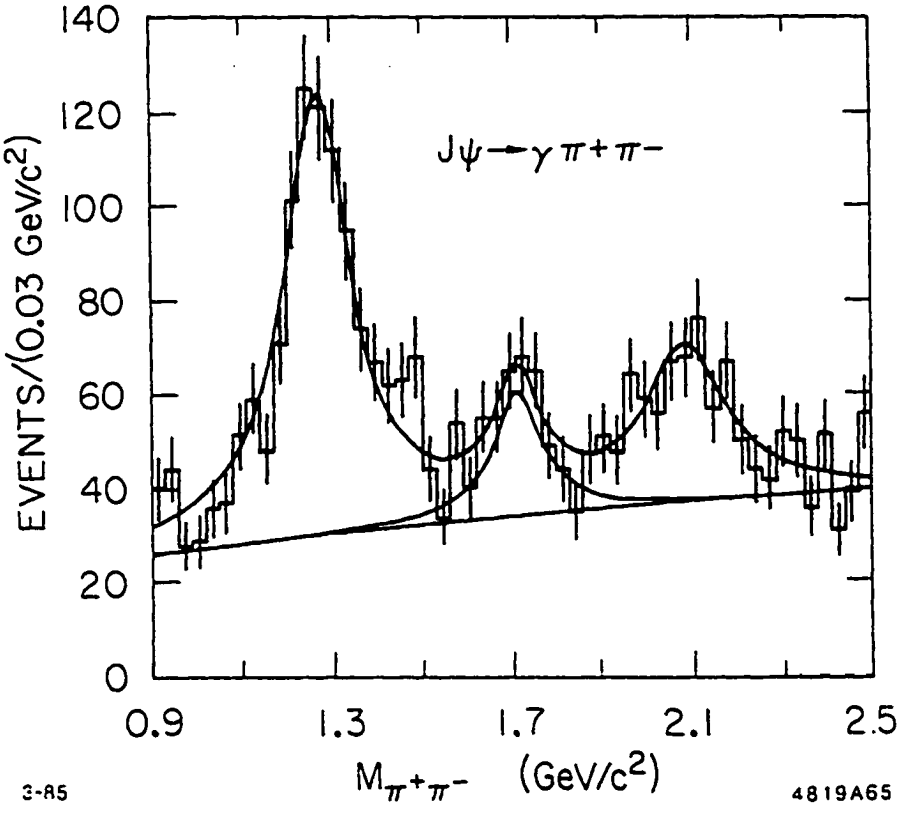

Figure 4.5: $M_{\pi^+\pi^-}$ in $J/\psi \to \gamma\pi^+\pi^-$ from Mark III

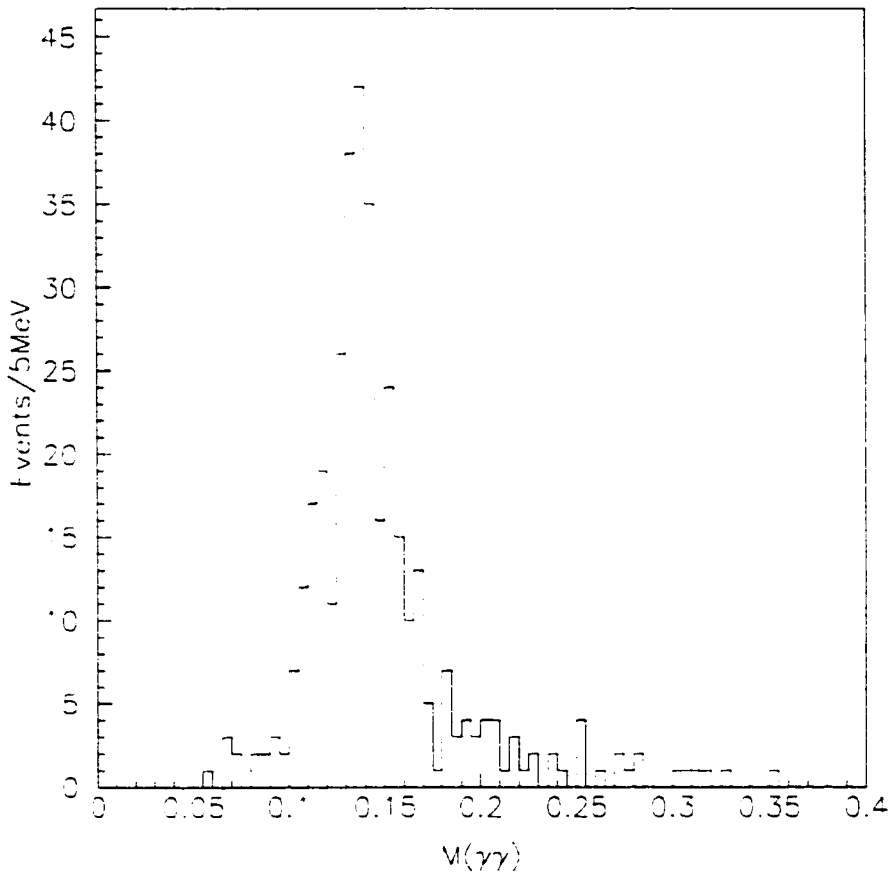

Figure 4.6: Invariant mass of $\gamma\gamma$

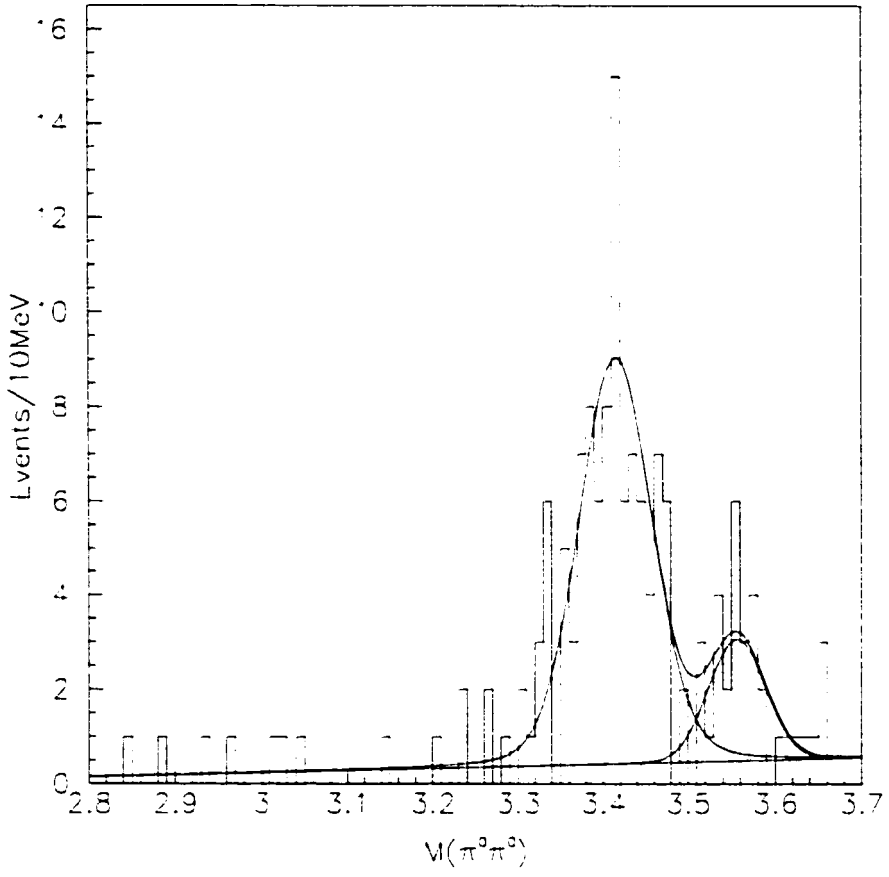

Figure 4.7: Invariant mass of $\pi^0\pi^0$

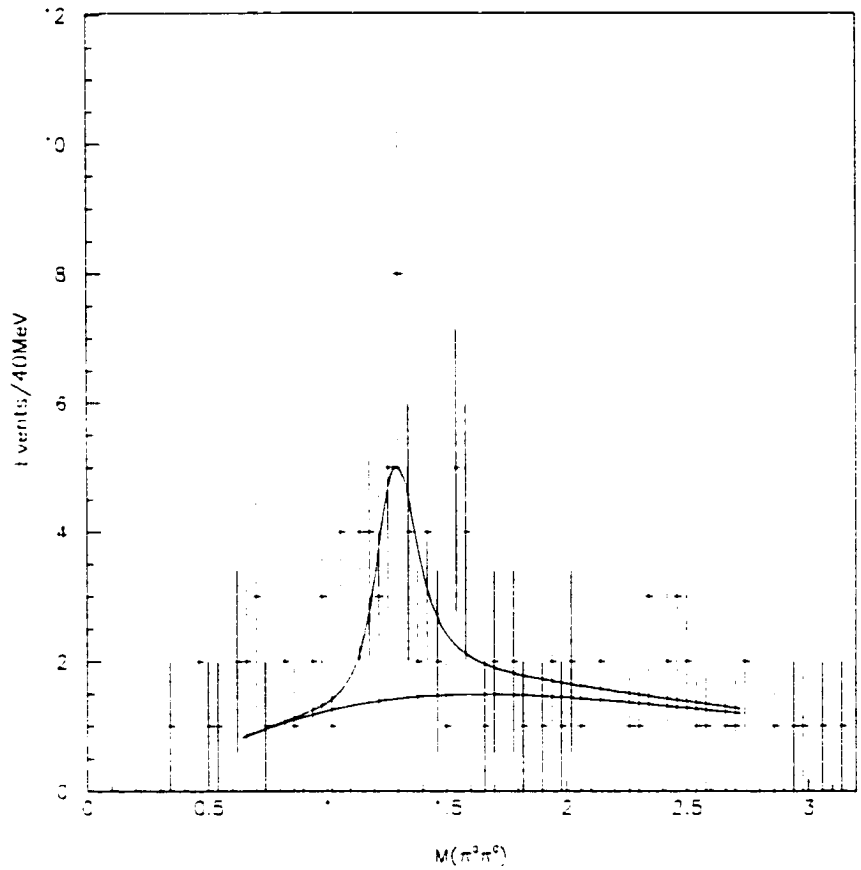

Figure 4.8: Invariant mass of $\pi^0\pi^0$

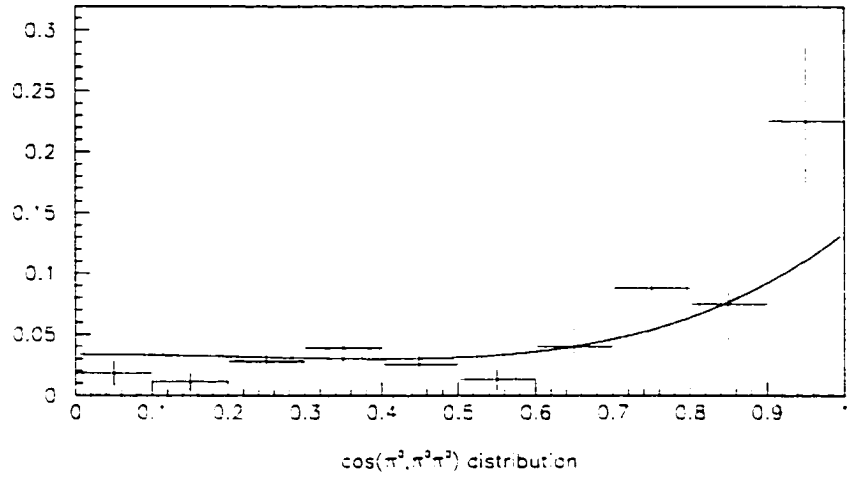

Figure 4.9: Helicity angle of $\pi^0\pi^0$ decay

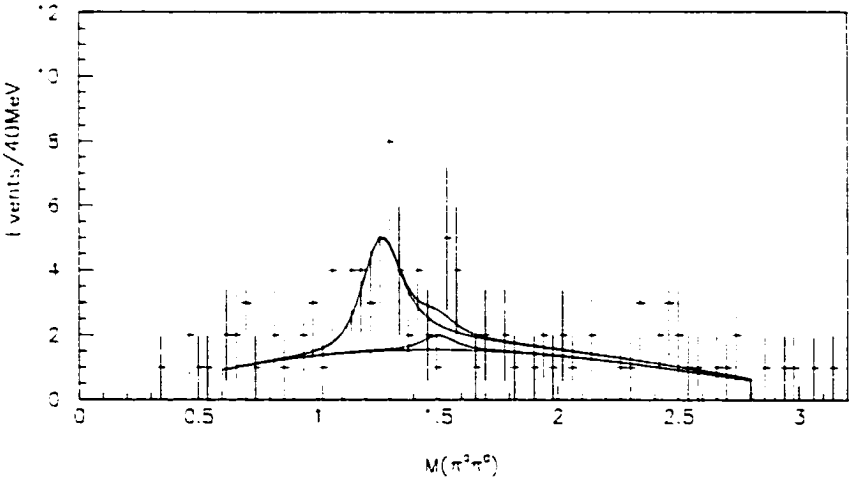

Figure 4.10: Fit the $\pi^0\pi^0$ mass with two peaks fixed at PDG value of $f_2(1270)$ and $f_0(1500)$

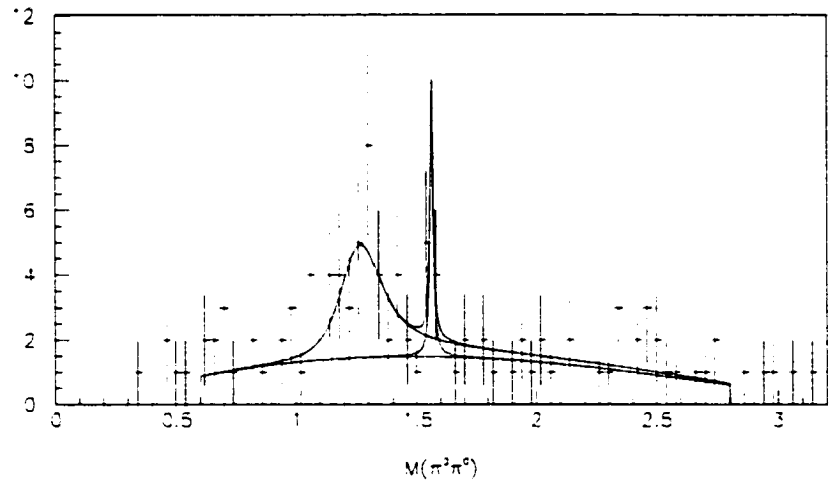

Figure 4.11: Fit the $\pi^0\pi^0$ mass with two peaks and the second peak's resonant parameters are free

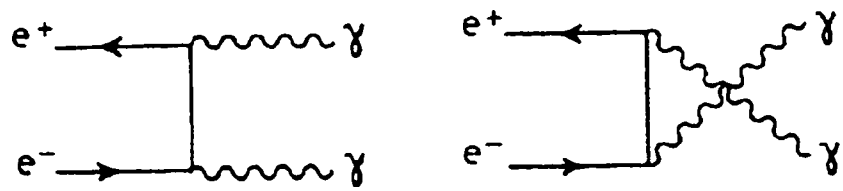

Figure 4.12: Lowest order QED two-photon annihilation process

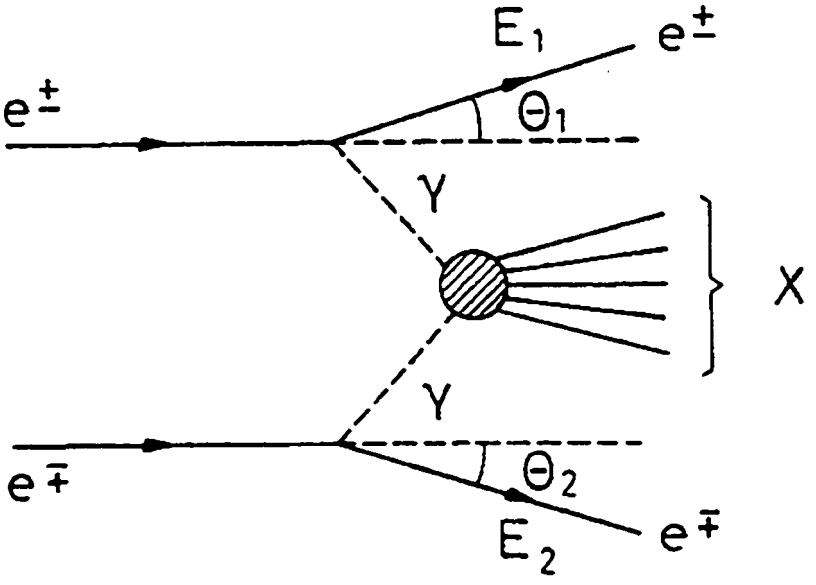

Figure 4.13: QED two photon process

Chapter 5

Study of $\psi(2S) \to \gamma K\overline{K}$ Final States

The $\psi(2S) \to \gamma K\overline{K}$ has been investigated through two channels, the $\psi(2S) \to \gamma K^+K^-$ and $\psi(2S) \to \gamma K^0_S K^0_S \to \gamma\pi^+\pi^-\pi^+\pi^-$. These decay modes are particularly interesting because of the production of the $f_J(1710)$, a possible glueball candidate. The $f_J(1710)$ has been observed in Fixed-Target experiment and J/ψ radiative decay. In pp central production in both K^+K^- and $K^0_S K^0_S$ study, the spin of $f_J(1710)$ is 2 [29]. In J/ψ radiative decay, both Mark III and DM2 observed signal in K^+K^- and $K^0_S K^0_S$ [22] [23]. A reanalysis of Mark III's result indicate a scalar at $\sim$ 1750 MeV and a tensor at $\sim$ 1620 MeV [27]. A recent BES moment analysis of the K^+K^- channel also indicated a lower mass tensor and a higher mass scalar [30], although the masses of tensor and scalar obtained from these two analyses are quite different. We will measure the decay branching fraction in the $\psi(2S)$ decay and will compare with that in the J/ψ decay.

5.1. Study of $\psi(2S) \to \gamma K^+K^-$ Final State

We chose events with two opposite charged tracks and at least one good photon. Cuts applied for this channel are similar to those described in Chapter 3 and Section 4.1 for $\gamma\pi^+\pi^-$ channel. In order to remove $\gamma\pi^+\pi^-$ background, we imposed:

$$CL_{(\chi^2_{TOF}+\chi^2_{dE/dx}+\chi^2_{KF})}(\gamma K^+K^-) > CL_{(\chi^2_{TOF}+\chi^2_{dE/dx}+\chi^2_{KF})}(\gamma\pi^+\pi^-) \qquad (5.1)$$

$$CL_{(\chi^2_{TOF}+\chi^2_{dE/dx}+\chi^2_{KF})}(\gamma K^+K^-) > 0.01 \qquad (5.2)$$

The invariant mass of K^+K^- is shown in Fig. 5.1(a). A $f_J(1710)$ signal is clearly presented in the plot. Again, QED background from reaction $e^+e^- \to \gamma o \to \gamma K^+K^-$ and $e^+e^- \to \gamma\mu^+\mu^-$ can also be seen in the plot.

We used the same technique we used in Section 4.1 to remove these backgrounds, that is, using the BES τ scan data. Fig. 5.1(b) is similar to Fig. 5.1(a) except it is from the τ scan data. The ratio of the number of events under the o signal

$$\frac{N_o(\psi(2S))}{N_o(\tau)} = 1.30$$

is consistent with the ratio yield from [17] [18] and Eq. (4.3). But is considered to be less accurate due to the limited number of events under o signal in both plots of Fig. 5.1.

The dot-line histogram in Fig. 5.2 from τ data has been normalized using Eq. (4.3). The data points with error bars in Fig. 5.4 are the result of subtraction of the two histograms in Fig. 5.2. The error bars are determined in the same way as described in Eq. (4.10). An S-wave Breit-Wigner function has been used to describe the $f_J(1710)$ signal. A D-wave Breit-Wigner at the mass region of $f_2'(1525)$ was added to describe the line-sharp at the region. Both Breit-Wigners are wide and Eq. (4.4) and Eq. (4.5) are used for them. Again, each τ events has been assigned a negative weight $-\omega = -1.43$ in the mass fit.

The efficiency of the analysis is 33.6%. The mass resolution is 8 MeV. They are both determined by a uniform phase space Monte Carlo simulation with Breit-Wigner function described in Eq. (4.4) (See Fig. 5.3). We fix the mass and width of $f_J(1710)$ and $f_2'(1525)$ to the PDG value, that is, $M_{f_J(1710)} = 1712\ MeV$, $\Gamma_{f_J(1710)} = 133\ MeV$, $M_{f_2'(1525)} = 1525\ MeV$ and $\Gamma_{f_2'(1525)} = 76\ MeV$ and we determined that there are $N = 71.9 \pm 14.4$ $f_J(1710)$ events and $N = 19.7 \pm 8.6$ $f_2'(1525)$ events under the fitting curve. The following branching ratios are determined from these numbers

$$\begin{aligned} B(\psi(2S) \to \gamma f_J(1710) \to \gamma K^+K^-) &= \frac{N}{N_{\psi(2S)} \times \epsilon} \\ &= (5.8 \pm 2.0 \pm 1.0) \times 10^{-5} \end{aligned} \tag{5.3}$$

$$B(\psi(2S) \to \gamma f_2'(1525)) = \frac{N}{N_{\psi(2S)} \times \epsilon \times B(f_2'(1525)) \to K\overline{K}) \times \frac{1}{2}}$$

$$= (3.60 \pm 1.57) \times 10^{-4} \tag{5.4}$$

where $\epsilon = 33.6\%$ is the analysis efficiency. The factor $\frac{1}{2}$ comes from the Clebsch-Gordan coefficients for isospin-0 particles (See. Eq. (4.11)).

The $f_J(1710)$ is considered to have spin-parity of $even^{++}$. The spin has not been determined yet. Some experiments prefer spin-0 while others gave spin-2. We include the difference from spin-2 hypotheses into our systematic error. Table. 5.1 listed the number of events survives each cut. Table. 5.2 listed the major sources of systematic errors.

Both Mark III and DM2 experiment measured the $B(J/\psi \to \gamma f_J(1710) \to \gamma K^+K^-)$ and their results are $(4.8 \pm 0.6 \pm 0.9) \times 10^{-4}$ and $(4.6 \pm 0.7 \pm 0.7) \times 10^{-4}$ respectively [22] [23]. Combining them together we have $B(J/\psi \to \gamma f_J(1710) \to \gamma K^+K^-) = (4.7 \pm 0.5 \pm 0.5) \times 10^{-4}$. Compare Eq. (5.3) with this, we have

$$Q = \frac{B(\psi(2S) \to \gamma f_J(1710) \to \gamma K^+K^-)}{B(J/\psi \to \gamma f_J(1710) \to \gamma K^+K^-)} = (12.3 \pm 4.3 \pm 4.6)\%$$

This shows that the theoretical prediction of "15%" is also followed in this decay mode. Similarly, if we compare the branching fraction of $\psi(2S) \to \gamma f_2'(1525)$ with $B(J/\psi \to \gamma f_2'(1525)) = (6.3 \pm 1.0) \times 10^{-4}$ from PDG, we have

$$Q = \frac{B(\psi(2S) \to \gamma f_2'(1525))}{B(J/\psi \to \gamma f_2'(1525))} = 57.1 \pm 24.9\%$$

Cuts	Data	Monte Carlo
Number of events come in	4786432	14305
$\sum Q_i = 0$; $N_\gamma > 0$; mfit=2	1062523	9165
γ hit at BSC, $E_\gamma > 10MeV$	971176	8176
$\lvert Z_1 - Z_2\rvert < 5cm$; $\lvert Z_V\rvert < 15cm$; $\theta_{\pi^+\pi^-} < 175^\circ$	402323	7277
Total μ layers$\geq$3; $\lvert\cos(\theta_K)\rvert < 0.85$; $R_{xy} < 2cm$; $Z < 15cm$; $E/P < 0.75$; $(E_+/P_+ - 1)^2 + (E_-/P_- - 1)^2 > 0.4$;	222326	6033
$P_{(\chi^2_{TOF}+\chi^2_{dE/dx}+\chi^2_{KF})}(\gamma K^+K^-) > P_{(\chi^2_{TOF}+\chi^2_{dE/dx}+\chi^2_{KF})}(\gamma\pi^+\pi^-)$ $P_{(\chi^2_{TOF}+\chi^2_{dE/dx}+\chi^2_{KF})}(\gamma K^+K^-) > 0.01$	1243	4818
$\theta_{\gamma\pi} > 15^\circ$	1237	4802

Table 5.1: Number of γK^+K^- events survive various cuts

which is much higher than the "15%" prediction.

According to Eq (4.14) and $B(f_2(1270) \to \gamma K^+K^-) = (4.6 \pm 0.5)\%$ from the PDG, we estimate that ~ 6.7 $\psi(2S) \to \gamma f_2(1270) \to \gamma K^+K^-$ events may appear at $\sim$ 1.3 GeV region in Fig. 5.4. Unfortunately we do not have good a fit in the region. Also by feeding $\psi(2S) \to \gamma\pi^+\pi^-$ Monte Carlo simulated events into the $\psi(2S) \to \gamma K^+K^-$ analysis procedure, we are able to estimate that only $\sim 1\%$ of the $\psi(2S) \to \gamma\pi^+\pi^-$ events may have both $\pi^\pm$ misidentified as $K^\pm$ and appeared in Fig. 5.4 at $\sim$ 1.5 GeV region (see Fig. 5.5(a)), which contribute ~ 5 events. Fig. 5.5(b) shows the contamination from $\psi(2S) \to \gamma\pi^+\pi^-$ with no intermediate $\pi^+\pi^-$ resonant. It is considered to be negligible.

Major cuts	$B(\psi(2S) \to \gamma f_J(1710)) \to K^+K^-$ difference(%)
$P_{\chi^2}(\gamma K^+K^-) > 0.01 \to 0.05$	8.1%
$\lvert Z_V \rvert < 15cm \to 10cm$	4.8%
$\theta_{\gamma\pi} > 15^\circ \to 10^\circ$	2.4%
$(E_+/P_+ - 1)^2 + (E_-/P_- - 1)^2 > 0.4 \to 0.6$	0%
Fitting Region $1.0 \sim 2.5$ GeV to $1.0 \sim 2.0$	4.8%
Assuming spin 2 for $f_J(1710)$	4%
Number of $\psi(2S)$ events	8%
Uncertainty of TELESIS	10%
Total	16.4%

Table 5.2: Systematic error estimation of $B(\psi(2S) \to \gamma f_J(1710)) \to \gamma K^+K^-$

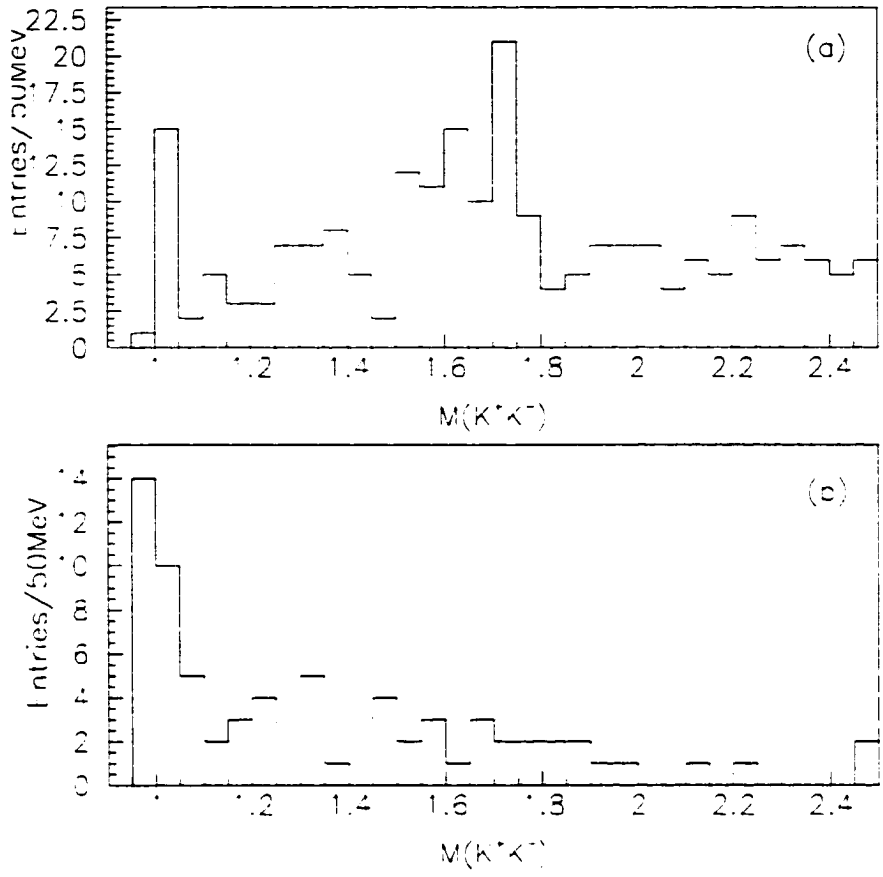

Figure 5.1: Invariant mass of K^+K^- from $\psi(2S)$ data(a) and τ data(b)

5.2. Study of $\psi(2S) \to \gamma K_S^0 K_S^0$ Final State

In the study of this channel, we look at the final state of $\gamma K_S^0 K_S^0 \to \gamma\pi^+\pi^-\pi^+\pi^-$ where each K_S^0 decay into a pair of $\pi^+\pi^-$. The event selection of this channel begins from the DST data by requiring for charged tracks. The selection criteria for a single track are similar to what we have done previously except that we replace $R_{xy} < 2$ cm by a much looser cut of $R_{xy} < 20$ cm due to the fact that K_S^0 can travel much longer

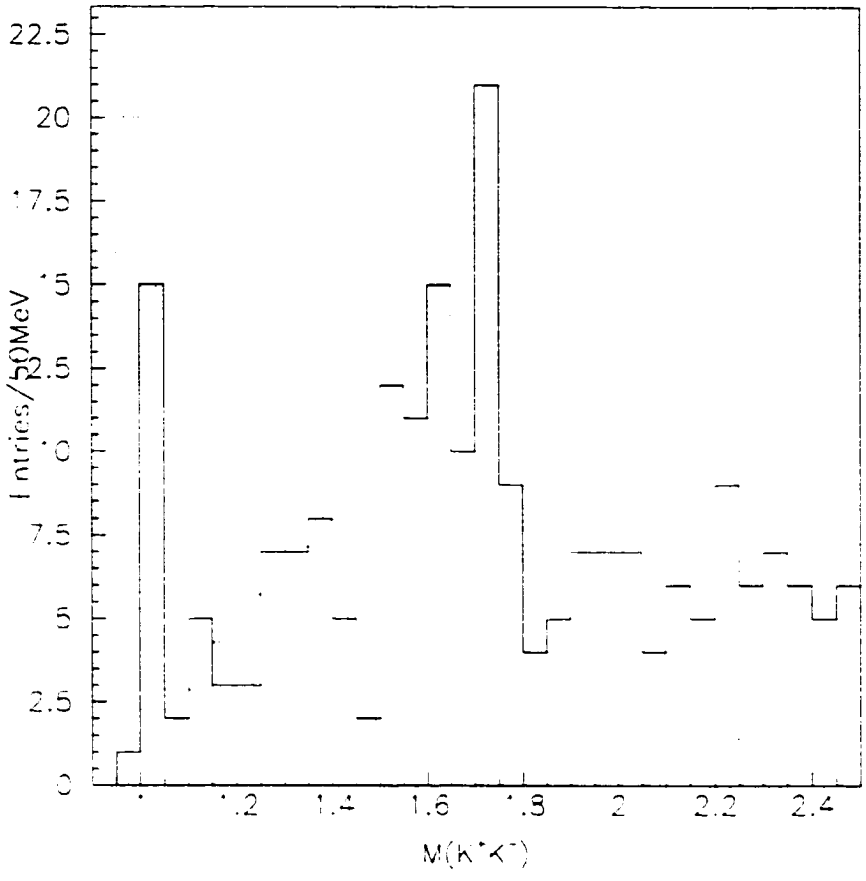

Figure 5.2: Invariant mass of K^+K^- from $\psi(2S)$ data and τ data (in dot-line histogram) after normalization

than 2 cm. In addition, we require

- A 4-constraint fit with all good photons as radiative photon candidate in all $\gamma\pi_1^+\pi_2^-\pi_3^+\pi_4^-$ combination. The successful combination should have 4-C fit χ^2 confidence level higher than 0.01. Both K_S^0 candidates should be also identified

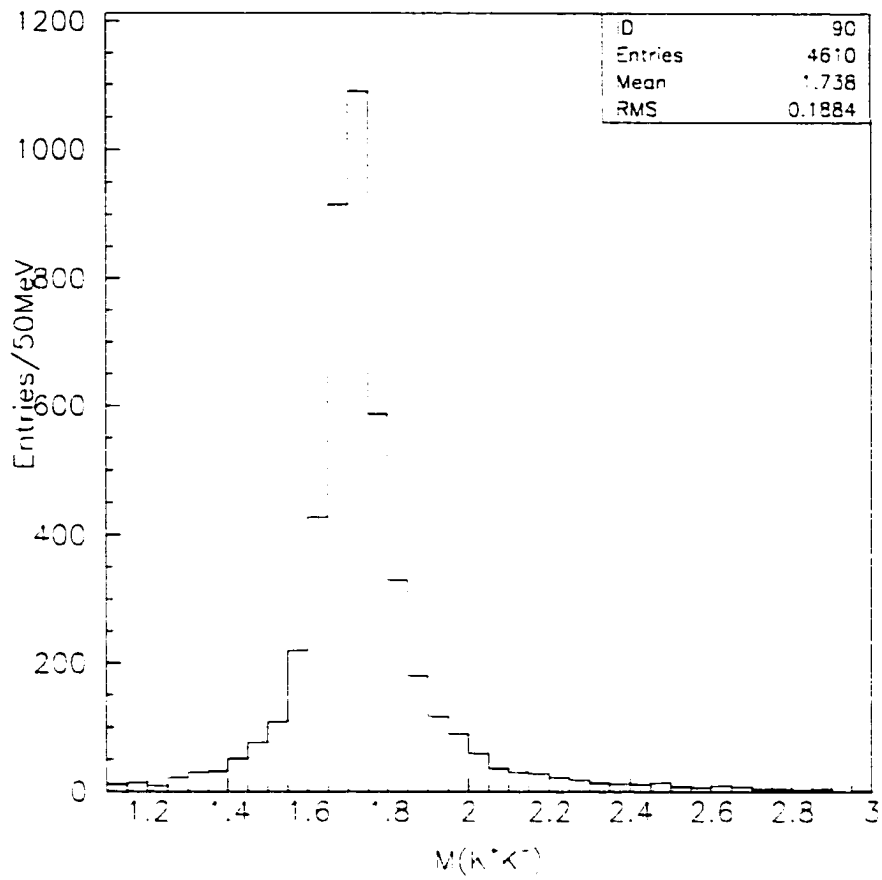

Figure 5.3: $M_{K^+K^-}$ from Monte Carlo simulated data.

by vertex finding program VEEFND and should have the minimum value of

$$\sqrt{(m_{\pi_1^+\pi_2^-} - m_{K_S^0})^2 + (m_{\pi_3^+\pi_4^-} - m_{K_S^0})^2}$$

amount all combinations.

- Each $\pi^+\pi^-$ pair should satisfy $|m_{\pi^+\pi^-} - m_{K_S^0}| < 20$ MeV (see Fig. 5.6(b)).

Fig. 5.8(a) is the χ^2 confidence level distribution. Fig. 5.8(b) is life time distribution of K^0_S in term of $c\tau$ where c is the speed of light and τ is the lifetime. From the relation:

$$N = N_0 e^{-t/\tau} = N_0 e^{-ct/c\tau}$$

$$ct = -c\tau \ln(N) + c\tau \ln(N_0)$$

where ct is the x-axis of Fig. 5.8(b) and $\ln(N)$ is the y-axis. $c\tau = 3.28 \pm 0.15$ cm from the fitted measurement of the life time of the K^0_S.

In Fig. 5.8(c) we see obvious χ_{c0} signal (and may be χ_{c2} signal). The $\chi_{c0,2}$ decay into $\pi^+\pi^-$, K^+K^- and $K^0_S K^0_S$ have been studied by BES collaboration elsewhere [13] [31]. What we are interested are those events around the $1 \sim 2$ GeV.

We use a S-wave Breit-Wigner to fit the invariant mass of $K^0_S K^0_S$. The number of $f_J(1710)$ events under the fitting curve in Fig. 5.10 is 6.8 ± 3.1. If we treat the fitting curve as a Gaussian function with central value at 6.8 and $\sigma = 3.1$, we can also give a upper limit of 10.8 events at 90% confidential level. Monte Carlo simulation shows that the detecting efficiency is 18.0% (Fig. 5.9). Consider that $B(f_J(1710) \to K^0\overline{K^0}) : B(f_J(1710) \to K^0_S K^0_S) = B(f_J(1710) \to K^0_L K^0_L) = 2 : 1 : 1$ due to the fact that decay process $f_J(1710) \to \gamma K^0_L K^0_S$ violate C-parity.

$$B(\psi(2S) \to \gamma f_J(1710) \to K^0\overline{K^0}) = (4.4 \pm 2.0 \pm 2.3) \times 10^{-5}$$

Cuts	Data	Monte Carlo
Starting Number of events	2370479	14305
$\sum Q_i = 0$; $N_\gamma > 0$; mfit=2	569865	6479
γ hit at BSC, $E_\gamma > 10MeV$	561215	5178
$\lvert\cos(\theta_\pi)\rvert < 0.85$: $R_{xy} < 2cm$: $Z < 15cm$: $E/P < 0.75$	407819	4455
$P_{\chi^2}(\gamma\pi^+\pi^-\pi^+\pi^-) > 0.01$	11900	3351
$\lvert m_{\pi^+\pi^-} - m_{K^0_S}\rvert < 20MeV$: VEEFND finds both vertexes	74	2580

Table 5.3: Number of $\gamma\pi^+\pi^-\pi^+\pi^-$ events survive various cuts

Major cuts	$B(\psi(2S) \to \gamma f_J(1710) \to \gamma K^0_S K^0_S)$ difference(%)
$P_{\chi^2}(\gamma\pi^+\pi^-\pi^+\pi^-) > 0.01 \to 0.05$	20%
$\lvert m_{\pi^+\pi^-} - m_{K^0_S}\rvert < 20MeV \to 10MeV$	28%
Number of Vee $\geq 2 \to 1$	38%
Number of $\psi(2S)$ events	8%
Uncertainty of TELESIS	10%
Total	52.8%

Table 5.4: Systematic error estimation in $B(\psi(2S) \to \gamma K^0_S K^0_S)$

or

$$B(\psi(2S) \to \gamma f_J(1710) \to K^0\overline{K^0}) < 8.3 \times 10^{-5} \quad (90\%\ C.\ L.)$$

The number of events surviving major cuts and the systematically error estimation can be found at Table. 5.3 and Table. 5.4.

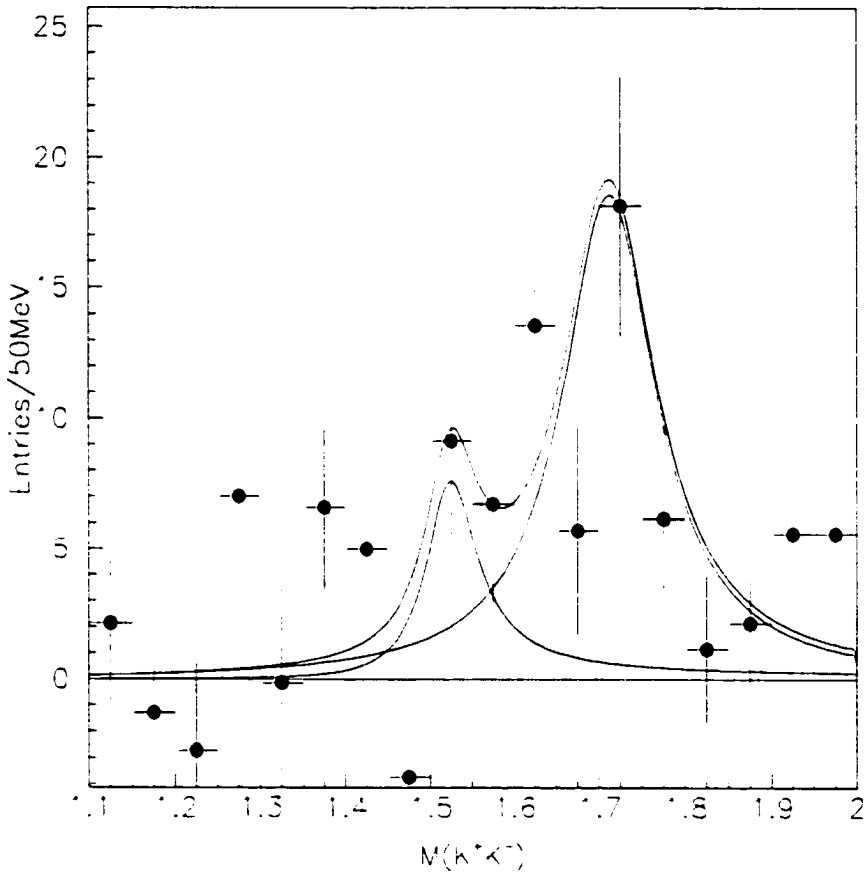

Figure 5.4: Data points with error bar are the difference between the two histograms in Fig. 5.2. The curve is the fitting result with Breit-Wigner function described by Eq. 4.4.

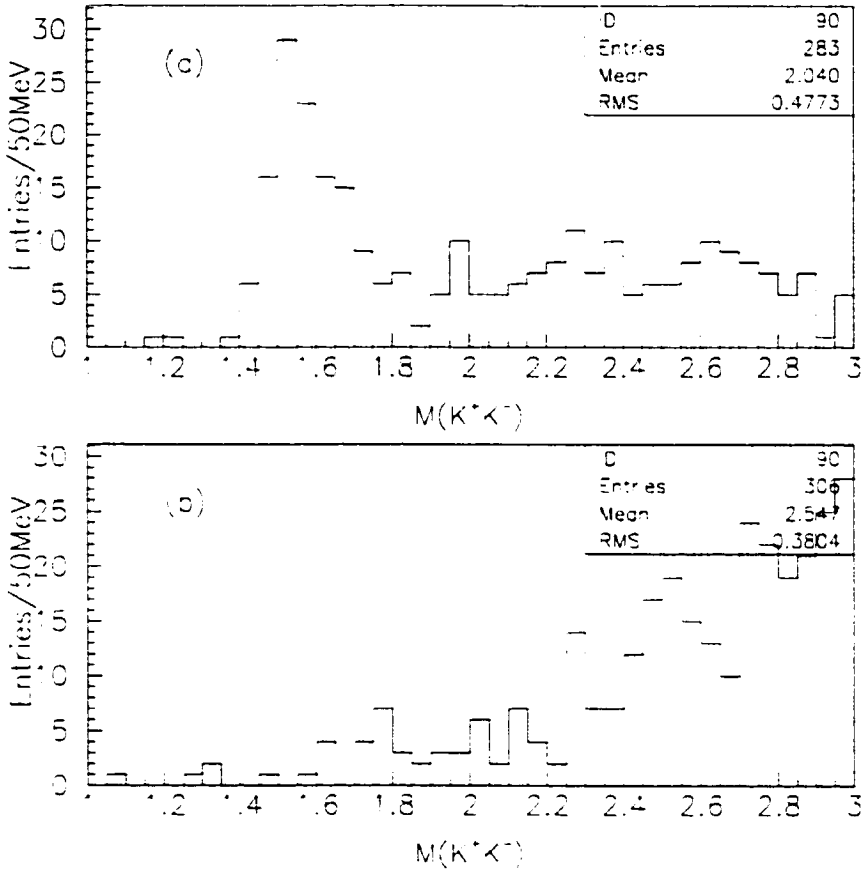

Figure 5.5: Invariant mass of K^+K^- in (a) $\psi(2S) \to \gamma f_2(1270) \to \gamma\pi^+\pi^-$ Monte Carlo (b) $\psi(2S) \to \gamma\pi^+\pi^-$ Monte Carlo following misidentification of both $\pi^\pm$ as $K^\pm$

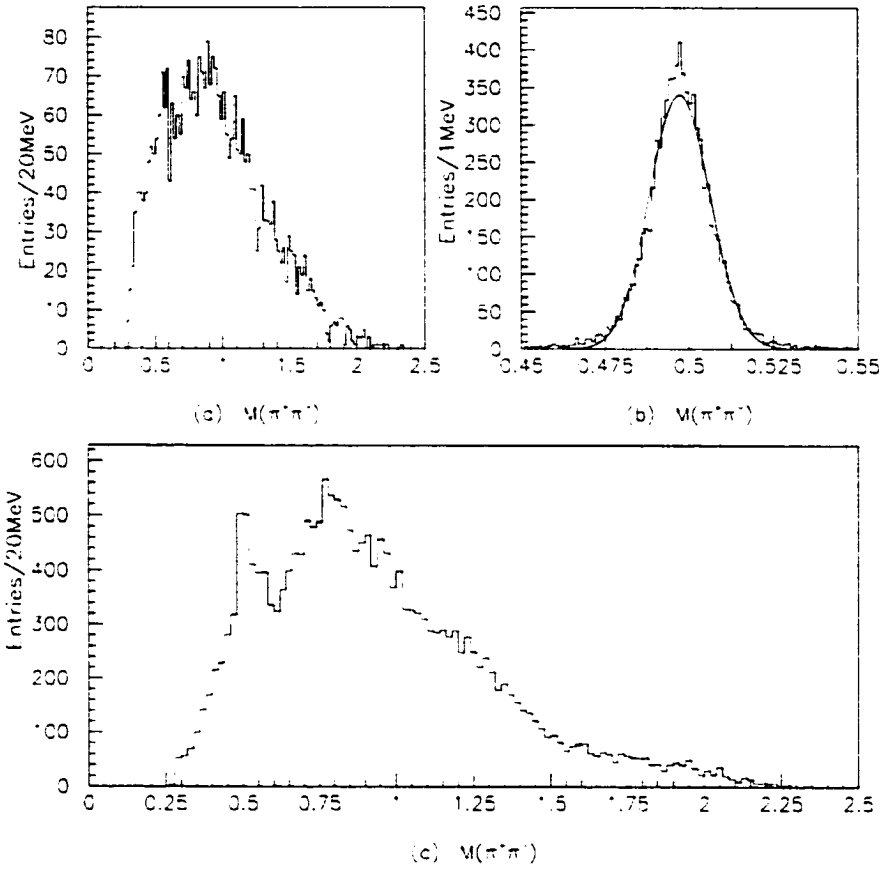

Figure 5.6: Invariant mass of $\pi^+\pi^-$ in (a) $\psi(2S) \to \gamma\pi^+\pi^-\pi^+\pi^-$ Monte Carlo (b) $\psi(2S) \to \gamma f_J(1710) \to \gamma K_S^0 K_S^0 \to \gamma\pi^+\pi^-\pi^+\pi^-$ Monte Carlo (c) $\psi(2S)$ data. A Gaussian fit over (b) gives a $M_{\pi^+\pi^-}$ mass resolution of 9.0 MeV.

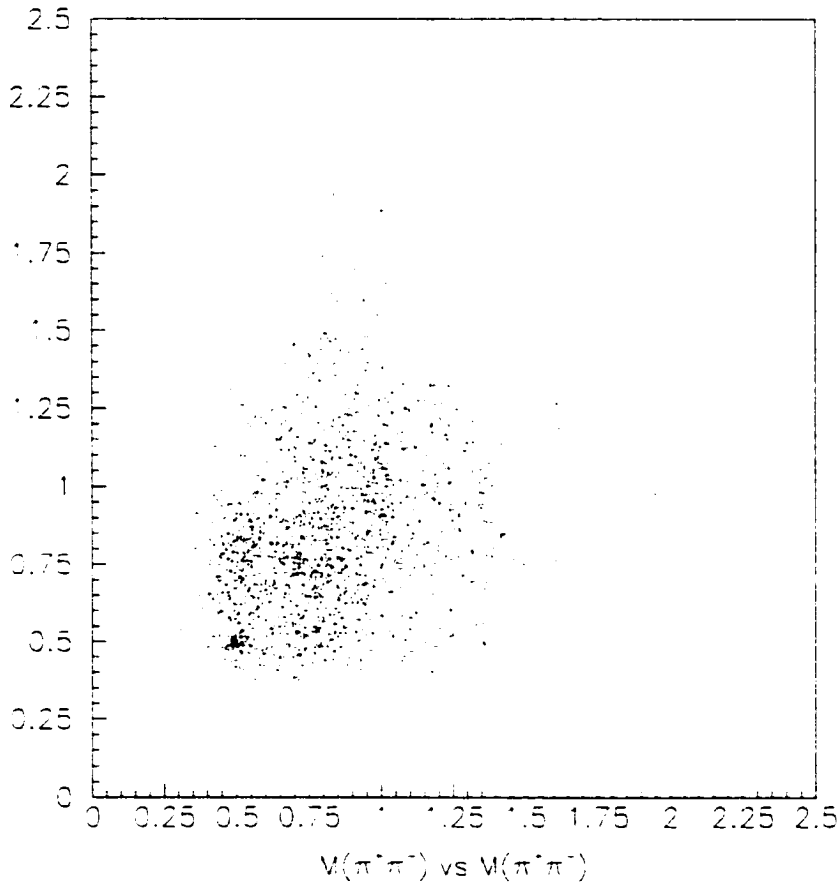

Figure 5.7: $M_{\pi^+\pi^-}$ vs. $M_{\pi^+\pi^-}$ in $\psi(2S)$ data.

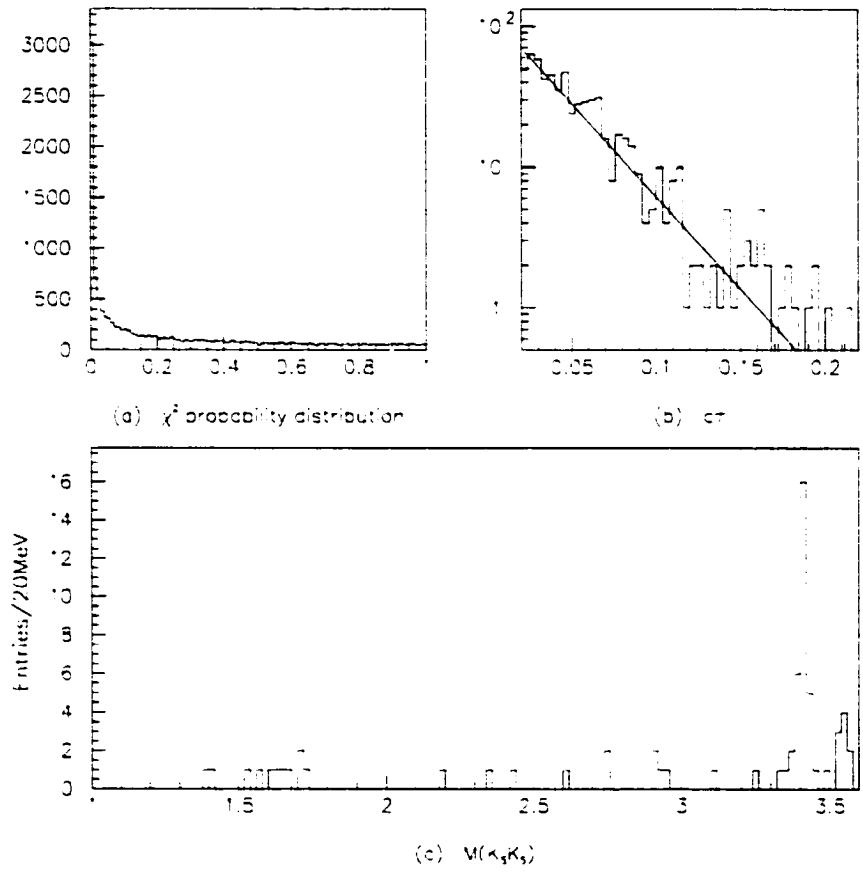

Figure 5.8: From $\psi(2S)$ data: (a) χ^2 distribution (b) lifetime of K^0_S. $c\tau = 3.28cm$ (c) Invariant mass distribution of $K^0_S K^0_S$.

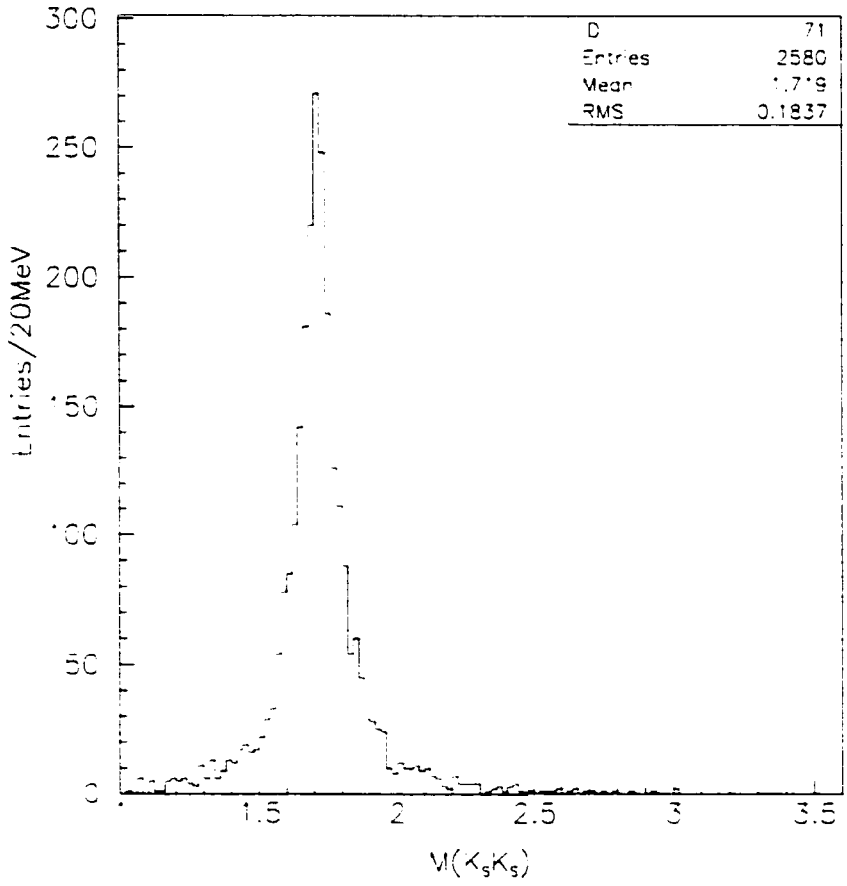

Figure 5.9: Invariant mass distribution of $K_S^0 K_S^0$ from Monte Carlo data.

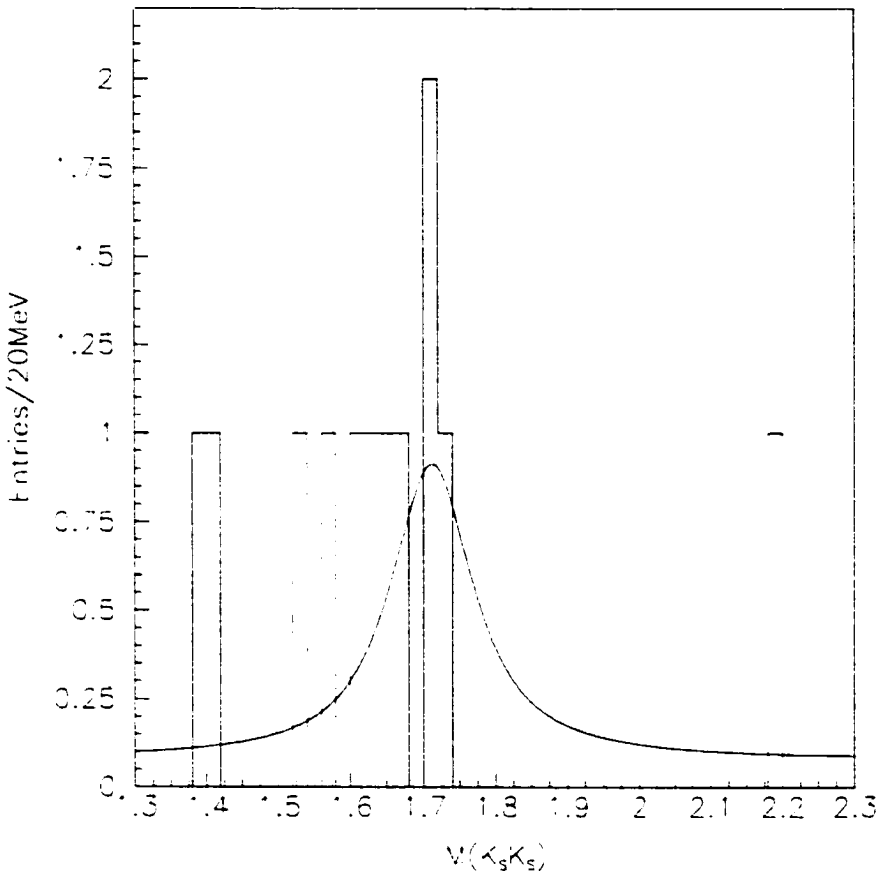

Figure 5.10: Invariant mass distribution of $K_S^0 K_S^0$ in $\psi(2S)$ data.

Chapter 6

Study of $\psi(2S) \to \gamma\eta\eta$ Final State

The event selection of the $\psi(2S) \to \gamma\eta\eta$ mode is the same as was done in $\psi(2S) \to \gamma\pi^0\pi^0$ channel except that we replace the restriction of $|M_{\gamma\gamma} - M_{\pi^0}| < 70$ MeV by $|M_{\gamma\gamma} - M_\eta| < 70$ MeV and replace the π^0 resonant mass in kinematic fit by η mass. Fig. 6.1 shows the invariant mass of photon pairs. In this channel, one of the difficulties that we did not meet in the $\psi(2S) \to \gamma\pi^0\pi^0$ mode is that the opening angle of the two photons are much wider than that in the π^0 decay due to the fact that on average, η momentum is smaller than π^0 momentum because of its higher mass. In this situation, the relatively good spatial resolution of the BSC does not help. In Fig. 6.1, the mass distribution of the η signal is wider than $M_{\gamma\gamma}$ for the π^0 in Fig. 4.6.

The invariant mass distributions of $\gamma\gamma\gamma\gamma$ are shown in Fig. 6.2 with $M_{\gamma\gamma}$ within 70 MeV of the η mass (Fig. 6.2(e)) and outside at sideband. Crystal Ball experiment

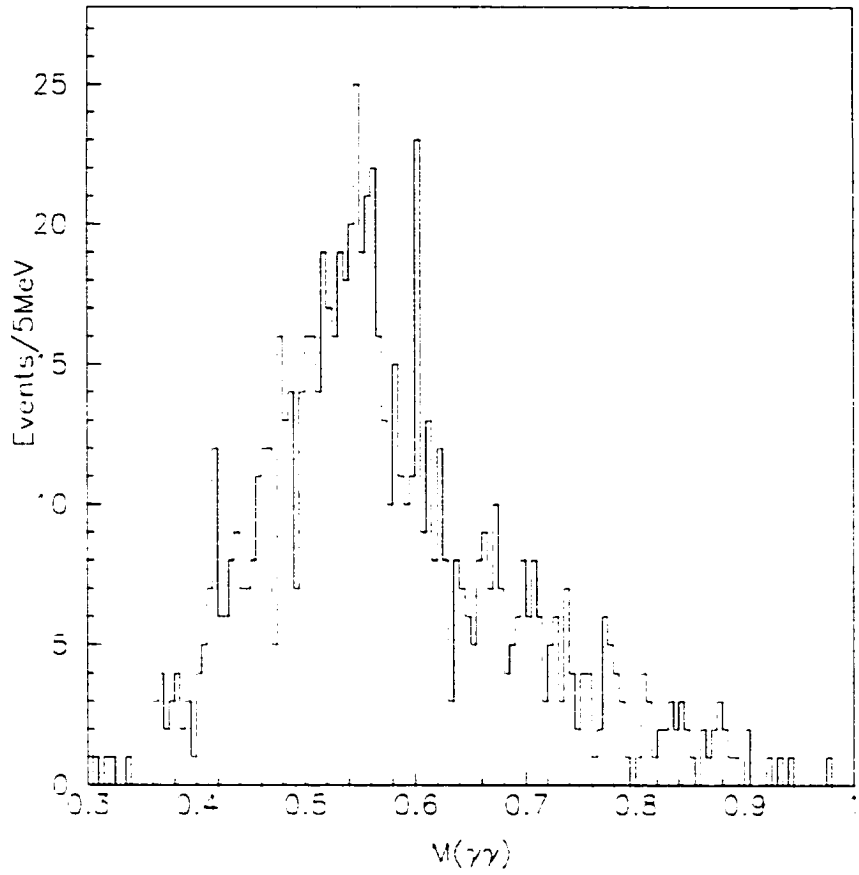

Figure 6.1: Invariant mass distribution of $\gamma\gamma$ from $\psi(2S)$ data.

observed an $\eta\eta$ signal at 1670 ± 50 MeV in $J/\psi \to \gamma\eta\eta$ [32]. In our case, in the region where $M_{\gamma\gamma\gamma} < 2$ GeV in Fig. 6.3, we see evidence of signals. But so far we can't claim any statistical significant signal from them. As a comparison, we also show the Crystal Ball's result of $\eta\eta$ invariant mass from $\psi(2S)$ radiative decay, which has nothing below 3 GeV.

The χ_{c0} signal and a weak χ_{c2} signal can be seen at above 3 GeV region in Fig.

6.2(e). An expanded version of mass plot at this region is shown in Fig. 6.5. We fit this plot with two Breit-Wigner plus a flat background (lowest of polynomial background) and obtain.

$$N(\chi_{c0}) = 12.7 \pm 5.3 \quad (6.1)$$

$$N(\chi_{c2}) = 2.1 \pm 3.0$$

$$< 5.9 \quad (90\%\ C.L.) \quad (6.2)$$

From the Monte Carlo simulation of these two channels we know that the detection and analyzing efficiency are 11.9% and 10.5% for χ_{c0} and χ_{c2} respectively. We used the PDG value of $B(\psi(2S) \to \gamma\chi_{c0}) = 9.3 \pm 0.8\%$ and $B(\psi(2S) \to \gamma\chi_{c2}) = 7.8 \pm 0.8\%$ to determine branching fractions of χ_{c0} and χ_{c2} decay into $\eta\eta$.

$$B(\chi_{c0} \to \eta\eta) = (2.03 \pm 0.84 \pm 0.61) \times 10^{-3} \quad (6.3)$$

$$B(\chi_{c2} \to \eta\eta) < 1.28 \times 10^{-3} \quad (6.4)$$

These branching fractions agree with the previous measurement by the Crystal Ball experiment [14][1]

$$B(\chi_{c0} \to \eta\eta) = (2.5 \pm 0.8 \pm 0.8) \times 10^{-3}$$

[1]These are the numbers from the PDG 96. see footnote in page 69

$$B(\chi_{c2} \to \eta\eta) = (7.9 \pm 4.1 \pm 2.4) \times 10^{-4}$$

As we discussed in Section 1.2.3, SU(3) flavor symmetric predicts that the decay branching fractions of χ_{c0} and χ_{c2} into $\pi^0\pi^0$ and $\eta\eta$ would be 0.95 (and 0.79 for χ_{c2}). The ratio from our measurement is

$$\frac{B(\chi_{c0} \to \eta\eta)}{B(\chi_{c0} \to \pi^0\pi^0)} = 0.73 \pm 0.31 \pm 0.23$$

It is consistent with the theoretical prediction.

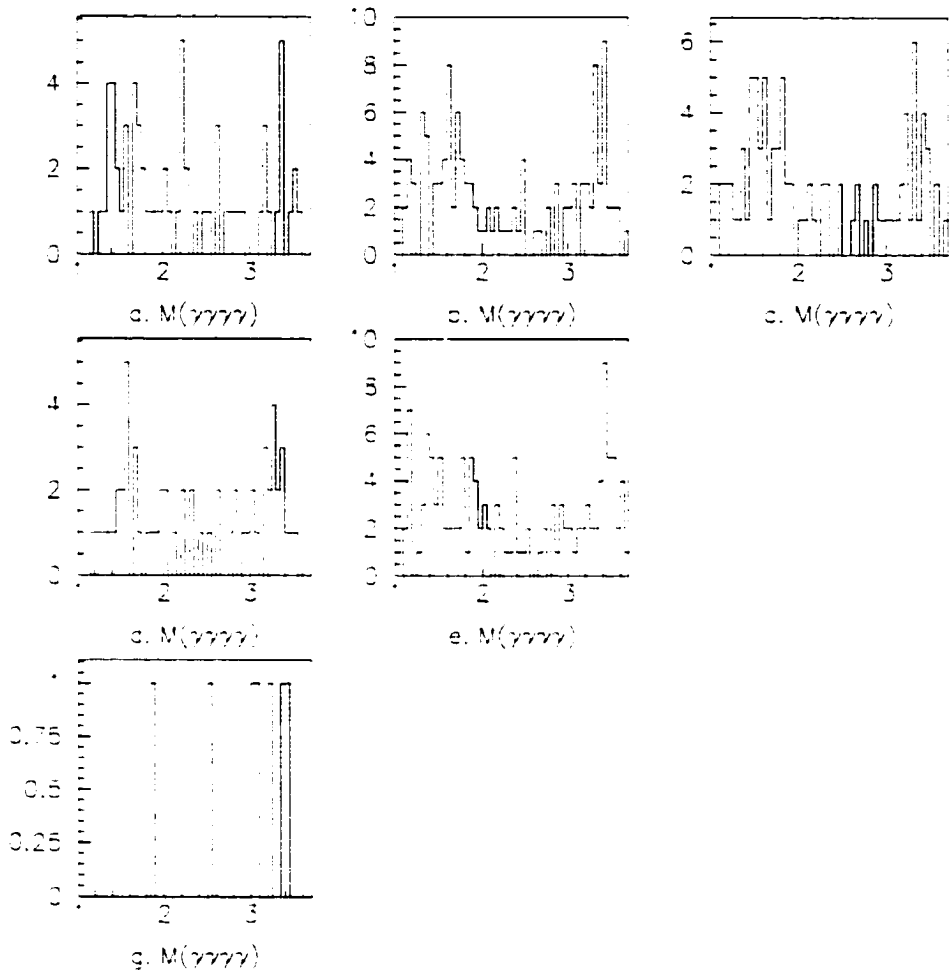

Figure 6.2: Mass of two pairs of γ's within η mass range or at sidebands. a: $M_{\gamma_2\gamma_3} < 0.472 MeV$ and $M_{\gamma_4\gamma_5} > 0.622 MeV$: b: $0.472 MeV < M_{\gamma_2\gamma_3} < 0.622 MeV$ and $M_{\gamma_4\gamma_5} > 0.622 MeV$: c: $M_{\gamma_2\gamma_3} > 0.622 MeV$ and $M_{\gamma_4\gamma_5} > 0.622 MeV$: d: $M_{\gamma_2\gamma_3} < 0.472 MeV$ and $0.472 MeV < M_{\gamma_4\gamma_5} < 0.622 MeV$: e: signal region $0.472 MeV < M_{\gamma_2\gamma_3} < 0.622 MeV$ and $0.472 MeV < M_{\gamma_4\gamma_5} < 0.622 MeV$: g: $M_{\gamma_2\gamma_3} < 0.472 MeV$ and and $M_{\gamma_4\gamma_5} < 0.472 MeV$

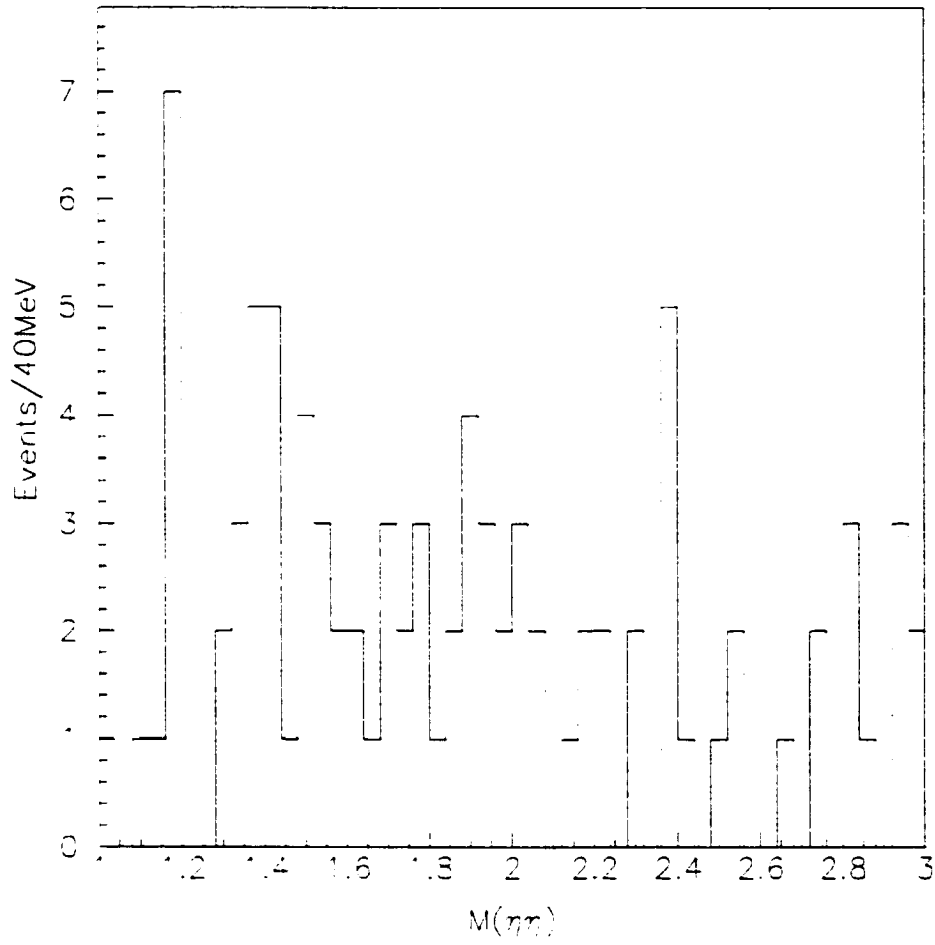

Figure 6.3: Mass of two pairs of γ's within 70 MeV of the η mass range. It is an expanded version of Fig. 6.2(e) from $1 \sim 3$ GeV.

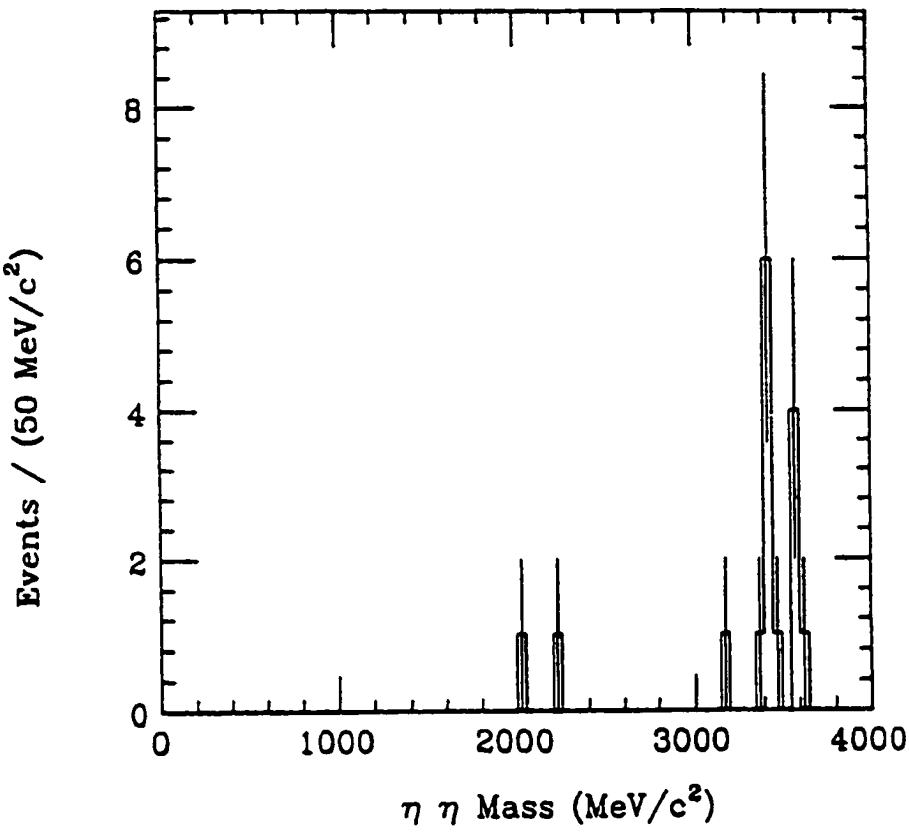

Figure 6.4: Crystal Ball's result of $M_{\eta\eta}$ from $\psi(2S)$ radiative decay.

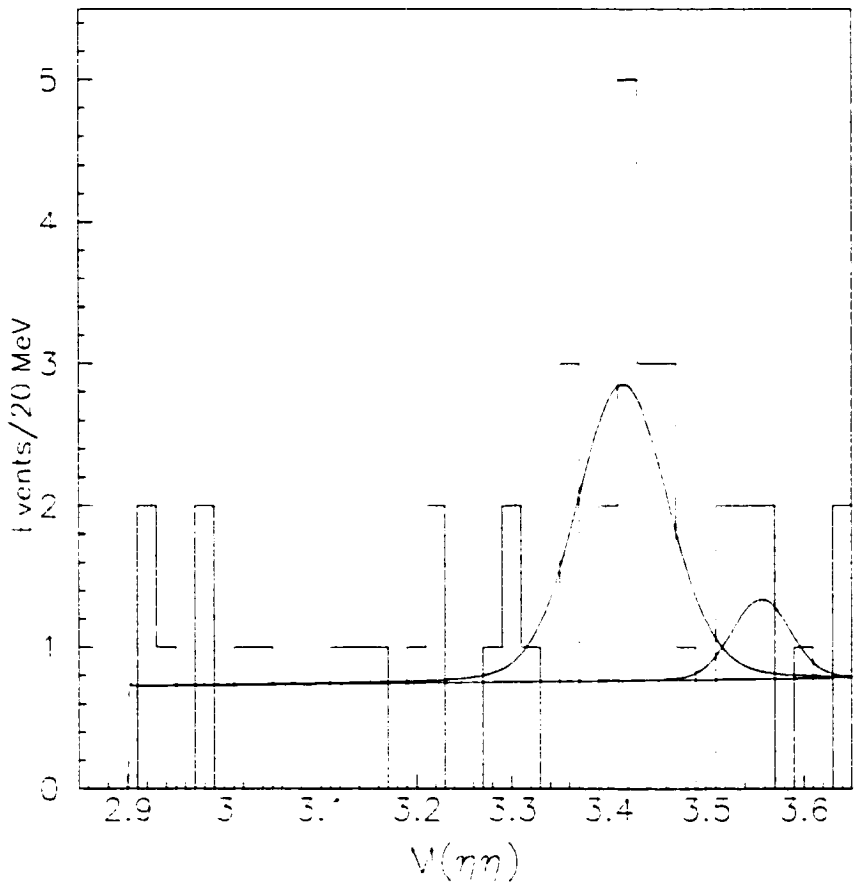

Figure 6.5: Invariant mass distribution of $\eta\eta$ at χ_c region.

Chapter 7

Summary and Conclusion

This analysis used the $\sim 3.79 \times 10^6$ $\psi(2S)$ data collected by the BES detector and measured various branching fractions for the $\psi(2S) \to \gamma$ + two pseudo-scalars in order to test the predicted "15%" relation in $\psi(2S)$ radiative decay, the SU(3) flavor symmetry in ω decay and to search for possible glueball candidates $f_0(1500)$ and $f_J(1710)$.

7.1. $\psi(2S) \to \gamma\pi\pi$ with Non-charmonium Resonance

In the $\psi(2S) \to \gamma\pi^+\pi^-$ and $\psi(2S) \to \gamma\pi^0\pi^0$ channels, we have measured

$$B(\psi(2S) \to \gamma f_2(1270)) = (2.31 \pm 0.27 \pm 0.39) \times 10^{-4} \tag{7.1}$$

$$B(\psi(2S) \to \gamma f_J(1710) \to \gamma\pi\pi) = (3.51 \pm 0.90 \pm 1.46) \times 10^{-5} \tag{7.2}$$

and

$$B(\psi(2S) \to \gamma f_2(1270)) = (3.01 \pm 1.12 \pm 1.12) \times 10^{-4} \tag{7.3}$$

respectively. We combined these two $f_2(1270)$ decay results together.

$$B(\psi(2S) \to \gamma f_2(1270)) = (2.37 \pm 0.26 \pm 0.37) \times 10^{-4} \tag{7.4}$$

Comparing to the theoretical prediction of the "15%" rule,

$$\frac{B(\psi(2S) \to \gamma f_2(1270))}{B(J/\psi \to \gamma f_2(1270))} = (17.2 \pm 1.9 \pm 2.6)\% \tag{7.5}$$

shows that *The "15% rule" is followed in $\psi(2S)$ radiative decay into $\gamma f_2(1270)$.* Also

$$\frac{B(\psi(2S) \to \gamma f_J(1710) \to \gamma\pi\pi)}{B(J/\psi \to \gamma f_J(1710) \to \gamma\pi\pi)} = (14.7 \pm 4.6 \pm 7.6)\% \tag{7.6}$$

Crystal Ball experiment also measured the decay of $\psi(2S) \to \gamma\pi^0\pi^0$ and obtained $B(\psi(2S) \to \gamma f_2(1270)) = (1.5 \pm 0.4 \pm 0.5) \times 10^{-4}$. Our result is much larger then theirs. Fig. 7.1 shows their result [14].

In the J/ψ radiative decay, $\pi^+\pi^-$ and $\pi^0\pi^0$ mass spectrum have been measured by Mark III and Crystal Ball respectively [22] [14], as are shown in Fig. 4.5 and Fig. 7.2. They both saw a strong $f_2(1270)$ signal and a $f_J(1710)$ signal along with bumps around 2 GeV. In $\psi(2S)$ radiative decay, these two signals also appear in our $\pi^+\pi^-$

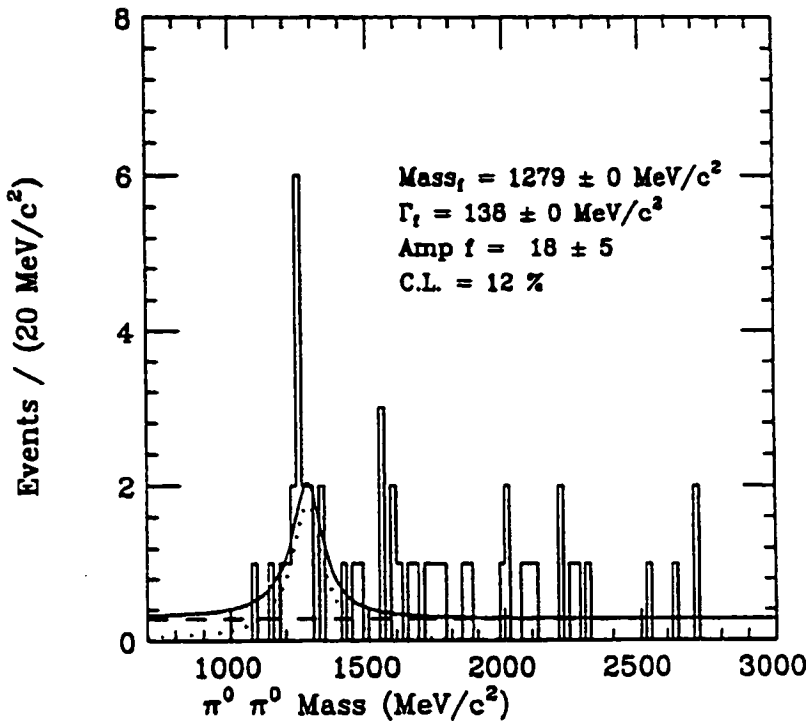

Figure 7.1: Crystal Ball's result of $M_{\pi^0\pi^0}$ from $\psi(2S) \to \gamma\pi^0\pi^0$

spectrum (Fig. 4.4) and maybe in Crystal Ball's $\pi^0\pi^0$ spectrum (Fig. 7.1). Only $f_2(1270)$ signal can be seen in our $\pi^0\pi^0$ spectrum (Fig. 4.8).

7.2. $\psi(2S) \to K\overline{K}$

In similar way, we measured $\psi(2S) \to \gamma K^+K^-$ channel and obtained,

$$B(\psi(2S) \to \gamma f_J(1710) \to \gamma K^+K^-) = (5.8 \pm 2.0 \pm 1.0) \times 10^{-5} \qquad (7.7)$$

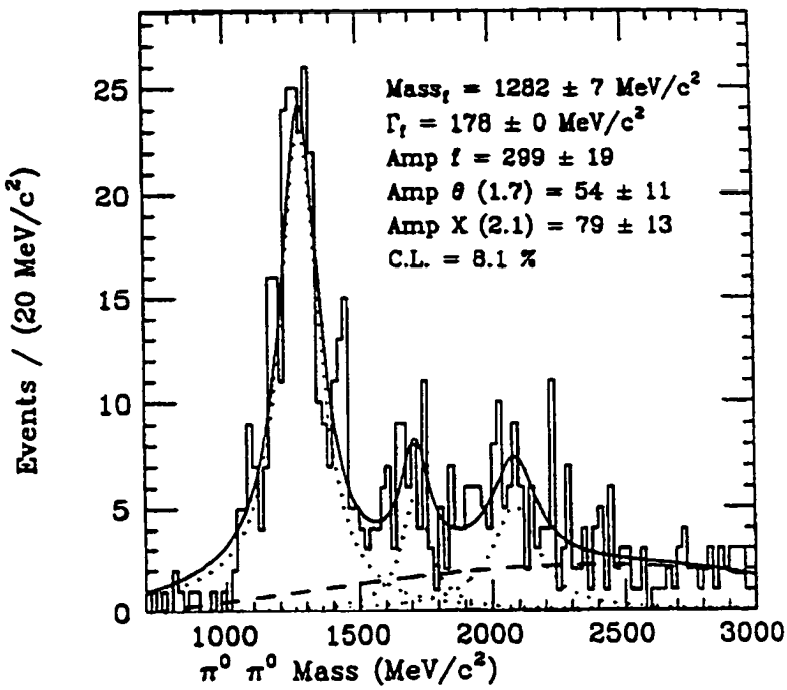

Figure 7.2: Crystal Ball's result of $M_{\pi^0\pi^0}$ from $J/\psi \to \gamma\pi^0\pi^0$

Assuming the isospin relation $B(f_J(1710) \to \gamma K\overline{K}) : B(f_J(1710) \to \gamma K^+K^-) : B(f_J(1710) \to \gamma K_S^0 K_S^0) = 4 : 2 : 1$ (see Appendix C).

$$B(\psi(2S) \to \gamma f_J(1710) \to \gamma K\overline{K}) = (1.16 \pm 0.40 \pm 0.20) \times 10^{-4} \qquad (7.8)$$

The K^+K^- mass spectrum we obtained in Fig. 5.4 has two bumps at $\sim$ 1.5 GeV and $\sim$ 1.7 GeV, which is similar to those measured by Mark III and BES in J/ψ radiative decay [22] [30], as shown in Fig. 7.3 and Fig. 7.4 respectively. However,

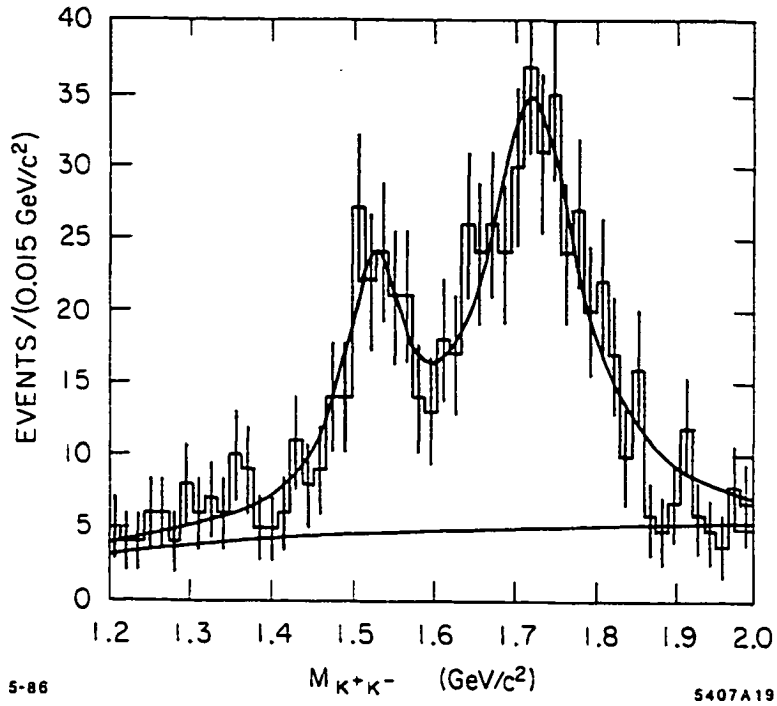

Figure 7.3: Invariant mass of K^+K^- from $J/\psi \to \gamma K^+K^-$ by Mark III

by using moment analysis method. they both claimed two particles at the region around 1.7 GeV. a low mass tensor and a high mass scalar. Several fixed-target experiments also observed spin-2 signal at $\sim$ 1.7 GeV region [29]. Due to the strong QED background and the lack of statistics. we have not tried to do any similar analysis to determine the spin of $f_J(1710)$.

Compared with a combined result of $B(J/\psi \to \gamma f_J(1710) \to \gamma K^+K^-) = (4.7 \pm 0.5 \pm 0.5) \times 10^{-4}$ from Mark III and DM2 [22] [23]. we have.

$$\frac{B(\psi(2S) \to \gamma f_J(1710) \to \gamma K^+K^-)}{B(J/\psi \to \gamma f_J(1710) \to \gamma K^+K^-)} = (12.3 \pm 4.3 \pm 4.6)\% \qquad (7.9)$$

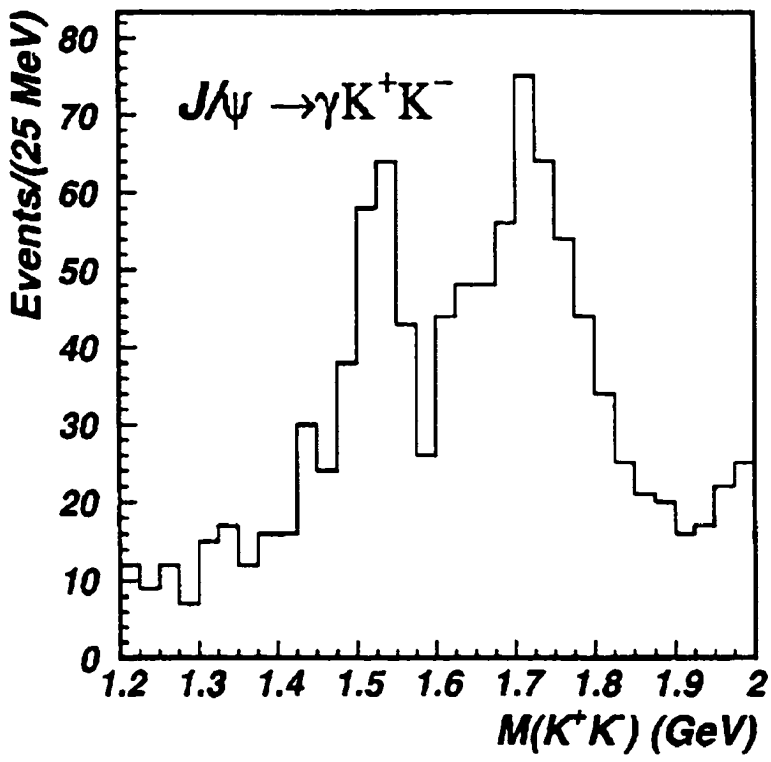

Figure 7.4: Invariant mass of K^+K^- from $J/\psi \to \gamma K^+K^-$ by BES

which shows that *The "15% rule" is followed in* $\psi(2S) \to \gamma f_J(1710) \to \gamma K^+K^-$.

Also, we measured this branching fraction in $\psi(2S) \to \gamma K^0_S K^0_S$ channel to be.

$$B(\psi(2S) \to \gamma f_J(1710) \to \gamma K^0\overline{K^0}) = (4.4 \pm 2.0 \pm 2.3) \times 10^{-5} \quad (7.10)$$

$$< 8.3 \times 10^{-5} \quad (90\%\ C.L.) \quad (7.11)$$

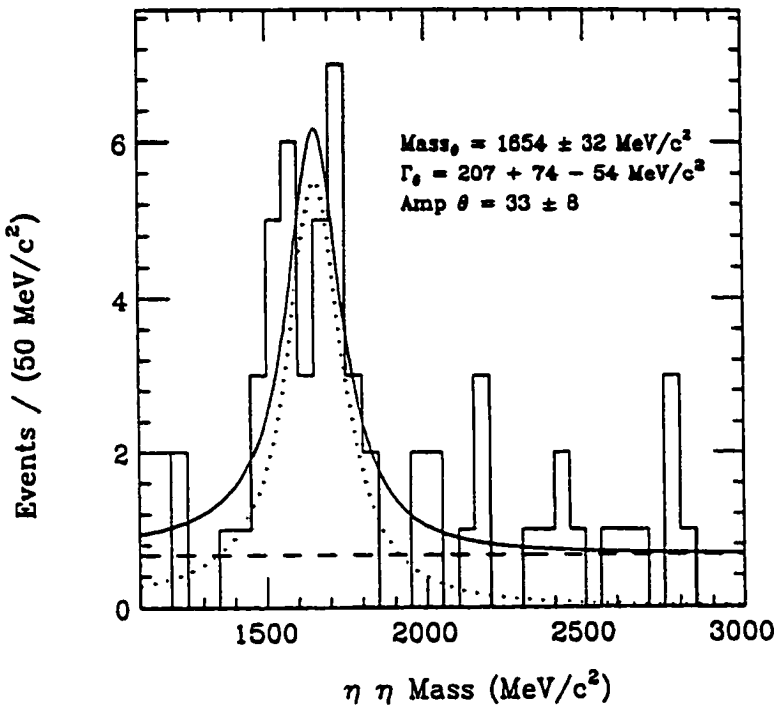

Figure 7.5: Crystal Ball's result of $M_{\eta\eta}$ in $J/\psi \to \gamma\eta\eta$ with one Breit-Wigner at $\sim$ 1655 MeV.

7.3. $\psi(2S) \to \gamma\eta\eta$ at Low $\eta\eta$ Mass Region

In the $\psi(2S) \to \gamma\eta\eta$ channel, neither us nor Crystal Ball observed any significant signal below 3 GeV (see Fig. 6.3 and Fig. 6.4). Crystal Ball observed signal(s) around 1.6 $\sim$ 1.75 GeV in radiative J/ψ decay into $\eta\eta$ [14]. It is possible to be either one signal at $\sim$ 1.65 GeV or two signals of $f_2'(1525)$ and $f_J(1710)$ (see Fig. 7.5 and Fig. 7.6).

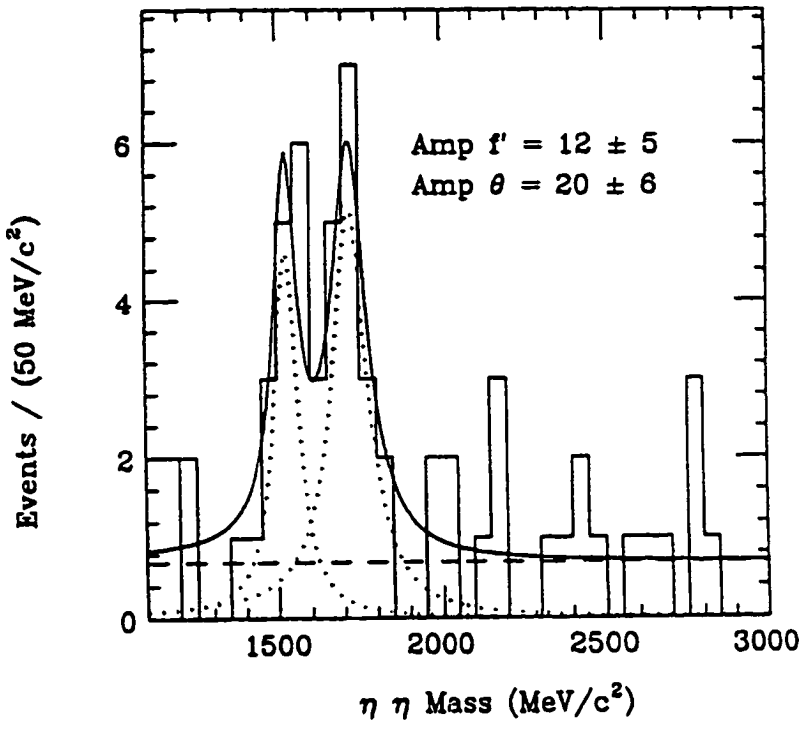

Figure 7.6: Crystal Ball's result of $M_{\eta\eta}$ in $J/\psi \to \gamma\eta\eta$ with two Breit-Wigners, the $f_2'(1525)$ and $\theta(1720)$.

7.4. χ_{c0} and χ_{c2} Decay

We observed the following branching fractions

$$B(\chi_{c0} \to \pi^0\pi^0) = (2.80 \pm 0.32 \pm 0.60) \times 10^{-3}$$

$$B(\chi_{c2} \to \pi^0\pi^0) = (9.2 \pm 2.7 \pm 5.3) \times 10^{-4}$$

$$B(\chi_{c0} \to \eta\eta) = (2.03 \pm 0.84 \pm 0.61) \times 10^{-3}$$

$$B(\chi_{c2} \to \eta\eta) < 1.28 \times 10^{-3} \quad (90\%\ C.L.)$$

These results are consistent with the Crystal Ball's measurement [14]. Our measurements have smaller errors in the first three channels.

The ratio of $\chi_{c0} \to \eta\eta$ and $\chi_{c0} \to \pi^0\pi^0$,

$$\frac{B(\chi_{c0} \to \eta\eta)}{B(\chi_{c0} \to \pi^0\pi^0)} = 0.73 \pm 0.31 \pm 0.23$$

is consistent with the predicted 0.95 based on the SU(3) flavor symmetry.

7.5. Conclusion

We used 3.79×10^6 $\psi(2S)$ data collected by the BES detector and we analyzed the $\psi(2S)$ decay into $\gamma\pi^+\pi^-$, $\gamma\pi^0\pi^0$, γK^+K^-, $\gamma K_S^0 K_S^0$ and $\gamma\eta\eta$ final states. Branching fractions of $\psi(2S) \to \gamma f_2(1270)$ and $\gamma f_J(1710)$ have been measured. Compare with the corresponding J/ψ decay branching fractions, these results follow the "15%" relation.

The glueball candidate $f_J(1710)$ has been observed in radiative decay of J/ψ into $K\overline{K}$, but not in the reaction of $K^-p \to KK\Lambda$. The later result exclude $f_J(1710)$ as an $s\bar{s}$ state. In our analysis, we see a clear signal of $f_J(1710)$ in $\psi(2S)$ radiative decay into K^+K^- final states. This is expected as $\psi(2S)$ differs from J/ψ only by the radial wave function.

In addition, we also measured the branching fractions of χ_{c0} and χ_{c2} decay into $\pi^0\pi^0$ and χ_{c0} decay into $\eta\eta$ as well as an upper limit of branching fraction of χ_{c2}

decay into $\eta\eta$. The results from $\chi_{c0} \rightarrow \pi^0\pi^0$ and $\eta\eta$ are consistent with SU(3) flavor symmetry.

Appendix A

The Breit-Wigner for $f_2(1270) \rightarrow \pi\pi$

In the studying of $\psi(2S) \rightarrow \gamma f_2(1270)$, one added complexity is that the $f_2(1270)$ is rather wide, and the spin of $f_2(1270)$ is not zero. So the non-relativistic S-wave form of Breit-Wigner

$$\frac{1}{\pi}\frac{\Gamma/2}{(m-m_0)^2+\Gamma^2/4} \tag{A.1}$$

which is used frequently at BES is no longer correct to describe the invariant mass distribution of $f_2(1270) \rightarrow \pi\pi$. A new form of Breit-Wigner is needed which should be in relativistic form, with mass dependent width, and with non-spin zero character considered [33].

In our studying, we are dealing with two consecutive two-body decays, $\psi(2S) \rightarrow \gamma f_2(1270)$ and $f_2(1270) \rightarrow \pi\pi$, [19]. The form of differential cross section is

$$\frac{d\sigma}{dm^2} = C|T|^2 \frac{P}{m_{\psi(2S)}}\frac{Q}{m} \tag{A.2}$$

where:

- m is the mass of the resonant mass.
- C is a constant that will be computed numerically based on the normalization.
- m is the invariant mass of the two pseudo-scalars.
- P is the momentum of the $\pi\pi$ resonant in $\psi(2S)$ rest frame which equals to $P = (m^2_{\psi(2S)} - m^2)/2m_{\psi(2S)}$ since the photon has zero mass.
- Q is the momentum of the π in the $\pi\pi$ rest frame. $Q = \sqrt{m^2/4 - m^2_\pi}$.
- T is the invariant amplitude describing the production and decay of $f_2(1270)$.

The differential on the left hand side of Eq. (A.2) is dm^2 instead of dm. This gives the correct Lorentz invariant phase space. We can also write this equation as

$$\frac{d\sigma}{dm} = C_1|T|^2Pq \tag{A.3}$$

where C_1 is a new constant that will be calculated numerically based on the normalization.

There are several factors that help us to determine the form of T:

- A vertex function describing the $\psi(2S) \to \gamma f_2(1270)$ vertex. V_1. Since the lowest orbital angular momentum which conserves parity is zero. we can treat this factor as a constant to a good approximation.

- A vertex function describing the vertex of $f_2(1270)$ decay to $\pi\pi$. This factor, $V_2 \sim q^s$ where s is the orbital angular momentum and equals to 2, the spin of $f_2(1270)$.

- A relativistic Breit-Wigner propagator, BW_{prop}, with mass dependent width describing the propagation of the $f_2(1270)$.

Putting these back to Eq. (A.3), we have

$$\frac{d\sigma}{dm} = C_2 \frac{Pq^{2s+1}}{|BW_{prop}|^2} \tag{A.4}$$

The relativistic form of BW_{prop} is

$$BW_{prop} = m_0^2 - m^2 - im_0\Gamma_{total} \tag{A.5}$$

where m_0 is the PDG mass of $f_2(1270)$ and Γ_{total} is the energy dependent total width which we are going to determine below.

The $f_2(1270) \to \pi\pi$ and $f_2(1270) \to K\overline{K}$ modes account for $\sim 90\%$ of $f_2(1270)$ decay width. Since we can not count all decay modes, as an approximation, we write:

$$\begin{aligned}
\Gamma_{total} &\simeq \Gamma_{\pi\pi} + \Gamma_{K\overline{K}} \\
\Gamma_{\pi\pi} &\sim |V_2|^2 \frac{q_\pi}{m} = \frac{q_\pi^{(2s+1)}}{m} \\
\Gamma_{K\overline{K}} &\sim |V_2|^2 \frac{q_K}{m} = \frac{q_K^{(2s+1)}}{m}
\end{aligned}$$

where q_π is q defined in Eq. (A.2) and q_K is similar to q_π except for a $K\overline{K}$ final state. We will need some rescaling of this Γ_{total} later because the above form doesn't include all decay modes. Similarly

$$\begin{aligned}
\Gamma^0_{total} &= \Gamma^0_{\pi\pi} + \Gamma^0_{K\overline{K}}; \\
\Gamma^0_{\pi\pi} &\sim |V_2|^2 \frac{Q_\pi}{m} = \frac{Q_\pi^{(2s+1)}}{m} \\
\Gamma^0_{K\overline{K}} &\sim |V_2|^2 \frac{Q_K}{m} = \frac{Q_K^{(2s+1)}}{m}
\end{aligned}$$

where Q_π and Q_K are defined the same way as q_π and q_K but with $m = m_0$. Γ^0_{total}, $\Gamma^0_{\pi\pi}$ and $\Gamma^0_{K\overline{K}}$ are the PDG value of these decay widths. It follows that

$$\begin{aligned}
\Gamma_{\pi\pi} &= \Gamma^0_{\pi\pi}(\frac{q_\pi}{Q_\pi})^{(2s+1)}\frac{m_0}{m} \\
\Gamma_{\pi\pi} &= \Gamma^0_{\pi\pi}(\frac{q_K}{Q_K})^{(2s+1)}\frac{m_0}{m} \\
\Gamma_{total} &= \Gamma^0_{total}\frac{B(f_2(1270) \to \pi\pi)(\frac{q_\pi}{Q_\pi})^{(2s+1)} + B(f_2(1270) \to K\overline{K})(\frac{q_K}{Q_K})^{(2s+1)}}{B(f_2(1270) \to \pi\pi) + B(f_2(1270) \to K\overline{K})}
\end{aligned} \tag{A.6}$$

The denominator in Eq (A.6) is there in order to re-scale a branching fraction sum to 1. Equations list here can be easily extend to other resonances in $\psi(2S) \to \gamma +$ two pseudo-scalars by making similar approximations.

Background can also be described by Eq. (A.2) and Eq. (A.3). Since we do not

know the underlying physics of the background process, we can not write out the expression of the matrix element T. Instead, we use Legendre polynomials

$$\frac{1}{m_{max} - m_{min}} \sum_{i=1}^{N_{poly}} b_i p_i(x) \tag{A.7}$$

to represent the lack of physical knowledge of T. x in the expression is defined as

$$x = 2\frac{m - m_{min}}{m_{max} - m_{min}} - 1; \quad x \in [-1, 1]$$

Appendix B

Combining Separate Measurements

It often happens that a physical quantity x is measured several times, perhaps with different experiments and have values

$$x_A \pm \sigma_{x_A} \tag{B.1}$$

$$x_B \pm \sigma_{x_B} \tag{B.2}$$

The question is how to combine them together to get a single best estimate [34]. Before we answer this question, we should realize that if the discrepancy $|x_A - x_B|$ between the two measurements is much greater than both uncertainties σ_A and σ_B, then we should suspect that something has gone wrong in at least one of the measurements.

Suppose that two measurements (B.1) and (B.2) are consistent: that is, $|x_A - x_B|$ is not significantly larger than both σ_A and σ_B. It then makes sense to ask what is the best estimate x_{best} of the true value X based on the two measurements.

Assuming that both measurements are governed by Gaussian distributions. We denote the unknown true value of x by X. Then the probability of A measurement obtaining x_A is

$$P_X(x_A) \propto \frac{1}{\sigma_A} e^{-(x_A - X)^2/2\sigma_A^2}$$

and that of B's getting x_B is

$$P_X(x_B) \propto \frac{1}{\sigma_B} e^{-(x_B - X)^2/2\sigma_B^2}$$

The probability that A find x_A and B find x_B is just the product of the above two probabilities.

$$\begin{aligned} P_X(x_A, x_B) &= P_X(x_A) P_X(x_B) \\ &\propto \frac{1}{\sigma_A \sigma_B} e^{-\chi^2/2} \end{aligned} \tag{B.3}$$

where we define

$$\chi^2 = \left(\frac{x_A - X}{\sigma_A}\right)^2 + \left(\frac{x_B - X}{\sigma_B}\right)^2 \tag{B.4}$$

According to the maximum likelihood principle, the best estimate for X is the value for which the probability (B.3) is maximum or, equivalently, the exponent χ^2 is minimum. To find the best estimation, we simply differentiate (B.4) with respect

to X and solve

$$\frac{d\chi^2}{dX} = 0$$

The solution of this equation for X is the best estimate x_{best}

$$x_{best} = (\frac{x_A}{\sigma_A^2} + \frac{x_B}{\sigma_B^2})/(\frac{1}{\sigma_A^2} + \frac{1}{\sigma_B^2}) \tag{B.5}$$

This analysis can be generalized to combine several measurements of a signal quantity. Supposed we have N separate measurements of a quantity x.

$$x_1 \pm \sigma_1, \quad x_2 \pm \sigma_2, \ldots, \quad x_N \pm \sigma_N$$

The best estimate based on these measurements is the weighted average:

$$x_{best} = \sum_{i=1}^{N} \frac{x_i}{\sigma_i^2} / \sum_{i=1}^{N} \frac{1}{\sigma_i^2} \tag{B.6}$$

To estimate the uncertainty of x_{best}, we take the derivative of x_{best} in (B.6).

$$dx_{best} = \sum_{i=1}^{N} \frac{dx_i}{\sigma_i^2} / \sum_{i=1}^{N} \frac{1}{\sigma_i^2} \tag{B.7}$$

And the uncertainty of x_{best} should be

$$\begin{aligned} \sigma_{x_{best}} &= \sqrt{\sum_{i=1}^{N}(\frac{\sigma_i}{\sigma_i^2})^2 / \sum_{i=1}^{N}\frac{1}{\sigma_i^2}} \\ &= \sqrt{\sum_{i=1}^{N}\frac{1}{\sigma_i^2}} \end{aligned} \tag{B.8}$$

Often times each measurement give several errors such as statistical error and systematic error. For several measurement

$$x_1 \pm \sigma_1, \quad x_2 \pm \sigma_2, \ldots, \ x_N \pm \sigma_N$$

Each $\sigma_i \quad i = 1, \ldots, N$ may have several components, say

$$\begin{aligned} \sigma_i &= \sigma_i^1 \pm \sigma_i^2 \pm \ldots \sigma_i^M \\ &= \sqrt{\sum_{j=1}^{M}(\sigma_i^j)^2} \end{aligned}$$

according to (B.7), the jth uncertainly for x_{best} is

$$\sigma^j_{x_{best}} = \sqrt{\sum_{i=1}^{N}(\frac{\sigma_i^j}{\sigma_i^2})^2 / \sum_{i=1}^{N}\frac{1}{\sigma_i^2}} \tag{B.9}$$

Appendix C

Isospin Determination of Decay Amplitude Among $K\overline{K}$ Final States

The isospin states of K and K^0 are similar to the nucleon-antinucleon states. The K^+ and K^0 forms an isospin doublet with $I_3 = 1/2$ and $-1/2$ respectively. The K^- and $\overline{K^0}$ also forms an isospin doublet.

$$\begin{pmatrix} K^+ \\ K^0 \end{pmatrix} \cdot \begin{pmatrix} \overline{K^0} \\ -K^- \end{pmatrix} \tag{C.1}$$

where we follow the Cordon-Shortley convention and assign a minus sign to the K^-. The most positively charged particle is chosen to have the maximum value of I_3. Note that both doublets transform in the same way under the rotation through π about

the 2-axis.

$$e^{-i\sigma_2\pi/2} = -i\sigma_2; \quad \sigma_2 = \begin{pmatrix} 0 & -i \\ i & 0 \end{pmatrix}$$

A composite system of a K-$\overline{K}$ pair has isospin states:

$$|I = 1, I_3 = 1 >= |K^+ > |\overline{K^0} > \tag{C.2}$$

$$|I = 1, I_3 = 0 >= \frac{1}{\sqrt{2}}(|K^+ > |K^- > -|K^0 > |\overline{K^0} >) \tag{C.3}$$

$$|I = 1, I_3 = -1 >= -|K^- > |K^0 > \tag{C.4}$$

$$|I = 0, I_3 = 0 >= \frac{1}{\sqrt{2}}(|K^+ > |K^- > +|K^0 > |\overline{K^0} >) \tag{C.5}$$

The last formula can be used to form an isoscalar decay of the K-$\overline{K}$ system. But we must be careful because a isoscalar also has a defined C-parity. For example, particle like o has $I = 0$ and $J^{PC} = 1^{--}$, thus the final K-$\overline{K}$ system state should be written as.

$$\frac{1}{2}\left[(|K^+ > |K^- > +|K^0 > |\overline{K^0} >) - (|K^- > |K^+ > +|\overline{K^0} > |K^0 >)\right] \tag{C.6}$$

$$= \frac{1}{2}\left[(|K^+ > |K^- > -(|K^- > |K^+ >) + (|K^0 > |\overline{K^0} > -|\overline{K^0} > |K^0 >)\right] \tag{C.7}$$

Both the first two items and the second two items of Eq. (C.6) has $I = 0$ and $I_3 = 0$

and thus the total has $I = 0$ and $I_3 = 0$. Let's now look at its C-parity. Since

$$|K^0>= \frac{1}{\sqrt{2}}(|K^0_L> +|K^0_S>) \qquad |\overline{K^0}>= \frac{1}{\sqrt{2}}(|K^0_L> -|K^0_S>) \tag{C.8}$$

$$|K^0_L>= \frac{1}{\sqrt{2}}(|K^0> +|\overline{K^0}>) \qquad |K^0_S>= \frac{1}{\sqrt{2}}(|K^0> -|\overline{K^0}>) \tag{C.9}$$

Eq. (C.7) can also be written as

$$\frac{1}{2}\left[(|K^+>|K^->-(|K^->|K^+>)+(|K^0_L>|K^0_S>-|K^0_S>|K^0_L>)\right] \tag{C.10}$$

The C-parity of a K^+K^- system is determined by the following argument:

$$(-1)^L C(|K^+>|K^->) = +|K^+>|K^-> \tag{C.11}$$

$$\Longrightarrow \quad C(|K^+>|K^->) = (-1)^L|K^+>|K^-> \tag{C.12}$$

where L is the orbital angular momentum. Also, since

$$C|K^0_L>= |K^0_L>: \quad C|K^0_S>= -|K^0_S>$$

the C-parity for $K^0_L - K^0_L$, $K^0_S - K^0_S$ and $K^0_L - K^0_S$ system are

$$C|K^0_L>|K^0_L>= +|K^0_L>|K^0_L> \tag{C.13}$$

$$C|K^0_S>|K^0_S>= +|K^0_S>|K^0_S> \tag{C.14}$$

$$C|K_L^0 > |K_S^0 >= -|K_L^0 > |K_S^0 > \qquad \text{(C.15)}$$

Thus, for a decay process with $L = 1$, Eq. (C.6) gives $C = -1$ which is the same as ϕ's C-parity.

The K-$\overline{K}$ system state from a $I^G(J^{PC}) = 0^+(even^{++})$ decay can be written as

$$\frac{1}{2}\left[(|K^+ > |K^- > +|K^0 > |\overline{K^0} >) + (|K^- > |K^+ > +|\overline{K^0} > |K^0 >)\right] \qquad \text{(C.16)}$$

$$= \frac{1}{2}\left[(|K^+ > |K^- > +(|K^- > |K^+ >) + (|K^0 > |\overline{K^0} > +|\overline{K^0} > |K^0 >)\right]$$

$$= \frac{1}{2}\left[(|K^+ > |K^- > +(|K^- > |K^+ >) + (|K_L^0 > |K_L^0 > -|K_S^0 > |K_S^0 >)\right] \qquad \text{(C.17)}$$

It follows that ratio of decay branching fractions among K-$\overline{K}$ final states are $B(K\overline{K})$: $B(K^+K^-) : B(K_S^0K_S^0) = 4 : 2 : 1$.

Appendix D

Principle of Kinematic Fitting

Kinematic fitting method uses the physical laws such as conservation of energy and momentum to improve the measurements describing the particle interaction or decay process. For example, the fact the several particles decay from a parent particle must come from a common space point can be used to improve the momentum vectors of the daughter particles, thus improve the mass resolution of the parent particle.

In the BES kinematic fitting packages, such as TELESIS, momentum and energy and their covariance matrices (also called error matrices) of charged and neutral tracks are used, regardless of how these quantities are measured by the detector.

Let $\mathbf{p}$ be a vertex of parameters of a set of n tracks in the final state. Since each

tracks has three parameters, the dimension of $\mathbf{p}$ would be $3n$.

$$\mathbf{p} = \begin{pmatrix} p_1 \\ p_2 \\ \vdots \\ p_n \end{pmatrix} ; \mathbf{p}_{charged} = \begin{pmatrix} o \\ 1/p_{xy} \\ \coth\theta \end{pmatrix} ; \mathbf{p}_{neutral} = \begin{pmatrix} o \\ \coth\theta \\ \sqrt{E} \end{pmatrix} ; \tag{D.1}$$

Let $\mathbf{p}_0$ be the initial unconstrained value of $\mathbf{p}$ obtained from reconstruction. The χ^2 is defined as:

$$\chi^2 = (\mathbf{p} - \mathbf{p}_0)^T \mathbf{V}^{-1}(\mathbf{p}_0)(\mathbf{p} - \mathbf{p}_0) \tag{D.2}$$

The values in $\mathbf{p}$ can not be adjust arbitrary to achieve a minimum value of χ^2 — they have to satisfy the conservation of 4-momentum! In order to write out the expression of 4-momentum constraints $\mathbf{C}(\mathbf{p}) = 0$, an array of 4 equations, the masses of each particles in the initial state and final state should be input as parameters. The constraints are then incorporated into the χ^2 using the Lagrange multiplier method.

$$\chi^2 = (\mathbf{p} - \mathbf{p}_0)^T \mathbf{V}^{-1}(\mathbf{p}_0)(\mathbf{p} - \mathbf{p}_0) + 2\lambda^T \mathbf{C}(\mathbf{p}) \tag{D.3}$$

where λ is a vector of 4 unknowns.

$\mathbf{C(p)}$ can be expanded at point $\mathbf{p}_A$ as

$$\mathbf{C}(\mathbf{p}_A) + \frac{\partial \mathbf{C}(\mathbf{p}_A)}{\partial \mathbf{p}}(\mathbf{p} - \mathbf{p}_A) = 0 \tag{D.4}$$

By solving equations

$$\frac{\partial \chi^2}{\partial \mathbf{p}} = 0; \quad \frac{\partial \chi^2}{\partial \lambda} = 0 \tag{D.5}$$

or

$$\mathbf{V}^{-1}(\mathbf{p}_0)(\mathbf{p} - \mathbf{p}_0) + \left(\frac{\partial \mathbf{C}(\mathbf{p})}{\partial \mathbf{p}}\right)^T \lambda = 0 \tag{D.6}$$

$$\mathbf{C}(\mathbf{p}_A) + \frac{\partial \mathbf{C}(\mathbf{p})}{\partial \mathbf{p}}(\mathbf{p} - \mathbf{p}_0) = 0 \tag{D.7}$$

We can solve $\mathbf{p}$ and λ that cause minimum χ^2.

The fitting χ^2 is determined by

$$\chi^2 = \lambda^T \left(\mathbf{C}(\mathbf{p}_A) + \frac{\partial \mathbf{C}(\mathbf{p})}{\partial \mathbf{p}}(\mathbf{p} - \mathbf{p}_0)\right) \tag{D.8}$$

In addition to the $4n$ input parameters we just mentioned, there are also 4-momentums of the entire events plus the number of resonance mass. The number of output parameters are $4n$ which are the 4-momentums from the daughter particles. Thus the degree of freedom is number of input parameters minus number of

output parameters.

$$N_{dof} = 4 + N_{resonance} \tag{D.9}$$

In order to evaluate the fit, "pull" is defined for each quantities:

$$Pull_i = \frac{p_i - p_{0i}}{\sqrt{V_{ii}}} \tag{D.10}$$

Apparently, "pulls" should have normal Gaussian distributions $N(0,1)$. A none-zero central value may indicate systematic error in the measurement while standard deviation does not equal to one may indicate a improper measurement error.

Bibliography

[1] S.L. Glashow, J. Iliopoulos, J. Maiani, Phys. Rev. D2(1970) 1285

[2] J.J Aubert *et. al.*, Phys. Rev. Lett. 33(1974) 1404

[3] J.E. Augustin *et. al.*, Phys. Rev. Lett. 33(1974) 1406

[4] E. Leader and E. Predazzi, An Introduction to Gauge Theories and the "New Physics", p155.

[5] R. Partridge *et. al.* Phys. Rev. Lett. 45 (1980) 1150

[6] M.E.B. Franklin et al., Phys. Rev. Lett. 51, 11(1983).

[7] BES Collaboration, J.Z. Bai *et al.*, Phys. Rev. Lett. 81, 5080(1998)

[8] BES Collaboration, J.Z. Bai *et al.*, Phys. Rev. Lett. 83, 1918(1999)

[9] BES Collaboration, J.Z. Bai *et al.*, Determination of J/ψ Leptonic Branching Fraction via $\psi(2S) \to \pi^+\pi^- J/\psi$, Phys. Rev. D58 (1998) 092006

[10] Mark I Collaboration, Phys. Rev. D17, 1731, 1978

[11] DASP Collaboration. Nucl. Phys. B160. 426. 1979

[12] DASP Collaboration. Z. Phys. C1. 233. 1979

[13] BES Collaboration. J.Z. Bai *et al.*. Study of the P-Wave Charmonium χ_{cJ} in $\psi(2S)$ decay. Phys. Rev. Lett. 81. 3091(1998).

[14] Roger Alan Lee. Ph. D. dissertation. Radiative decays of the PSI Prime to all-photon final states. SLAC-PUB-282

[15] H.b. Li. Ph. D. dissertation. Studying of $\psi(2S)$ decay into all-photon final state

[16] BES Collaboration. J.Z. Bai *et al.*. Measurement of the Mass of the τ Lepton. Phys. Rev. D53.20(1995)

[17] Derrick Kong and Cui Xianzhong. Integrated Luminosity of $\psi(2S)$ data. BES Analysis Note. Nov. 27th 1998 The value of integrated luminosity is $6011 \pm 26 \pm 155\ nb^{-1}$.

[18] Huang Guangshun and Zhao Zhengguo. Measurement of the Luminosity with Large Angle Bhabha Events for the Data Around 3.55 GeV Collected with BES and BEPC. BES Analysis Note. Apr. 1998. The integrated luminosity values are 4220.6 nb^{-1}. 4232.4 nb^{-1} and 4187.8 nb^{-1} by using three events selection criteria. Errors are not available for some of these values.

[19] Private communication with Bill Dunwoodie.

[20] Yuang Changzheng, "Is TELESIS Reliable?", BES memo, Nov. 1997; Private communication with Yuang Changzheng and Fred Harris; It is agreed within the BES collaboration to include a 10% error in the final systematic error due to the problem of TELESIS.

[21] Bill Dunwoodie, SLAC-PUB 7163, Nov. 1997

[22] Mark III Collaboration, R. Baltrusaitis *et. al.* Radiative decay of the J/ψ into $\gamma\pi^+\pi^-$ and γK^+K^-, Phys. Rev. D 35, 2077(1987)

[23] DM2 Collaboration, Augustin *et. al.* Phys. Rev. Lett. 60 2238(1988)

[24] C. Edwards *et al.*, Phys. Rev. D 25, 3065(1982)

[25] T. Armstrong *et al.*, Crystal Barrel Collaboration, Phys. Lett. B353, 425(1995)

[26] M. Reyes *et al.* Phys. Rev. Lett. 81, 4079(1998)

[27] D. Bugg *et al.*, Phys. Lett. B353, 378(1995)

[28] BES Collaboration, J.Z. Bai *et al.*, Branching fractions of $\psi(2S) \to \gamma\eta'$ and $\gamma\eta$, Phys. Rev. D58 097101(1998)

[29] T. Armstrong *et al.*, Phys. Lett. B227, 186(1989)

[30] BES Collaboration, J.Z. Bai *et al.*, Structure Analysis of the $f_J(1710)$ in the Radiative Decay $J/\psi \to \gamma K^+K^-$, Phys. Rev. Lett. 77, 3959(1996)

[31] BES Collaboration, J.Z. Bai *et al.*, Study of the hadronic decays of χ_c states Phys. Rev. D 60, 072001, 1999

[32] C. Edwards *et al.*, Phys. Rev. Lett. 48, 458(1982)

[33] Kevin F. Einsweiler, Radiative decay of the Psi(3097) to two meson Final States. SLAC-PUB-272

[34] John R. Taylor, An Introduction of Error Analysis, University Science Book, 1982